2018

Proportion and performance evaluation of fly ash-based geopolymer and its application in engineered composites

Yifeng Ling
Iowa State University

Proportion and performance evaluation of fly ash-based geopolymer and its application in engineered composites

by:

Yifeng Ling

A dissertation submitted to the graduate faculty

in partial fulfillment of the requirements for the degree of

DOCTOR OF PHILOSOPHY

Major: Civil Engineering (Civil Engineering Materials)

Program of Study Committee:
Kejin Wang, Co-major Professor
Say-Kee Ong, Co-major Professor
Franciszek Hasiuk
Ashley Buss
Xuhao Wang

The student author, whose presentation of the scholarship herein was approved by the program of study committee, is solely responsible for the content of this dissertation. The Graduate College will ensure this dissertation is globally accessible and will not permit alterations after a degree is conferred.

Iowa State University

Ames, Iowa

2018

TABLE OF CONTENTS

ACKNOWLEGEMENTS

I wish to express my sincere thanks to my major advisors, Dr. Kejin Wang and Dr. Say Kee Ong, for their generous support during my doctoral program. I greatly appreciate not only their professional guidance but also the opportunities to teach classes as a teaching assistant and to participate in projects sponsored by Midwest Transportation Center and Iowa Department of Transportation as a research assistant. These activities made my graduate experience busy but rewarding.

I am also grateful to Dr. Ashley Buss, Dr. Franciszek Hasiuk and Dr. Xuhao Wang for their service as my committee members. The comments and questions that I have received from them have encouraged me to read more and think deeper for my research. During the course of my PhD study, I have received a lot of comments, suggestions, discussions, and help in performing laboratory work from my colleagues in Civil, Construction and Environmental Engineering (CCEE) Department at Iowa State University. They include, but not limited to, Dr. Gilson Lomboy, Robert Steffes, Dr. Chuanqing Fu, Douglas Wood, Dr. Song Han, Yu-an Chen, Dr. Peng Zhang, Dr. Jianzhong Liu and Dr. Sudong Hua. Their presences and involvements have assisted me in developing ideas for my experiments.

I will never forget the support from my family for their selfless love, sacrifice and encouragement without which I could never successfully complete my Ph.D. degree. My overseas studies has made me miss them much.

Finally, I would like to give my most gratitude to my wife, Yunyun Yao. She shared her love with me against half of the Earth in distance during past two years and makes my life beautiful every day. I humbly dedicate this piece of study to her and love her with my whole life.

ABSTRACT

It is well known that the use of Portland cement (PC) in concrete construction is causing severe environmental issues primarily due to vast quantity of carbon dioxide released to the atmosphere leading to global warming during its manufacture. On the other hand, disposal of industrial solid wastes such as fly ash and slag in landfills creates another threat to the environment. The development of a fly ash geopolymer binder, produced from the reaction of fly ash and an alkaline solution, may replace Portland cement as a construction material while simultaneously reducing the amount of fly ash needing to be disposed of in landfills.

This dissertation reports on efforts to optimize mix proportion, predictive modeling on early age properties, shrinkage control, and mechanical performance of an engineered composite made with fly ash-based geopolymer. It's four component studies are: (1) Optimization of Mix Design Parameters on Thermal, Setting and Stiffening Behaviors of High-Calcium Fly Ash Geopolymer; (2) Prediction of Strength, Setting Time and Heat Generation of Fly Ash Geopolymer Using An Artificial Neural Network; (3) The Effects of Activator and Shrinkage Reducing Admixture on Shrinkage Behavior of Fly Ash Geopolymer, and (4) The Effect of Slag on Mechanical Properties of An Engineered Geopolymer Composite.

Due to the paucity of knowledge to optimize the mix proportion of fly-ash-based geopolymer in the published literature, Paper 1 is focused on the effects of design parameters including SiO_2/Na_2O molar ratio (Module) and solute (NaOH and Na_2SiO_3) mass concentration on both fresh and hardened PC properties (i.e., setting time, compressive strength, heat of hydration). The knowledge gained from this study is expected to assist in the optimization of the mix proportions for the fly ash geopolymer. Results from Paper 1 have shown that modules less than 1.5,

concentrations between 40% and 50%, L/F ratios less than 0.40, and higher curing temperature, (such as 50℃) were preferred to synthesize a geopolymer system using high-calcium fly ash.

In Paper 2, an artificial neural network (ANN) approach was applied to analyze the complexity between geopolymer properties and various parameters for geopolymer mix proportion design. The predictive models for setting time and compressive strength of geopolymer were established to simplify mix design. Paper 2 concluded that ANN was an effective tool for conducting a parametric study of fly ash geopolymer properties. The effects of mix design parameters on setting time, compressive strength and heat generation were discussed in accordance with the prediction profiler generated by the ANN models. The proposed model can be used to guide high-calcium fly ash geopolymer mix design in the future.

Shrinkage of cement-based materials is a major cause of cracking. The work discussed in Paper 3 characterized the shrinkage behavior (e.g., free drying shrinkage and restrained ring shrinkage) of fly-ash-based geopolymer in comparison with that of traditional PC paste. The effects of activator (Module and Concentration) and shrinkage reducing admixture (SR) on the shrinkage behavior of fly-ash-based geopolymer have been explored. In addition, the flowability of the geopolymer using a mini slump test and compressive strength test were also carried out. The results indicate that the fly ash geopolymer has comparable flowability to that of traditional PC. Increased SR slightly decreased flowability of both PC and fly ash geopolymer. It was also found that the drying shrinkage of fly ash geopolymer was of similar magnitude to that of PC, but that this similarity was not due to mass loss in the fly ash geopolymer. The SR significantly reduced (up to 52%) the drying shrinkage of fly ash geopolymer as well as in PC. The SR decreased the restrained shrinkage up to 16%, delayed the cracking time, reduced the crack width and lowered the cracking potential for both PC and fly ash geopolymer. The fly ash geopolymer mixtures had

lower cracking potential than PC. The effects of Module and Concentration on drying shrinkage and restrained ring shrinkage were also concluded.

The last paper (Paper 4) investigated the mechanical performance of fly ash-based geopolymer in a fiber-reinforced composite, namely an engineered geopolymer composite (EGC). Fly ash was replaced with slag in the geopolymer. The physical and chemical interactions of these two cementitious materials have resulted in a high strength (up to 110 MPa) and workable EGC. The mechanical properties including compressive strength, tensile strength, tensile strain capacity, toughness, elasticity, flexural bending strength, ductility and pullout bond strength were assessed. Experimental results in Paper 4 revealed that all EGCs exhibited strain hardening behavior. The addition of 20% slag had the largest effect on engineering strength. However, as slag addition increased, the tensile strain capacity, ultimate deflections, toughness and ductility decreased. In addition, bond strength can be estimated precisely based on the compressive strength of EGCs.

CHAPTER 1. INTRODUCTION

Background

Concrete is the most widely used construction material in the world and typically is produced using Portland cement (PC) as the binder. The mass of PC used in concrete construction brings a critical environmental issue due to the high emission of carbon dioxide gas during its manufacture from the calcination of limestone and the combustion of fossil fuel. It has been reported that around 5% of global carbon dioxide emissions is from the cement industry (IPCC 1997). Moreover, producing a ton of PC requires 4.9 million kilojoule of energy, equivalent to about 400 pounds of coal. Together, production of one ton of PC generates nearly a ton of CO_2.

On the other hand, fly ash, a by-product of burning coal in power plants, is abundant worldwide. The constituents of fly ash vary considerably depending on the source of the coal burned but the main components are SiO_2 (40-60%), Al_2O_3 (20-30%), Fe_2O_3 (4-10%) and CaO (5-30%). Fly ash usually contains toxic elements including arsenic, cadmium, chromium, lead and mercury. The majority of fly ash is currently dumped in landfills, creating a threat to the environment due to the impacts to groundwater and encroaching upon valuable open space and biodiversity (ACI 232). Over the years, many attempts have been made to divert fly ash from landfills, one of which is to use it as a supplementary cementitious material (SCM) for PC. Fly ash, with a low CaO content (Class F fly ash specified by ASTM C618), does not possess binding properties by itself. However, in the presence of water and at an ambient temperature, Class F fly ash reacts with the calcium hydroxide, a hydration product of PC, to form calcium silicate hydrate (C-S-H) gel. This process is called a pozzolanic reaction. It is the C-S-H gel formed from the pozzolanic reaction that possesses cementing properties. Based on this concept, high volume fly ash (HVFA) concrete, which has more than 60% by mass of its PC replacemed by fly ash has been

developed (Malhotra 2002; Malhotra and Mehta 2002). The advantages of using HVFA concrete are not only reducing CO_2 emissions and cost, but also having improved workability, reduced free-drying shrinkage and enhanced ultimate strength.

While SCMs are increasingly used in PC, another class of binders, first termed as geopolymer by Joseph Davidovits in 1978, has been developed. Different from HVFA concrete, geopolymerdoes not need the presence of PC. Instead, the source materials that are rich in silicon (Si) and aluminum (Al), such as fly ash or slag, are activated by alkaline chemicals. In this technology, the alkalinity of the activator can be low, mild, or high. The activator, with a low to medium alkalinity is generally used to activate silicon- and calcium-rich minerals (e.g., slag and Class C fly ash). The main reaction product is C-S-H gel. A high alkaline activator is frequently used to activate silicon- and aluminum-rich minerals, such as low calcium (ASTM Class F) fly ash (Palomo, Grutzeck et al. 1999). In this case, the cementing properties were generated through a process of polymerization. It has been known that geopolymer possesses excellent early strength, resistance to sulfates, various acids, temperature extremes and minimal shrinkage. However, the disadvantages of using geopolymer including complex mix design parameters, strict curing condition and decreased workability cannot be disregarded.

In 2015, during the initial stages of this dissertation, there were some research publications on geopolymer regarding the mix proportion, predictive modeling on strength, shrinkage behavior and the mechanical performance of engineered geopolymer composite. (Jo et al. 2015; Patankar et al. 2014; Khale and Chaudhary 2007; Krizan et al. 2002; Yadollahi et al. 2015; Ridtirud et al. 2011; Deb et al. 2015; Palacios and Puertas 2005; Nematollahi et al. 2015). However, the overall consideration of mix design parameters in geopolymer early properties was limited. The effects of all mix design parameters need to be assessed. Moreover, the thermal behavior of geopolymer,

which largely controls its early properties, has not been fully explored in terms of mix design parameters. Additionally, because it is known that binder shrinkage is a critical cause for cracking in PC concrete, the shrinkage behavior of geopolymer should be investigated. To reduce shrinkage, shrinkage reducing admixtures (SR) have been effectively used in PC concrete. In order to provide a shrinkage control method for geopolymer, the evaluation of the effect of SR on geopolymer can be beneficial. Its relatively low strength is one of the biggest limitations of fly-ash-based engineered geopolymer composite (EGC). Replacing fly ash with slag could be an acceptable alternative to enhance the strength of fly ash-based EGC due to its high-calcium content, but maintaining strain hardening behavior because of fiber addition.

Objective of Dissertation

The overall goal of the research presented in this dissertation is to develop a high performance (highly workable, high strength, and high cracking resistance) engineered geopolymer composite (EGC). Several steps were made to achieve this goal:

1. Exploration of the effects of mix design parameters (e.g., SiO_2/Na_2O mole ratio, solute mass concentration, activator to fly ash mass ratio, temperature and curing time) on basic geopolymer properties (e.g., strength, thermal and setting behaviors).
2. Optimization of mix proportions based on the understanding of materials and mix proportion effects.
3. Investigation of shrinkage cracking behavior of geopolymer made with various mix proportions and to effectively reduce shrinkage potential.
4. Development of an EGC that possesses good workability, excellent mechanical properties (high strength and ductility) for cracking and impact resistance.

Dissertation Organization

This dissertation consists of eight chapters.

Chapter 1 provides a background and objectives of this dissertation.

Chapter 2 includes a brief literature review on geopolymer theory, constituents, properties, and applications.

Chapter 3 to 6 describe experimental methods, main findings, and interpretations. Each chapter comprises a paper that is ready for peer-review publication. The papers are ordered in the dissertation as follows:

- Chapter 3

Yifeng Ling, Kejin Wang, Xuhao Wang, Sudong Hua, Scott M. Schlorholtz. *Optimization of Mix Design Parameters on Thermal, Setting and Stiffening Behaviors of High-calcium Fly Ash Geopolymer*

Chapter 3 explores the effect of mix design parameters on setting time, compressive strength and hydration characteristics of fly ash geopolymer. The optimized mix proportion of fly ash geopolymer is concluded. The mix design parameters considered in this chapter are SiO_2/Na_2O mole ratio (Module), NaOH and Na_2SiO_3 solute mass concentration (Concentration), activator solution-to-fly-ash ratio, curing temperature and time.

- Chapter 4

Yifeng Ling, Kejin Wang, Xuhao Wang. *Prediction of Strength, Setting time and Geopolymerization Heat of Fly Ash Geopolymer Using Artificial Neural Network.*

Chapter 4 presents a study that applies artificial neural networks to develop predictive models for setting time, compressive strength and geopolymerization heat of fly ash geopolymer. These models better account for the effect of each parameter on geopolymer performance .

- Chapter 5

Yifeng Ling, Kejin Wang, Chuanqing Fu. *The Effects of Activator and Shrinkage Reducing Admixture on Shrinkage Behavior of Fly Ash Geopolymer*.

Chapter 5 covers a study on the effect of Module, Concentration and shrinkage reducing admixture (SR) on the flowability, compressive strength and shrinkage behavior of fly ash geopolymer compared to Portland cement. The shrinkage potential of fly ash geopolymer paste and PC is evaluated as well as the shrinkage reduction by using SR.

- Chapter 6

Yifeng Ling, Kejin Wang, Guyu Shi. *The Effect of Slag on Mechanical Properties of Engineered Geopolymer Composite.*

Chapter 6 includes the findings of the study concerning the addition of slag in fly-ash-based engineered geopolymer composite (EGC) to improve its strength. The mechanical properties (e.g., compressive strength, tensile strength, flexural bending strength and pullout bond strength) are conducted with from 0% to 30% slag. The effects of slag on mechanical properties and strain hardening behavior of fly-ash-based EGC are investigated.

Chapter 7 summarizes the major conclusions of this dissertation followed by the recommendations for future research in Chapter 8.

CHAPTER 2. LITERATURE REVIEW

Geopolymer Theory

Geopolymer development

To date, the increasing demands to reduce the use of Portland cement (PC) in concrete and the increasing environmental issues caused by CO_2 which is from production of PC have accelerated the development of geopolymer binder that was a product from the reaction of industrial aluminosilicate wastes (e.g., fly ash, slag and metakaolin) and alkali solution (Sumajouw et al., 2004). As a new type of concrete binder, geopolymer has been recognized as an alternative to traditional PC due to its high temperature, acid resistance and environmental benefits (e.g., list some environmental benefits). Since Joseph Davidovits coined the term "geopolymer" in 1978, its properties and uses have been explored by many scientific and industrial researchers (Davidovits 1994).

Geopolymers are characterized by a three-dimensional Si-O-Al structure. They are able to provide ceramic and zeolitic properties not normally present in PC (McDonald and Thompson 2005). Geopolymer develops through several distinct reaction processes from initial pozzolanic activation to final microstructure development (Fernandez et al., 2005). The major procedural steps in geopolymer formation are 1) dissolution of the aluminosilicate species within a highly alkaline environment, 2) polymerization of the dissolved ions into temporary structural gel, 3) precipitation of formed hydration products, 4) final hardening of the matrix by excess water evaporation and 5) the growth of crystalline structures. Fig. 1 illustrates the overall polymerization process in geopolymer which can be summarized as three processes: Dissolution, Polymerization and Growth (Rangan 2008). Dissolution occurs immediately after the contact of the alkaline solution and the

pozzolanic materials and creates ionic interface that facilitate the breaking of covalent bonds among silicon, aluminum and oxygen atoms. Similar to PC, this process generates rapid and intense heat (Fernandez et al. 2006). The rate of dissolution correlates to the amount and composition of the activating solution (Xie and Xi 2001). The polymerization process involves a rapid chemical reaction in an alkaline solution on Si-Al species, resulting in a three-dimensional polymeric chain-and-ring structure consisting of Si-O-Al-O bonds (Skvara et al. 2006). The formed gel contains alkaline cations that compensate for the charge deficit associated with the Al-for-Si substitution (Xie and Xi 2001). An intermediate, Al-rich phase is first formed, which then gives way to a more stable, silicon-rich, three-dimensional gel that is dependent upon curing conditions and activator type (Fernandez et al. 2006). During this process, the slow growth of crystalline structures become evident as the nuclei of the polymerized gel reaches critical size. The degree of crystallinity relates to the rate at which precipitation occurs. It should be noted that the fast reactions between alkali and pozzolanic materials do not allow enough time for the growth of a well-structured crystalline environment. Therefore, most hardened geopolymer is referred to as zeolitic precursors rather than actual zeolites. The final product of geopolymerization is an amorphous, semi-crystalline cementitious material (Petermann et al. 2010).

Geopolymer Constituents

Pozzolanic materials

Fly ash

Most available pozzolanic material around the world is fly ash, which is by-product obtained from the combustion of coal during industrial processes like power generation (Reference). It is considered one of the most important source materials for geopolymer binder (Khale et al. 2007). Most fly ashes from the combustion of coal are made up of an inhomogeneous mix of

aluminosilicate and silica glasses plus small amounts of crystalline materials including mullite, quartz, hematite and magnetite (Song et al. 2000). Particle size distribution and particle fineness are the physical characteristics of fly ashes as shown in Fig. 2, most strongly governing their reactivity (Krizan et al. 2002). The presence of highly reactive silica in the fly ash increases the formation potential of the aluminosilicate gel, which contributes mechanical strength of geopolymer. The aluminum content of fly ash material is critical to the hardening properties of a geopolymer binder and believed to be the critical factor for setting (Rangan 2008).

Slag

Another pozzolanic material used to synthesize geopolymer is ground granulated blast furnace slag (GGBFS) resulting from rapid water-cooling of molten steel. It has been used extensively in the concrete industry as a cementitious material since it is relatively inexpensive to obtain, highly resistant to chemical attack and maintains excellent thermal properties (Dan and Janotka 2003). Major components of the slag product include SiO_2, CaO, MgO and Al_2O_3. Alkali activation yields a highly amorphous calcium silicate hydrate (C-S-H) gel product with high aluminum content (Pacheco et al. 2007). This product is referred to alkali-activated slag (AAS). While shrinkage in AAS pastes is more common than in PC, it maintains a much higher ultimate strength by comparison.

Alkaline activator

NaOH

The NaOH is a commonly employed alkaline activator to provide OH^-. Its concentration in activator solution determines the geopolymer paste properties. While high NaOH concentrations accelerate chemical dissolution, it depresses ettringite and CH formation during binder formation (Khale et al. 2007). While a higher concentration of NaOH promotes higher strength at early stages

of reaction, the strength of activated geopolymer can be compromised due to excessive OH^- in solution causing non-uniform morphology of the final products (Khale et al. 2007). It is found that geopolymer activated with NaOH develops greater crystallinity thus improving stability in aggressive environments of sulfates and acids (Criado et al. 2007). There is a linear relationship between NaOH concentration and the heat generation (Chareerat et al. 2006).

Na_2SiO_3

Sodium silicate is manufactured by fusing silica sand (SiO_2) with sodium carbonate (Na_2CO_3) at temperatures in excess of 1100ºC and dissolving the product with high pressure steam into a semi-viscous liquid referred to as "waterglass" (Fernandez et al. 2005). Waterglass is rarely used as an independent activating unit because it does not possess enough OH^- as activation potential to initiate pozzolanic reaction alone. Rather, it is commonly mixed with NaOH as a fortifying agent to enhance alkalinity and increase overall strength. The most utilized alkaline activator in geopolymerization is a combination of sodium hydroxide and sodium silicate (Kong et al. 2008).

Feng et al. (2004) asserted that soluble silicates reduce alkali saturation in pore solutions and promote greater inter-particle bonding with geopolymer binders. As well, the presence of Na_2SiO_3 improves interfacial bonding between aggregates and geopolymer mortars (Feng et al. 2004).

Geopolymer proportioning

Geopolymer proportioning is very complex due to various parameters need to be considered.

Activator concentration (Concentration)

The alkaline activator concentration (i.e., solute mass concentration) is the most critical factor for successful geopolymer formation and the evolution of high compressive strength. An increase in concentration increases the reaction rate and degree leading to a less porous and stronger

geopolymer for the fly ash-based systems (Chareerat et al. 2006). Consequently, a higher alkaline concentration increases setting time and delays polymer formations since excessive ion presence limits polymer mobility and potential to interact with available reactive species. Furthermore, the increase in alkaline concentration in the paste mix increases the degree of hydration reactions (Pacheco et al. 2007) and reduces pore volumes improving microstructural properties of the C-S-H product. Thus, concentration must be addressed clearly in a geopolymer mix design.

SiO_2 / Na_2O mole ratio (Module)

Module is a highly significant parameter in geopolymer design. It is well known that variations in Module significantly modify the degree of polymerization of the dissolved species in the reacting solution, thus determining the mechanics and overall properties of the synthesized gel product (Rangan 2008). Higher percentages of soluble silic in geopolymer systems retard dissolution of fly ash due to increased saturation of the ionic silica species and promote the precipitation of larger molecular species, resulting in a stronger gel with an enhanced density (Zuda et al. 2006). The presence of soluble silica directly influences the reaction kinetics and the rate of crystallization as well as promoting gel formation, which is beneficial for strength development. A module range of 1.0-2.0 was recommended by Fernandez (Fernandez et al. 2005). Drying shrinkage is a direct result of hydration heat and increases with increased module and dosage of waterglass activators (Fernandez et al. 2007).

Activator to fly ash mass ratio (L/F)

The ratio of a selected activator-to-pozzolanic-material (fly ash) appeared to be the most critical parameter regarding general strength and fire resistance of the geopolymer paste (Fernandez et al. 1999). The L/F is recommended to be maintained in the range of 0.30 to 0.45

(Skvara et al. 2006). High compressive strengths were obtained up to 70 MPa when L/F was lower than 0.43 (Krizan et al. 2002).

Curing temperature and time

As with traditional PC, geopolymer responds better to heated curing methods. Previous work has demonstrated that curing time and temperature greatly affect the mechanical development of geopolymer binders. However, a temperature threshold exists, beyond which the strength gain rate is extremely slow (Rangan 2008). Temperatures in the range of 50-80°C are widely accepted values used for successful geopolymer hydration. Both curing temperature and curing time directly influence final compressive strength values of geopolymer specimens. Elevated temperature curing methodologies were evaluated on the use of steam- or dry-heat, the test data shows that dry-curing yields a compressive strength increase of 15% over the steam-curing methods (Skvara et al. 2006). Geopolymer sets rapidly and attains a significant percentage of its total compressive strength within the first few hours of reaction (Khale et al. 2007). However, the strength increase for specimens cured beyond 48 hours was not significant. Testing has shown that compressive strength values of 60 MPa can be achieved after only five hours at 85ºC (Khale et al. 2007). Longer curing times will increase the strength of geopolymer, but the strength is developing at a much slower rate as time progresses due to alkaline saturation and product densification (Skvara et al. 2006).

Characterization of Geopolymer Properites

Fresh properties of geopolymer mixture

The fresh properties of geopolymer mixtures, (e.g., setting time, flowability and calorimetry) are very significant for the practical application of binder materials (Zivica et al., 2014). While

these fresh properties of PC pastes have been investigated in depth, they have not yet been explored for geopolymer pastes. Consequently, research to understand the fresh properties of geopolymer pastes in relation to the effect of the activator nature is needed. The significant properties of fresh geopolymer mixtures are: setting time, flowability and calorimetry, depending strongly also on the quantity of activator added. This quantity significantly influences the workability of the mixtures, their setting time and calorimetry, but even the mechanical properties of the hardened mixture (Gourley, 2003; Nicholson et al., 2005; Banfill, 2006). The setting time represents a very important property of the fresh geopolymer mixtures influencing the time interval needed for the possibility of their placing *in situ*. Alkaline activator types, concentration of activators, ratio of liquid-to-solid and curing temperatures are all relevant in the characterization of geopolymer pastes calorimetry and directly influence the degree of reaction observed in a mixed geopolymer paste and either enhance or detract from the polymerization process (Williams et al. 2002).

Setting time

In ASTM WK27337, a pocket penetrometer is used to measure the setting time of a paste mixture. The initial and final setting times are respectively determined as the times required for paste to reach 24 kPa and 430 kPa of resistance to penetration of the pocket penetrometer. Rupnow evaluated this method for setting time on cement and fly ash paste and concluded that it is a convenient approach (Rupnow 2013).

Flowability

The flowability of paste can be measured using the mini slump cone in accordance with modified ASTM C1611, which is used to describe the rheology behavior of paste. Especially in field conditions, the availability and practicability of using a rheometer is limited. In such cases a mini slump cone has been proposed by several authors and several empirical relationships (Collins

and Sanjayan 1998, Roussel 2006). In their studies, it is shown that the workability of the paste is directly related to the spread it attains. Some researchers even proposed a relationship between the yield stress and spread diameter for concrete (Roussel and Coussot 2005):

$$\tau = \frac{7200\rho g v^2}{128\pi^2 D^5} \quad (1)$$

Where v is the volume of paste, τ is the yield stress, ρ is density of paste, g is the gravity and D the spread diameter. The units should be consistent in international unit.

Calorimetry measurement

Calorimetry measures heat changes during a chemical reaction such as cement hydration. It can be used to assess hydration-related properties, such as setting time, stiffening, and maturity according to the recorded temperature-time curve. It can also be used to evaluate the hydration kinetics and the geopolymerization process of geopolymer (Yao et al. 2009). It can be performed under isothermal conditions on paste in accordance with ASTM C1679. Fig. 3 illustrates the typical calorimetric curves of geopolymer and pozzolanic reaction (Yao et al. 2009).

Hardened properties of geopolymer mixture

Mechanical properties

For geopolymer as a novel cementitious material, its mechanical properties including compressive strength, tensile strength, flexural strength and bond strength are very important to apply in concrete. Its better mechanical properties over PC have been perceived as advantages in previous studies (Palacios et al. 2008 and Chindaprasirt et al. 2007). It has been shown that compressive strength, flexural strength, and tensile strength of geopolymers increase as NaOH solution concentration increases (Zivica et al. 2014).

The compressive strength of geopolymer paste havs been investigated following ASTM C109 by many researchers (Hardjito et al. 2008, Karakoca et al 2014). A tensile strength test is commonly used to determine strain-hardening behavior of fiber reinforced engineered geopolymer composite (EGC) (Nematollahi et al. 2015). A flexural bending test was carried out to evaluate mechanical properties for fabric reinforced geopolymer composite (Alomayri et al. 2014). The bond strength between geopolymer and embedded steel, which was essential for geopolymer as a binder in concrete, was measured using pullout test (Sarker 2011). Fig. 4 indicates that the bond strength of geopolymer concrete is higher than that of PC concrete.

Shrinkage behavior

In alkali activated systems, it is thought that there is an increase in drying shrinkage as compared to that of Portland cement (PC) due to the pore sizes are comparatively smaller and that leads to higher capillary tension as shown in Fig. 5 (Collins and Sanjayan 2000). Fig. 6 shows the drying shrinkage measurements taken for various SiO_2/Na_2O ratios. All samples were observed to shrink rapidly during the early stages and plateau was attained at around 50 days. The samples with SiO_2/Na_2O ratios of 1.0, 1.5 and 2.0 are reported to display almost the same trend at later ages and the sample with a ratio of 1.0 displayed the most drying shrinkage (Zheng 2009).

If paste is restrained against drying shrinkage, tensile stress develops and can cause cracks. Such shrinkage cracks are widely evident in bridge decks, industrial and parking garage floors and highway pavement slabs, that have large thickness and exposed areas (Filho et al. 2005). The restrained ring shrinkage test has been used widely to measure such restrained shrinkage, cracking time, crack width and shrinkage cracking potential of concrete according to ASTM C1581 (Wang 2011, Yuan et al. 2011). Many advantages of ring tests include high and nearly constant restraint, its applicability to both mortar and concrete samples, and lower effects of geometry and boundary

conditions due to symmetry (Tang et al. 1996). The theory of restrained ring testing has been addressed (Hossain and Weiss 2006). The apparatus of restrained ring specimens is shown in Fig. 7. Rare literature reports use the restrained ring test to investigate the free shrinkage of geopolymer paste (Wang et al. 2012).

Predictive models on geopolymer

Mix design of geopolymer is very complicated because it involves many parameters. On the other hand, artificial neural networks (ANN) have been successfully utilized to develop predictive models of setting time, compressive strength and slump for PC concrete (e.g., Dias 2001, Suryadi et al. 2011, Diab et al. 2014). Table 1 presents the comparison between ANN predicted values and experimental values on compressive strength of geopolymer (Yadollahi et al. 2017). It can be seen that ANN-established model predicted the compressive strength of geopolymer well.

Geopolymer Application

Engineered geopolymer composite

Fibers are broadly used to modify the brittle behavior of plain cementitious materials (Li and Wu 1992). Engineered cementitious composites (ECC) are a special class of high performance, fiber-reinforced cementitious composites that utilize a small amount of fibers (typically 2% by volume) and exhibit very high tensile strain capacity of up to 6% (Li and Kanda 1998).

Recently, feasibility studies have been undertaken to develop geopolymer-based ECCs with complete replacement of the PC binder with fly-ash-based geopolymer binders. These engineered geopolymer composites (EGCs) demonstrated strain-hardening behavior in tension (Lee et al. 2012). The developed fly-ash-based EGC exhibited very high tensile strain capacity (up to 4.3% on average), but low to moderate compressive and tensile strengths (17.4-27.6 MPa and 2.9-3.4

MPa, respectively), which may limit its widespread application in the construction industry due to low ability to withstand load without failure or plastic deformation (Ohno and Li 2014).

General applications

One motivator for adopting geopolymer binder is its ability to resist sulfate and other chemical intrusions and maintain excellent thermal loading capacities. The tests reported by Sumajouw et al. (2004) revealed that geopolymer concretes possess high compressive strength, undergo very little drying shrinkage and exhibit moderately low creep. Their data also indicate that geopolymer concretes possess excellent resistance to sulfate attack, resulting in a promising construction material for some harsh environments (Sumajouw et al. 2004).

Generally, the properties of geopolymers significantly depends upon the silica/alumina ratio, thus the applications of geopolymer are also related to this ratio. It is evident that the applications of geopolymer are broad associated with Si/Al ratio as shown in Table 2 (Jaarsveld et al. 2003).

Table 1. Comparison between predicted and experimental compressive strength (Yadollahi et al. 2017)

No	Experimental results	Predicted with ANN
1	13.2	15.47
2	6.14	7.07
3	9.45	9.44
4	7.9	7.63
5	29.08	32.15
6	13.6	14.91
7	23.12	21.04
8	28.07	27.72
9	38.59	36.75
10	8.68	8.37
11	18.78	18.62
12	9.55	9.25
13	16.4	12.44
14	26.11	23.37
15	15.2	12.46

Table 2. Applications of geopolymer associated with the inherent Si/Al ratio (Jaarsveld et al. 2003)

Si:Al Ratio	Applications
1	• Bricks • Ceramics • Fire Protection
2	• Low CO_2 Cements and Concretes • Radioactive and Toxic Waste Encapsulation
3	• Fire Protection Fiberglass Composites • Foundry Equipment • Heat Resistant Composites, 200°C to 1000°C • Tooling for Aeronautics Titanium Process
>3	• Sealants for Industry, 200°C to 600°C • Tooling for Aeronautics SPF Aluminum
20-35	• Fire Resistant and Heat Resistant Fiber Composites

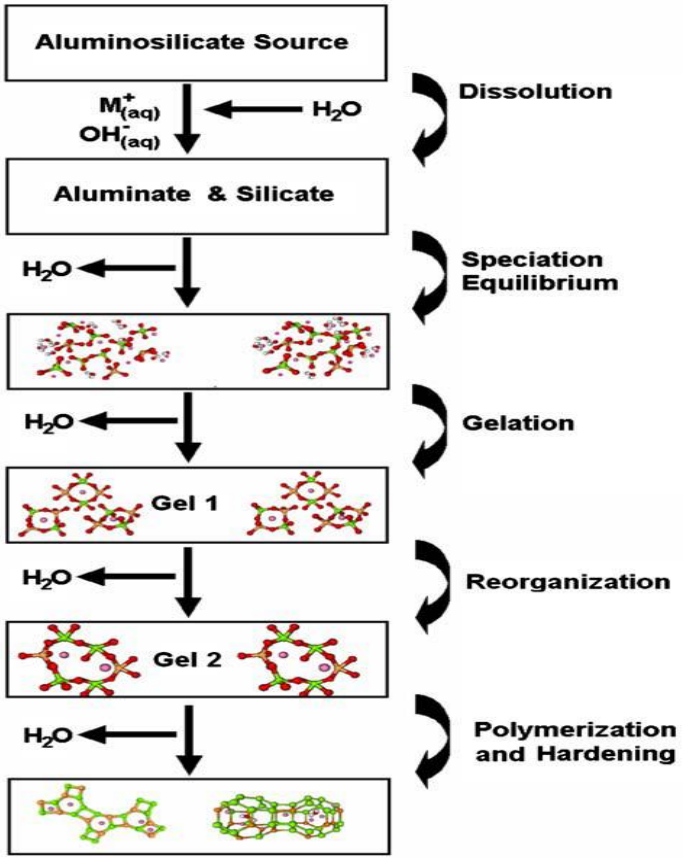

Figure 1. Geopolymer development model (Rangan 2008)?

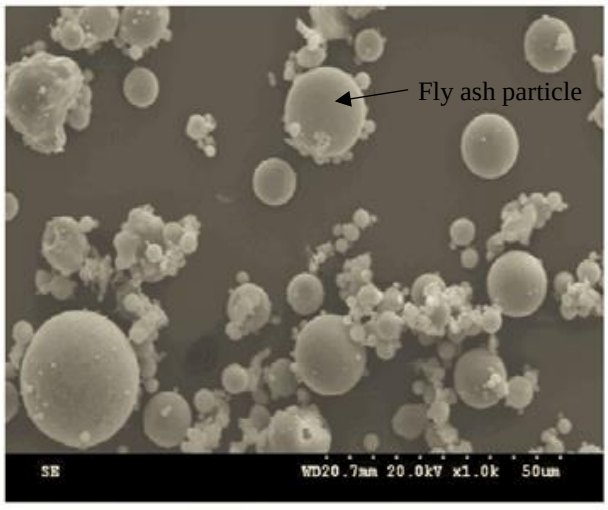

Figure 2. Microscopic image of raw fly ash (Krizan et al. 2002)

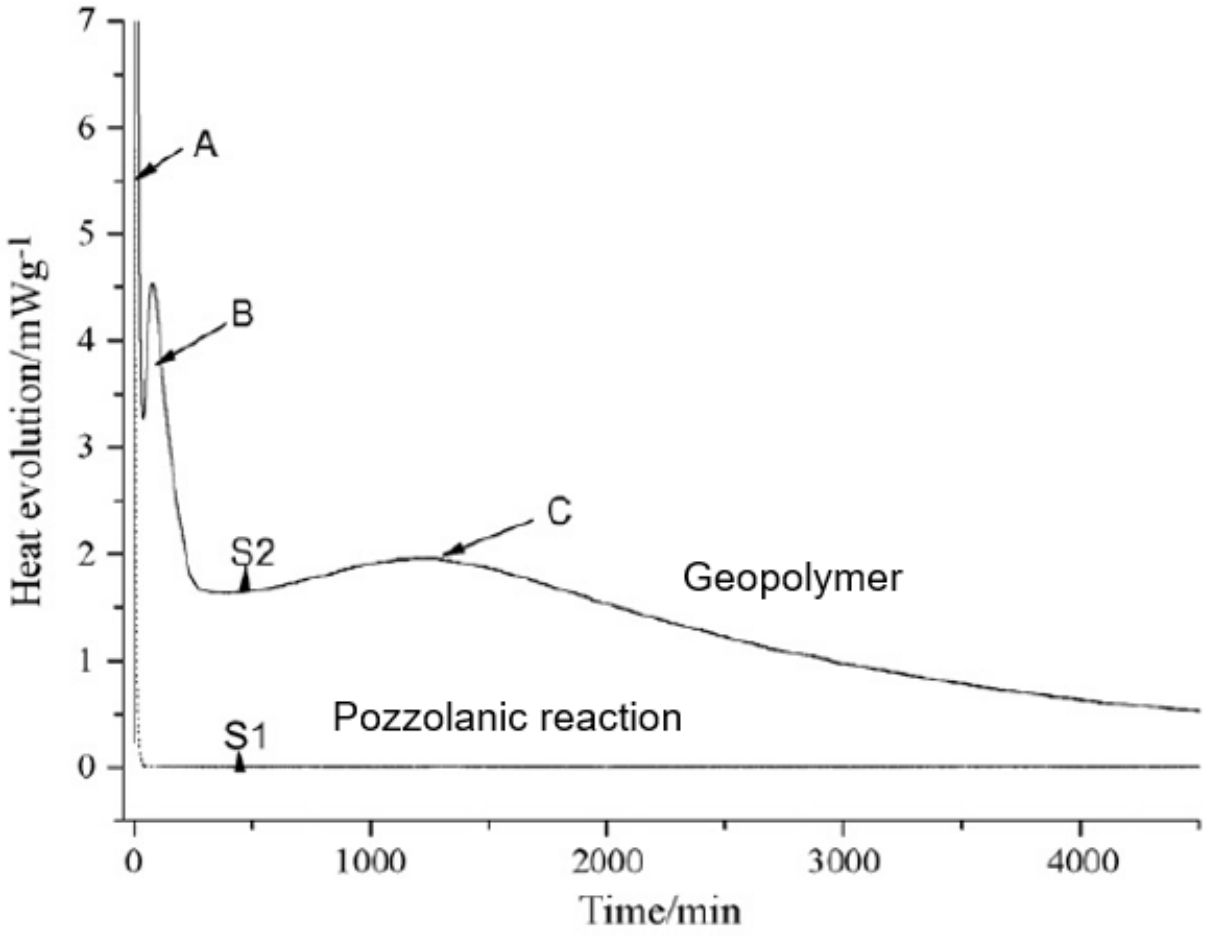

Figure 3. Typical calorimetric curves of geopolymer and pozzolanic reaction (Yao et al. 2009)

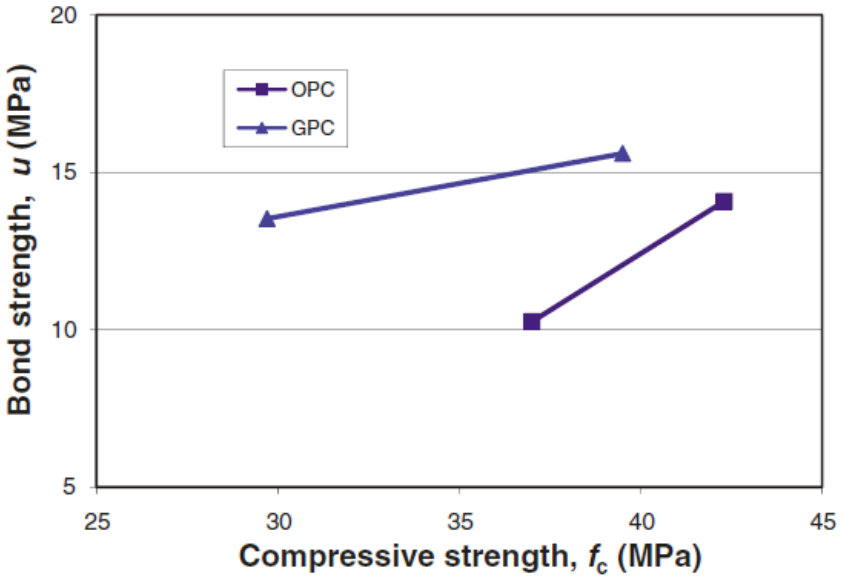

Figure 4. Bond strength versus compressive strength (Sarker 2011)

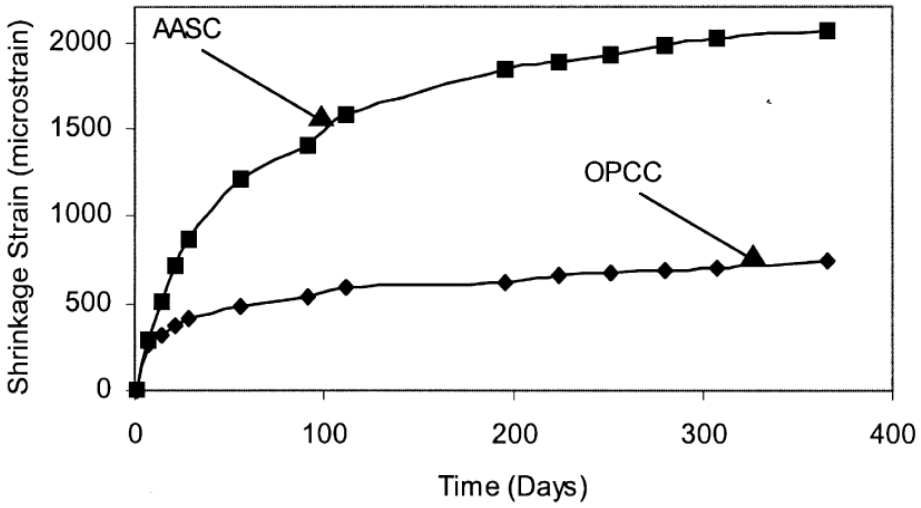

Figure 5. Drying shrinkage of concrete made with Portland cement (OPCC) and geopolymer (AASC) (Collins and Sanjayan 2000)

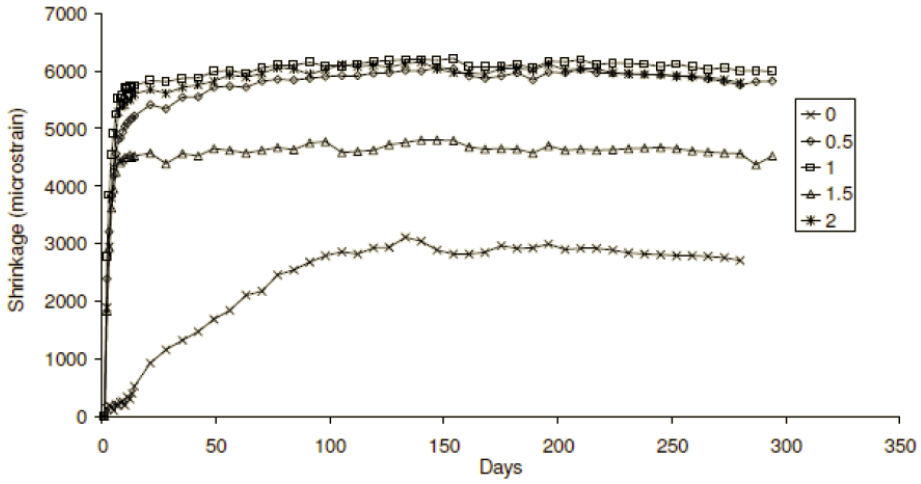

Figure 6. Drying shrinkage of geopolymers with varying Module (Zheng 2009)

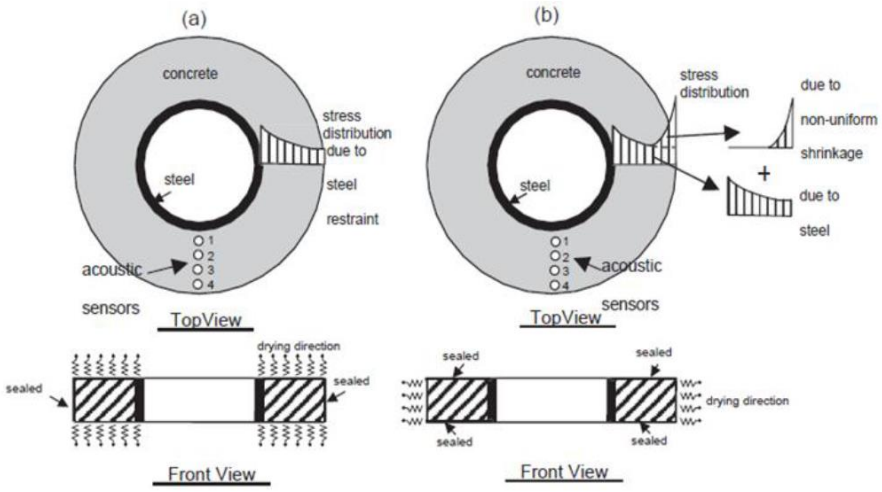

Figure 7. Restrained ring specimen apparatus (Hossain and Weiss 2006)

CHAPTER 3. OPTIMIZATION OF MIX DESIGN PARAMETERS ON THERMAL, SETTING AND STIFFENING BEHAVIORS OF HIGH-CALCIUM FLY ASH GEOPOLYMER

Yifeng Ling, Kejin Wang, Xuhao Wang, Sudong Hua, Scott M. Schlorholtz

Department of Civil, Construction and Environmental Engineering, Iowa State University, Ames IA 50010

Abstract

In this study, the effects of critical design parameters, such as SiO_2/Na_2O molar ratio (Module), concentration of solute in alkaline solution (Concentration), liquid-to-fly-ash mass ratio (L/F), temperature and elapsed time of curing on setting time, compressive strength, and heat of hydration behaviors of high-calcium fly ash geopolymer mixtures were investigated. Results indicated that increasing Module accelerated setting time, but reduced strength, total heat generation, reaction time and geopolymerization peak time. As Concentration increased, setting time for mixtures of 1.0 and 1.5 Modules became longer, but shorter for mixtures with 2.0 Module. Make this its own sentence: while compressive strength, total heat, terminated time and peak time increased. Modules less than 1.5, Concentrations between 40% and 50%, L/F ratios less than 0.40, and higher curing temperature (such as 50°C) were preferred to synthesize a geopolymer system using high-calcium fly ash in order to obtain excellent strength and workable setting time.

Key words: Geopolymer, Fly ash, Early age performance, Optimization of mix design parameters

Introduction

The increasing environmental threats caused by CO_2 produced during manufacture of Portland cement have promoted the development of geopolymer binders that were activated from alumina-silicate source materials (e.g., fly ash, slag and metakaoline) by alkaline solutions (Sumajouw et al 2004, Davidovits 1994). On the other hand, the rising demands to reduce the cost of binder in concrete desiderate an alternative source of Portland cement. Geopolymer binders, in this case, can be a best fit.

Coal combustion waste fly ash has been studied and known as a readily available alumina-silicate material to meet the demands due to its rich in Si and Al. It is in nature of sphere shape with a larger surface area and smaller specific gravity than Portland cement. The classification of fly ash in accordance with chemical and physical properties can be found in ASTM C618. Geopolymerization is the condensation of aluminum and silicon precursor species that are dissolved in alkaline solutions to attain polymers in three-dimensional Si-O-Al network. The fly-ash-based geopolymer concrete generally yields higher strength compared to a similar proportioned Portland cement concrete, especially with a longer curing time (Babaee and Castel 2016).

Research in recent years has applied alkali silicate solutions to activate fly ash to form geopolymer (Kong and Sanjayan 2010). It has been shown that silicate activation increases the dissolution of fly ash and gives rise to mechanical properties (Rees et al. 2004). A solution of sodium silicate (Na_2SiO_3) and sodium hydroxide (NaOH) is the most commonly recommended alkaline activator (e.g., Hardjito et al. 2004, Wongpa et al. 2010). The ratio of SiO_2/Na_2O mole module (i.e., Module) and the concentration of activator (i.e., Concentration) are critical parameters in designing activators. It has been recommended that Module from 1.0 to 2.0 be

employed with commercial fly ash (Fernandez et al 2005). 30%-50% Concentration were usually selected to synthesize geopolymer (References). While it is generally accepted that a higher Concentration will result in higher strength capabilities, there seems to be an optimum limit for each activator type, such that crossing this limit results in the reverse affect (Khale and Chaudhary 2007). The alkaline liquid-to-fly ash ratio (by mass) is recommended to be maintained in the range of 0.30 to 0.45 (Skvara et al. 2006). The biggest challenge of fly ash geopolymer is the retardation of strength development and many researchers have focused on adjusting design parameters and curing conditions to improve strength development (e.g., Kovalchuk et al. 2007, Sathonsaowaphak et al. 2009, Jo et al. 2015, Chareerat et al. 2006, Song 2007, Krizan and Zivanovic 2002). For example, because of the slow reactivity of fly ash at ambient curing temperature, elevating temperature is a way to increase the kinetics energy and degree of the reaction, thus increasing the density of the pore structure and improving the mechanical properties of geopolymer (Kovalchuk et al. 2007). Calorimetric characterization provides real-time heat generation during the whole process of geopolymerization that cannot be achieved by other intermittently recording methods in studying the rate and the extent of geopolymerization (Khale and Chaudhary 2007, Provis et al. 2005, Provis et al. 2005). A relatively small number of investigations on isothermal measurements for alkali–fly ash reaction systems have already been performed (Vijayakumar 2013). Those investigations showed that calorimetric analysis is a powerful method to characterize the geopolymerization process. However, little research has been focused on assessing the setting and thermal behaviors of fly ash geopolymer to extrapolate strength development of alkali-activated high-calcium fly ash geopolymer binders. The research in this chapter is sought to provide a comprehensive study on critical mix design parameters, such as Module, Concentration, L/F and curing condition, to seek an optimal strength development strategy of geopolymer binders.

Materials and Test Methods

Materials

An ASTM C618 Class C fly ash from Ash Grove with a specific gravity of 2.52 and fineness of 419.6 m^2/kg was used as a polymerizing material in this research. Where was the fly ash obtained from? Table 1 summarizes the chemical composition of the fly ash obtained from X-ray fluorescence (XRF) test. The activator was a combination of NaOH and Na_2SiO_3 where solid NaOH was added to an aqueous solution of Na_2SiO_3 (known as waterglass or liquid glass). Specifications for these reagents are listed in Table 2.

Mix design

Mix parameters were SiO_2/Na_2O mole ratio (Module) of 1.0, 1.5 and 2.0, solute (NaOH + Na_2SiO_3) mass percent in alkaline solution (Concentration) of 30%, 40% and 50% and liquid to fly ash mass ratio (L/F) of 0.33, 0.40, 0.50 and 0.60 as presented in Table 3. Based on the specification of sodium silicate solution, the initial SiO_2/Na_2O Module is 2.58. Adding NaOH solid to adjust this ratio was the approach to obtain the designed Modules. Deionized water dilution was also applied for the Concentration acquirement. Deionized water was also used as a reference activator source. Therefore, the design matrix contains nine alkali solutions with varying Modules, Concentrations and deionized water as well as 10 types of activator. They were prepared to mix with a single source fly ash with L/F of 0.33, 0.40, 0.50 and 0.60 for setting behavior and strength development investigations.

It is noted that all samples are marked as A-B-C-D in the following section for simplicity. (A: Module, B: Concentration in %, C: L/F, D: temperature). If solution is water, A and B equal to 0

and 0%, respectively. For instance, 1.0-40%-0.4-50 represents the geopolymer sample activated by the alkali solution of 1.0 Module, 40% Concentration with 0.4 L/F curing at 50°C.

Test methods

Mixing

Fly ash was mixed with the ten activators following designated L/F. The mix procedure was in accordance with ASTM C305 and used a Hobart mixer similar to a hydrated cement paste mixture. The fresh mixtures were used to further investigate setting behavior and strength development.

Setting time

Rupnow evaluated three common test methods for setting time on cement and fly ash paste, including Vicat needle, Gillmore needle and pocket penetrometer (Rupnow 2013). The pocket penetrometer was selected to measure setting time in this study due to its simplicity and comparable results to other techniques as present in Fig. 1. In this test, penetration resistance was measured to evaluate the setting and hardening behavior of a geopolymer mixture. The effects of Module, Concentration and L/F on setting time were determined in accordance with ASTM WK27337. A pan of fresh paste was cast to perform setting time measurement at 23℃. Time interval of penetration was controlled at five minutes. At each time point, the pocket penetrometer was pressed into paste until the tick mark reached the paste surface and the scale from the bottom of ring was recorded as penetration resistance. The reading was done within 15 seconds sooner or later than the time point. The setting time test stopped only if the penetrometer reading was greater than 4.5 tons per square foot. The initial and final setting times were respectively determined as the times required for paste to reach 24 kPa and 430 kPa of resistance to penetration of the pocket penetrometer.

Compressive strength

After mixing, 50.8 mm cubes were cast in brass molds. The specimens were compacted with two-layer placing and tamping as described in the ASTM C109. The specimens and molds were then wrapped with vinyl sheeting to prevent moisture loss. Sixteen cubes were cast for each mix where two cubes were cured in a sealed bag stored in a preset oven at a specific curing temperature, i.e., 23℃ and 50℃ and tested at different ages (i.e., 1 day, 3 days, 7 days and 28 days, respectively). The compressive strength tests were performed in accordance with ASTM C109.

Isothermal calorimetry

The isothermal calorimetry device consists of a temperature control chamber and a calorimeter containing eight separate channels that each hold a sample during the test (Fig. 2). A detailed description of the isothermal calorimetry apparatus can be found elsewhere (e.g., Wang et al. 2007). The main route for heat exchange between the sample and the surroundings is through the heat flow detector. The heat flow, caused by the temperature difference across the sensor, creates a voltage signal proportional to the heat flow. This voltage signal is corrected by the reference and converted to the rate of heat evolution by applying the calibration factor. In this research, the effects of Module, Concentration, L/F and temperature on dynamic process of geopolymerization were evaluated by isothermal calorimetry. The heat generation process of the geopolymer activated by the the activators (see Table 3) was tested at both 23℃ and 50℃ by using the isothermal calorimeter. In order to maintain the whole reaction proceeding under constant temperature, the materials (fly ash and activator) were weighed in cups with different L/F and conditioned to the internal temperature of equipment at 23℃ or 50℃ prior to mixing. To minimize the heat loss during mixing, fly ash and activator were manually mixed until uniform paste formed (approximately two minutes). Then the cups were tightly capped and placed in the calorimeter

cells. The test was finished when the measured voltage returned to its initial value that indicated the reaction was terminated. A summary flowchart for the experimental procedure is shown in Fig. 3.

Results and Discussion

Setting time

The pocket penetrometer setting time test was conducted under 23°C to evaluate consistency and unconfined compressive strength of geopolymer mixtures. Fig. 4 reveals the defined initial and final setting times in accordance with ASTM WK respectively. As shown in Fig. 4 (a), for 1.0 and 1.5 Module mixtures, the higher Concentration increases the initial setting time with increased L/F up to 0.60. This phenomenon is more apparent at 1.0 Module due to more NaOH content. A higher alkaline concentration increases initial setting time since excessive ion presence hinders their mobility and potential to interact with available reactive species (Khale and Chaudhary 2007). However, with respect to 2.0 Module mixtures, the initial setting time is decreasing with increased Concentration for all L/F ratios. it is most likely due to higher percentages of soluble silica in geopolymer systems retards dissolution of fly ash, while increased Concentration may help the dissolution of Si^{4+} and Al^{3+} ions from fly ash (Zuda et al. 2006, Rattanasak and Chindaprasirt 2009, Chindaprasirt et al. 2012), which improved the geopolymerization and thus shortened the initial setting time. The final setting time was exactly the same trend as initial setting time. The longest initial and final setting times 3900 and 4400 mins, respectively, can be observed in the mixture of 1.0-50%-0.6-23.

The geopolymer mixtures with 2.0 Module seems to set tremendous faster than 1.0 and 1.5 Module mixtures as shown in Figs. 4(a) and (b). The reduced setting times can be the result of

improved dissolution of the fly ash into alkaline liquid that is leading to improved polymerization and hardening of the gel phase (Temuujin et al. 2009). Atiş et al. (2009) and Topark et al. (2014) concluded similarly that setting times of liquid sodium silicate and sodium hydroxide activated paste reduced with increased silica Module and solute Concentration. In contrast, setting was controlled by the presence of calcium, and the high Concentration inhibits the dissolution of calcium to the system and thus setting was delayed (Chindaprasirt et al. 2012). The setting time of alkali-activated mixture is longer than the mixture without alkali solution. Moreover, as the L/F ratio increases, the setting times of geopolymer mixture are also increased. The similar trend can be observed for akali-activated slag paste (Yang et al. 2012).

Compressive strength

In order to take an overall evaluation of parameters on compressive strength for geopolymer mixtures, the results of compressive strength are presented in Figs. 5 to 7 including reference mixtures.

It can be observed that the geopolymer mixtures with 50% Concentration exhibit highest compressive strength at all testing ages. It reveals that, higher Concentration of alkali solution improves compressive strength of geopolymer mixtures at certain module, L/F, curing temperature and time because of sufficient OH^-. An increase of Concentration promotes the reaction rate and degree leading to a less porous and stronger geopolymer system. It may therefore result in an increased volume of smaller pores and lower total porosity for the fly ash-based systems, thus increasing strength of the geopolymer mixtures (Fernandez and Palomo 2005).

The L/F is also effective in changing the compressive strength of the geopolymer mixtures as shown in Figs. 5 to 7. For example, it can be observed in Fig. 5 that when the L/F increases from

0.33 to 0.60, a decreased compressive strength over 40 MPa can be derived with 1.0 Module, 40% Concentration, curing at 50℃ at 28 days. This effect seems to be similar to how hydraulic Portland cement paste with higher water-to-cementitious-materials ratio can yield a reduced compressive strength. In addition, the rates of strength development strength decreasing rates are higher when Concentrations are 40% or 50%, regardless of Module because excessive activator solution brings superfluous water or deficient alkali reaction to weaken bonding and reduce mechanical properties (Yang et al. 2012).

In general, higher curing temperature resulted in increased compressive strength for geopolymer mixtures as observed in Figs. 5 to 7 for various Modules. Higher curing temperature is more effective on strength gain at any age with the addition of activator. The strength gain can be ten times higher at 50℃ than that was cured at 23℃, e.g., the geopolymer mixture with 0.33 L/F, 30% activator Concentration, and at the curing age of 1 day. It is likely attributed to there was no sufficient time and temperature to remove the unconjugated water, and the geopolymer slurries were still gelatinous and moist for early age, while the initial geopolymerization reaction was easy to occurred at 50℃ curing condition with a larger reaction rate that developed strength quickly (Hanehara et al. 2001). Higher curing temperature increases the kinetics energy and degree of the reaction that produces the geopolymer with a stronger Al-Si-O network (Petermann et al. 2010). The only exception can be observed that there is no dramatic increase in strength at 50℃ compared to 23℃ curing temperature for geopolymer mixtures without adding activators, i.e., 0% activator serving for geopolymerization reaction, up to 7 days. However, the higher curing temperature can accelerate the pozzolanic reaction of fly ash system yielding an increased strength gain at 28 days. It can also be observed that longer curing time improved the polymerization process resulting in

higher compressive strength with the addition of activator at various Modules as shown in Figs. 5 to 7.

When considering Module effect on strength development, Figs. 5 to 7 should be compared. In general, a lower Module seems to achieve a higher compressive strength with the constant Concentration, curing temperature, L/F ratio and curing age. For example, a mixture of 1.0-50%-0.33-50 had the highest strength (about 76 MPa at 28 days) compared to 1.5-50%-0.33-50 and 2.0-50%-0.33-50 mixtures, which had strengths of 60 MPa and 50MPa respectively. It is well known that Module can significantly modify the degree of polymerization of the dissolved species in the alkaline/silicate solution, thus determining the mechanics and overall properties of the synthesized gel product (Rangan 2008). Higher compressive strength can be observed in geopolymer mixture of lower Module due to more OH^- taking part in geopolymerization, generating glassy phases. Higher percentages of soluble silica in geopolymer systems retard dissolution of the fly ash due to increased saturation of ionic silica species and promote the precipitation of larger molecular species, resulting in a stronger gel with an enhanced density (Zuda et al. 2006). The presence of soluble silica directly affects the reaction kinetics, the rate of crystallization, and promotes a Si-rich gel formation which is responsible for material strength development.

Heat generation

The heat generation of geopolymerization was evaluated by isothermal calorimetry test. The total heat generation, rate of heat generation, terminal time and geopolymerization peak heat and time were determined from the calorimetry curves. Fig. 8 shows the typical heat evolution of the hydraulic cement paste hydration process compared to that of a 2.0-40%-23C geopolymer mixture with different L/F ratios.

In Fig. 8(a), the cement hydration typically consists of rapid heat evolution period (stage 1), dormant period (stage 2), end of the dormant period (stage 3), slowing of heat generation (stage 4) and steady state (stage 5). Unlike cement paste hydration, as shown in Fig. 8(b), the fly ash geopolymer hydration has no apparent dormant period. The exothermic geopolymerization peak (second peak) occurred right after the first peak, which is associated with the dissolution of fly ash into alkali solution. The total heat generation for each L/F is the area within the curve and base line, determined by integration from time zero to terminated time of heat generation curve. The terminated time is when the heat generation goes back to initial base value, which indicates the duration of heat generation. The *geopolymerization peak time* is defined as the time to reach the peak heat of geopolymerization while the *geopolymerization peak heat* is the maximum heat value of geopolymerization peak indicating the geopolymerization degree. The overall heat generation characteristics of geopolymer mixtures with different parameters (Module, Concentration, L/F and temperature) were investigated by the total heat generation, terminated time, geopolymerization peak heat and geopolymerization peak time.

Fig. 9 exhibits the total heat generation derived from the heat generation curves of mixtures with varied Modules, Concentration and L/F ratios curing at 23 and 50°C. Without alkali activation (i.e., Module of 0), a slight increase on total heat generation with increased L/F ratio can be observed when curing at 23°C while higher curing temperature of 50°C results in a decreased total heat with increased L/F ratio. It may be attributed to the greater temperature decrease with the degree of fly ash hydration (Acquaye 2006). However, with the addition of activators, the higher curing temperature leads to an increase in heat generation of geopolymer mixtures. The 50°C external curing temperature provides the extra energy to promote the alkaline reactivity of fly ash.

Apparently, the total heat increases with the increased Concentration and L/F at either 23℃ or 50℃ external curing temperature during hydration. This is due to the increased alkali content improving the reaction extent. This trend is apparent at the Module of 1.0 and 1.5, but marginal at Module of 2.0 because the high silicate concentration hindered alkali dissolution by reducing its saturation, thus reducing the effect from concentration, L/F and temperature (Lee and Van Deventer 2004).

Fig. 10 shows the terminated time of heat generation at varied Module, Concentration and temperature. The range of times at which the geopolymerization process terminated varied from ~20-180 hours. At Module 0, the terminated times of heat generation are ~ 22and ~40 hours at 50 and 23℃ external curing temperatures, respectively. At the Modules of 1.0, 1.5 and 2.0, increased concentration can dramatically extend the termination time. The higher Concentration contains a higher amount of soluble silica in geopolymer system that retards dissolution of the fly ash material due to increased saturation of the ionic silica species, therefore elongates the geopolymerization process (Zuda et al. 2006). It may also delay polymer formation because the excessive ion presence limits mobility of ionic silica species and potential to interact with available reactive species (Khale and Chaudhary 2007). However, the higher Module yields a shortened geopolymerization process due to more soluble silicate promoteing the precipitation of larger molecular species (Zuda et al. 2006).

In general, higher temperature is a key thermodynamic and kinetic parameter for gel formation and promotes the geopolymerization process (Fernandez et al. 2006). OH^- acts as a catalyst for reactivity, and metal cations serve to form a structural element and balance the negative framework carried by the tetrahedral aluminum (Rangan 2008). Geopolymerization needs more time to proceed compared to typical pozzolanic reaction or hydraulic cement hydration due to higher

percentage of OH^- available in geopolymer matrix that elongates the reaction process (Petermann et al. 2010).

The magnitude and elapsed time of the geopolymerization peak on the calorimetry curve is an indicator for the degree of geopolymerization and strength development. The elapsed time to reach the geopolymerization peak (i.e., peak time) is presented with varied Modules, Concentrations, L/F and temperatures in Fig. 11. The peak time of fly ash-water mixtures increased somwhat with L/F increasing for both 23℃ and 50℃ curing while the peak time was slightly delayed for 50℃. However, for alkali-activated mixtures, the increased curing temperature accelerates the time to reach geopolymerization peak regardless Modules and Concentrations due to high temperature speeding up the geopolymerization reaction rate. It can be observed that increasing Concentration and L/F dramatically prolong peak time, especially at 23℃ curing temperature with 1.0 and 1.5 Modules. This is because the higher Concentration and L/F introduced a large amount of OH^- that restrained the rate of gel formation and geopolymerization. However, higher temperature significantly accelerated the geopolymerization process, therefore compensating for the longer time to reach the geopolymerization peak. This can be the reason why there is no significant prolonged effect on peak time with increased Concentration and L/F at 50℃ curing temperature.

At Module 2.0, the peak time is marginally affected by Concentration and L/F since the high concentration of dissolved silica could prompt geopolymerization thereby greatly reducing the effect from Concentration and L/F. It's also notable that with certain Concentration, L/F and temperature, the peak time decreased with an increase of Module. This is likely caused by the higher soluble silica Concentration in geopolymer mixtures promoting formation of a Si-rich gel as well as crystallization and precipitation of larger molecular species due to increased saturation of the ionic silica species.

Fig. 12 presents the peak heat of geopolymer derived from isothermal calorimetry curve for each geopolymer mixture. The highest peak heat for geopolymer mixtures is 5.5 mw from 2.0-50%-0.33-50 mixture while the lowest peak heat is 0.3 mw from 1.5-50%-0.6-23 mixture. Apparently, the geopolymerization peak heat decreases with increased L/F at given Modules, Concentrations and curing temperatures for both water-activated and alkali-activated mixtures. It can be attributed to the residue liquid is able to absorb some heat released from geopolymerization around peak point. It should be noted that only L/F plays a vital role on peak heat generation. The effects from Concentration and Module on peak heat generation of geopolymerization are marginal. Similar findings were drawn from Chareerat et al. (Chareerat et al. 2006). Again, higher curing temperature boosted peak heat for alkali-activated mixtures due to more intense geopolymerization.

Conclusions

The various and complex parameters are always a big concern in designing geopolymer mix proportions. This comprehensive research work studied a wide range of parameter combinations for high-calcium fly ash geopolymer that can guide optimized mix designs for further research and applications in concrete. For example, to prepare a geopolymer system using high-calcium fly ashto produce a geopolymer concrete with good compressive strength development, heat of hydration kinetics and setting behavior of geopolymer mixtures, one should select Modules less than 1.5, Concentrations between 40% and 50%, L/F ratios less than 0.40, and higher curing temperatures (such as 50°C). The effects of Module, Concentration, L/F, temperature and age time on setting time, compressive strength and heat of geopolymerization of fly-ash-based geopolymer mixtures are summarized as following:

1. Compared to water-activated mixtures, alkali-activated mixtures generally prolong the setting time, increase the compressive strength, lower total heat generation, raise the geopolymerization peak heat, shorten termination time and geopolymerization peak time in calorimetry.
2. Increasing the Module in geopolymer can accelerate setting time except for high Module (i.e., Module 2.0), but with negative effects on strength development, total heat generation, termination time of geopolymerization and geopolymerization peak time.
3. Increased Concentration of geopolymer resulted in prolonged setting time for 1.0 and 1.5 Module, but retarded setting time for 2.0 Module. In general, higher Concentration, up to 50% in this case, leads to increased compressive strength and total heat generation, while the geopolymerization termination time and peak time are prolonged.
4. When L/F was increased from 0.33 to 0.60, longer setting time and higher total heat generation were observed. Increasing L/F increases the time to reach peak point of geopolymerization dramatically (from X to Y). In addition, higher L/F can yield a lower strength and peak heat.
5. The elevated curing temperature of geopolymer improved strength development, increased total heat and peak heat generation and decreased terminated time and peak time.

Acknowledgements

The authors acknowledge help provided by Dapeng Jin from Materials Analysis and Research Laboratory of the Iowa State University Office of Biotechnology (MARL) and Jianzhong Liu from State Key Laboratory of High Performance Civil Engineering Materials in Nanjing.

References

Acquaye, L. (2006). "Effect of the High Curing Temperatures on the Strength, Durability and Potential of Delayed Ettringite Formation in Mass Concrete Structures," Doctoral Thesis, Graduate school of the University of Florida.

ASTM C109/C109M, (2013). "Standard Test Method for Compressive Strength of Hydraulic Cement Mortars," Philadelphia: ASTM International.

ASTM C305, (2014). "Standard Practice for Mechanical Mixing of Hydraulic Cement Pastes and Mortars of Plastic Consistency," Philadelphia: ASTM International.

ASTM C618, (2017). "Standard Specification for Coal Fly Ash and Raw or Calcined Natural Pozzolan for Use in Concrete," Philadelphia: ASTM International.

ASTM WK27337, (2010). "New Test Method for Pocket Penetrometer Test," ASTM International.

Atiş, C. D., Bilim, C., Çelik, O., Karahan, O. (2009). "Influence of Activator on the Strength and Drying Shrinkage of Alkali-Activated Slag Mortar," Construction and Building Materials, 23(1), pp. 548-555.

Babaee, M., Castel, A. (2016). "Chloride-induced Corrosion of Reinforcement in Low-calcium Fly Ash- based Geopolymer Concrete," Cement and Concrete Research 88, pp. 96–107.

Chareerat, T., Lee-Anansaksiri, A., Chindaprasirt, P. (2006). "Synthesis of High-calcium Fly Ash and Calcined Kaoline Geopolymer Mortar," International Conference on Pozzolan, Concrete and Geopolymer, Khhon Kaen, Thailand, May 24-25.

Chindaprasirt, P., De Silva, P., Sagoe-Crentsil, K., and Hanjitsuwan, S. (2012). "Effect of SiO_2 and Al_2O_3 on the Setting and Hardening of High-calcium Fly Ash- Based Geopolymer Systems," Journal of Materials Science 47(12), pp. 4876–4883.

Davidovits, J. (1994). "Properties of geopolymer cements," Alkaline cements and concretes, KIEV Ukraine.

Fernandez-Jimenez, A., Palomo, A. (2005). "Composition and Microstructure of Alkali Activated Fly Ash Binder: Effect of the Activator," Cement and Concrete Research 35(10), pp. 1984-1992.

Fernandez-Jimenez, A., Palomo, A., Criado, M. (2005). "Microstructure Development of Alkali-Activated Fly Ash Cement: A Descriptive Model," Cement and Concrete Research 35(6), pp. 1204-1209.

Fernandez-Jimenez, A., Palomo, A., Sobrados, I., Sanz, J. (2006). "The Role Played by the Reactive Alumina Content in the Alkaline Activation of Fly Ashes," Microporous and Mesoporous Materials 91(1-3), pp.111-119.

Hanehara, S., Tomosawa, F., Kobayakawa, M., Hwang, K. (2001). "Effects of Water/Powder Ratio, Mixing Ratio of Fly Ash, and Curing Temperature on Pozzolanic Reaction of Fly Ash in Cement Paste," Cement and Concrete Research 31(1), pp. 31-39.

Hardjito, D., Wallah, S.E., Sumajouw, D.M.J., Rangan, B.V. (2004). "On the Development of Fly Ash-based Geopolymer Concrete," ACI Materials Journal 101(6), pp. 467–472.

Jo, M., Soto, L., Arocho, M., John, J., and Hwang, S. (2015). "Optimum Mix Design of Fly Ash Geopolymer Paste and Its Use in Pervious Concrete for Removal of Fecal Coliforms and Phosphorus in Water," Construction and Building Materials 93, pp. 1097-1104.

Khale, D., Chaudhary, R. (2007). "Mechanism of Geopolymerization and Factors Influencing Its Development: A Review," Journal of Materials Science 42(3), pp.729-746.

Kong, D.L.Y., Sanjayan, J.G. (2010). "Effect of Elevated Temperatures on Geopolymer paste, Mortar and Concrete," Cement and Concrete Research 40(2), pp. 334-339.

Kovalchuk, G., Fernandez-Jimenez, A., Palomo, A. (2007). "Alkali- Activated Fly Ash: Effect of Thermal Curing Conditions on Mechanical and Microstructural Development - Part II," Fuel 86(3), pp. 315–322.

Krizan, D., Zivanovic, B., (2002). "Effects of Dosage and Modulus of Water Glass on Early Hydration of Alkali-Slag Cements," Cement and Concrete Research 32(8), pp. 1181-1188.

Lee, W.K.W., and Van Deventer, J.S.J. (2004). "The Interface between Natural Siliceous Aggregates and Geopolymers," Cement and Concrete Research 34(2), pp. 195-206.

Petermann, J.C., Saeed, A., and Hammons, M.I. (2010). "Alkali- Activated Geopolymers: A Literature Review," Air Force Research Laboratory Materials and Manufacturing Directorate.

Provis, J.L., Duxson, P., Van Deventer J.S.J., Lukey, G.C. (2005). "The Role of Mathematical Modelling and Gel Chemistry in Advancing Geopolymer Technology," Chemical Engineering Research and Design 83(7), pp. 853–860.

Provis, J.L., Lukey, G.C., Van Deventer, J.S.J. (2005). "Do Geopolymers Actually Contain Nanocrystalline Zeolites? A Reexamination of Existing Results," Chemistry of Materials 17(12), pp. 3075–3085.

Rangan, B.V. (2008). "Fly Ash-Based Geopolymer Concrete," Curtin University of Technology Research Report GC 4.

Rattanasak, U., and Chindaprasirt, P. (2009). "Influence of NaOH Solution on the Synthesis of Fly Ash Geopolymer," Minerals Engineering 22(12), pp. 1073–1078.

Rees, C., Lukey, G.C., Van Deventer, J.S.J. (2004). "The Role of Solid Silicates on the Formation of Geopolymers Derived from Coal Ash," In International Symposium of Research Student on Material Science and Engineering, Chennai: India, 1-13.

Rupnow, T.D. (2013). "Quality Control Tools to Identify Source Variability of Class C Fly Ash and Its Impact on Freshly Mixed Cement- Fly Ash Paste," World of Coal Ash (WOCA) conference, April 22-25, Lexington, KY.

Sathonsaowaphak, A., Chindaprasirt, P., and Pimraksa, K. (2009). "Workability and Strength of Lignite Bottom Ash Geopolymer Mortar," Journal of Hazardous Materials 168(1), pp. 44–50.

Skvara, F., Dolezal, J., Svoboda, P., Kopecky, L., Pawlasova, S., Lucuk, M., Dvoracek, K., Beksa, M., Myskova, L., Sulc, R. (2006). "Concrete Based on Fly Ash Geopolymers," project report CEZ: MSM 6046137302.

Song, X. (2007). "Development and Performance of Class F Fly-ash-based Geopolymer Concretes against Sulphuric Acid Attack," Doctoral Thesis, School of Civil and Environmental Engineering, University of New South Wales, Sydney, Australia.

Sumajouw, D.M.J., Hardjito, D., Wallah, S.E., and Rangan, B.V. (2004). "Geopolymer Concrete for a Sustainable Future," Green Processing Conference, Fremantle, WA. 10-12 May.

Temuujin, J., Williams, R.P., Riessen, A.V. (2009). "Effect of Mechanical Activation of Fly Ash on the Properties of Geopolymer Cured at Ambient Temperature," Journal of Materials Processing Technology 209(12-13), pp. 5276–5280.

Topark-Ngarm, P., Chindaprasirt, P., and Sata, V. (2014). "Setting Time, Strength, and Bond of High-Calcium Fly Ash Geopolymer Concrete," Journal of Materials in Civil Engineering 27(7): 04014198.

Vijayakumar, R. M. (2013). "Evaluating Shrinkage of Fly Ash- Slag Geopolymers," Master thesis, University of Illinois at Urbana-Champaign.

Wang, K., Ge, Z., Grove, J., Ruiz, J. M., and Rasmussen, R. (2006). "Developing a Simple and Rapid Test for Monitoring the Heat Evolution of Concrete Mixtures for Both Laboratory and Field Applications," project report, Center for Transportation Research and Education.

Wang, K., Ge, Z., Grove, J., Ruiz, J.M., Rasmussen, R., and Ferragut, T. (2007). "Developing a Simple and Rapid Test for Monitoring the Heat Evolution of Concrete Mixtures for Both Laboratory and Field Applications," project report, Center for Transportation Research and Education.

Wongpa, J., Kiattikomol, K., Jaturapitakkul, C., Chindaprasirt, P. (2010). "Compressive Strength, Modulus of Elasticity, and Water Permeability of Inorganic Polymer Concrete," Materials & Design 31(10), pp.4748–4754.

Yang, T. R., Chang, T.P., Chen, B.T., Lin, W.L. (2012). "Effect of Alkaline Solutions on Engineering Properties of Alkali-Activated GGBFS Paste," Journal of Marine Science and Technology 20(3), pp. 311-318.

Yang, T.R., Chang, T.P., Chen, C.T., Lee, Y.K., and Chen, B.T. (2012). "Effects of Activating Solution and Liquid/Solid Ratio on Engineering Properties of Metakaolin- Based Geopolymer," Applied Mechanics and Materials 204-208, pp. 4101-4104.

Zuda, L., Pavlik, Z., Rovnanikova, P., Bayer, P., Cerny, R. (2006), "Properties of Alkali Activated Aluminosilicate Material after Thermal Load," International Journal of Thermophysics 27(4), pp. 1250-1263.

Table 1: Chemical Composition of Fly ash

SiO_2	Al_2O_3	Fe_2O_3	SO_3	CaO	MgO	Na_2O	K_2O	P_2O_5	TiO_2	SrO	BaO	LOI
30.7	16	6.8	3.47	28.8	6.74	2.97	0.27	0.64	1.43	0.51	0.7	0.49

Note: All values in mass %, expressed on an oven-dry basis; LOI is loss on ignition at 1000°C

Table 2: Specification of Sodium silicate solution and sodium hydroxide

Product	Sodium silicate solution (Na_2SiO_3)	Sodium hydroxide (NaOH)
Company	Sigma-Aldrich	Fisher Scientific
Grade	Reagent	Certified ACS
Composition	Na_2O: 10.6%, SiO_2: 26.5%	NaOH Solid
Density	1.39 g/ml	2.13g/ml
Formula	$(NaOH)_x(Na_2SiO_3)_y \cdot zH_2O$	NaOH

Table 3. Design matrix of geopolymer mixtures

Module	Concentration (%)	Liquid/Fly ash (L/F)
0	0	0.33, 0.4, 0.5,0.6
1.0	30	0.33, 0.4, 0.5,0.6
1.0	40	0.33, 0.4, 0.5,0.6
1.0	50	0.33, 0.4, 0.5,0.6
1.5	30	0.33, 0.4, 0.5,0.6
1.5	40	0.33, 0.4, 0.5,0.6
1.5	50	0.33, 0.4, 0.5,0.6
2.0	30	0.33, 0.4, 0.5,0.6
2.0	40	0.33, 0.4, 0.5,0.6
2.0	50	0.33, 0.4, 0.5,0.6

Figure 1. Setting time apparatus: Pan (left) and penetrometer (right)

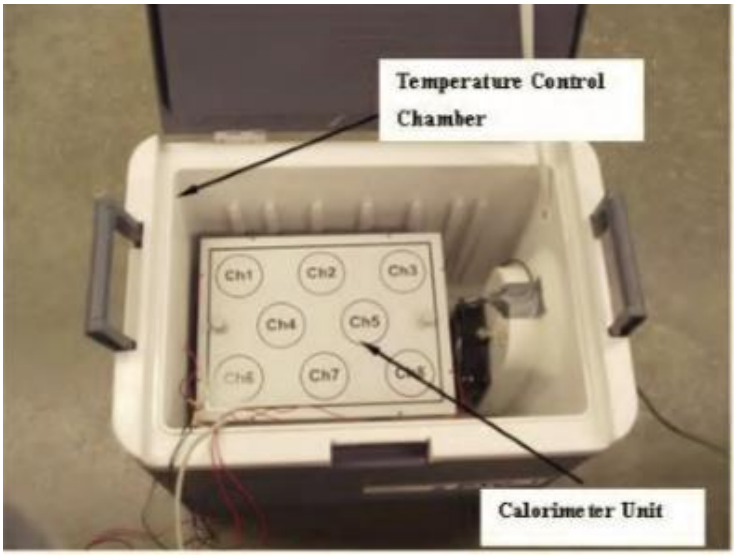

Figure 2. Calorimeter apparatus (Wang et al. 2007).

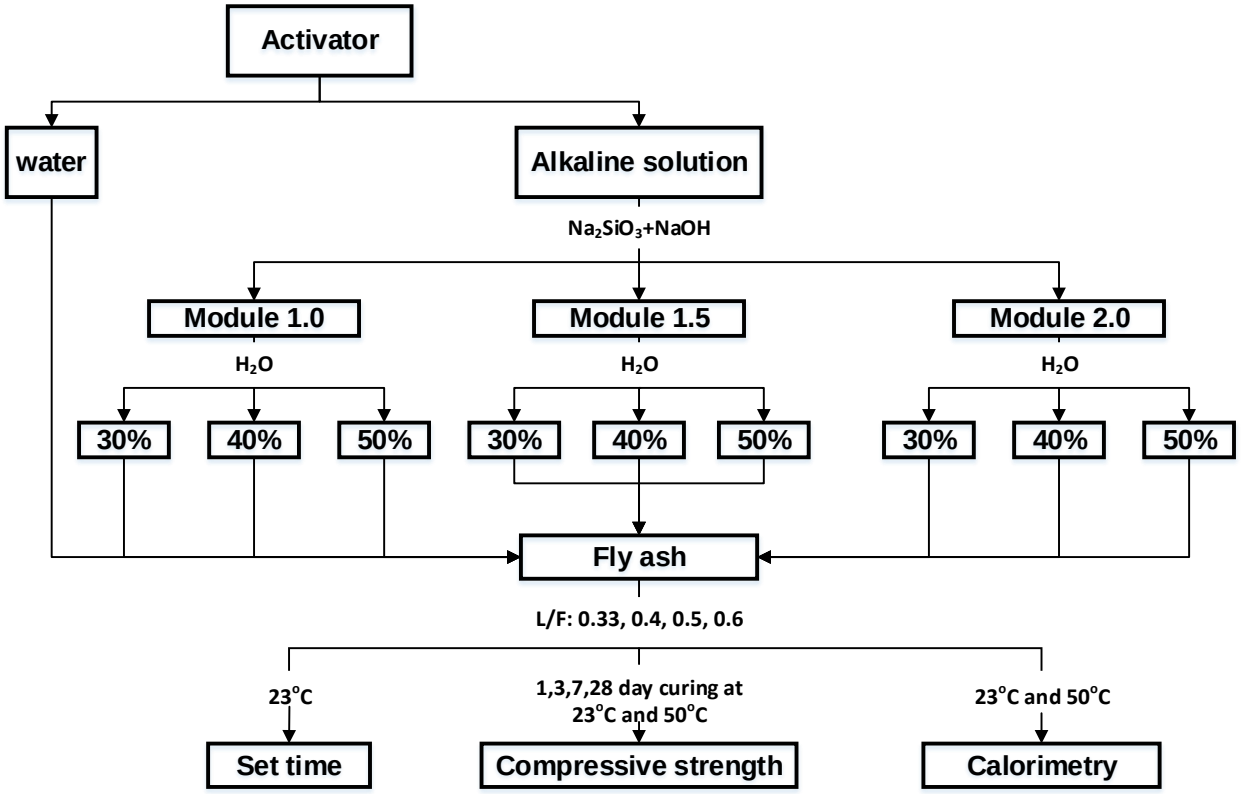

Figure 3. Flowchart of geopolymer mixture design and tests

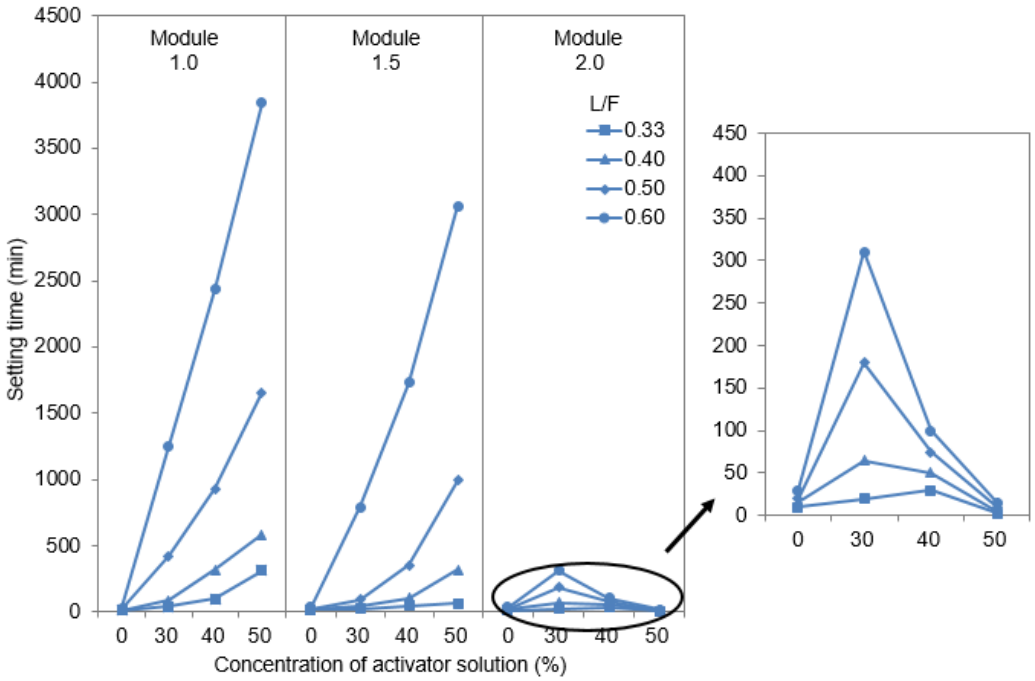

(a)

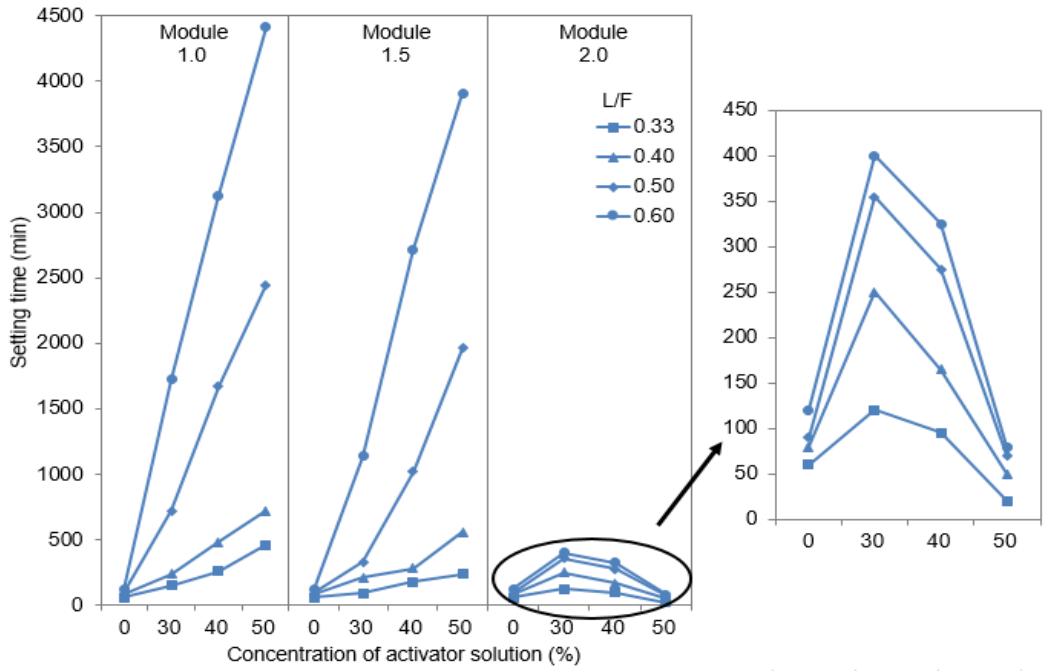

(b)

Figure 4. Setting time results for mixtures (a) initial setting time (b) final setting time

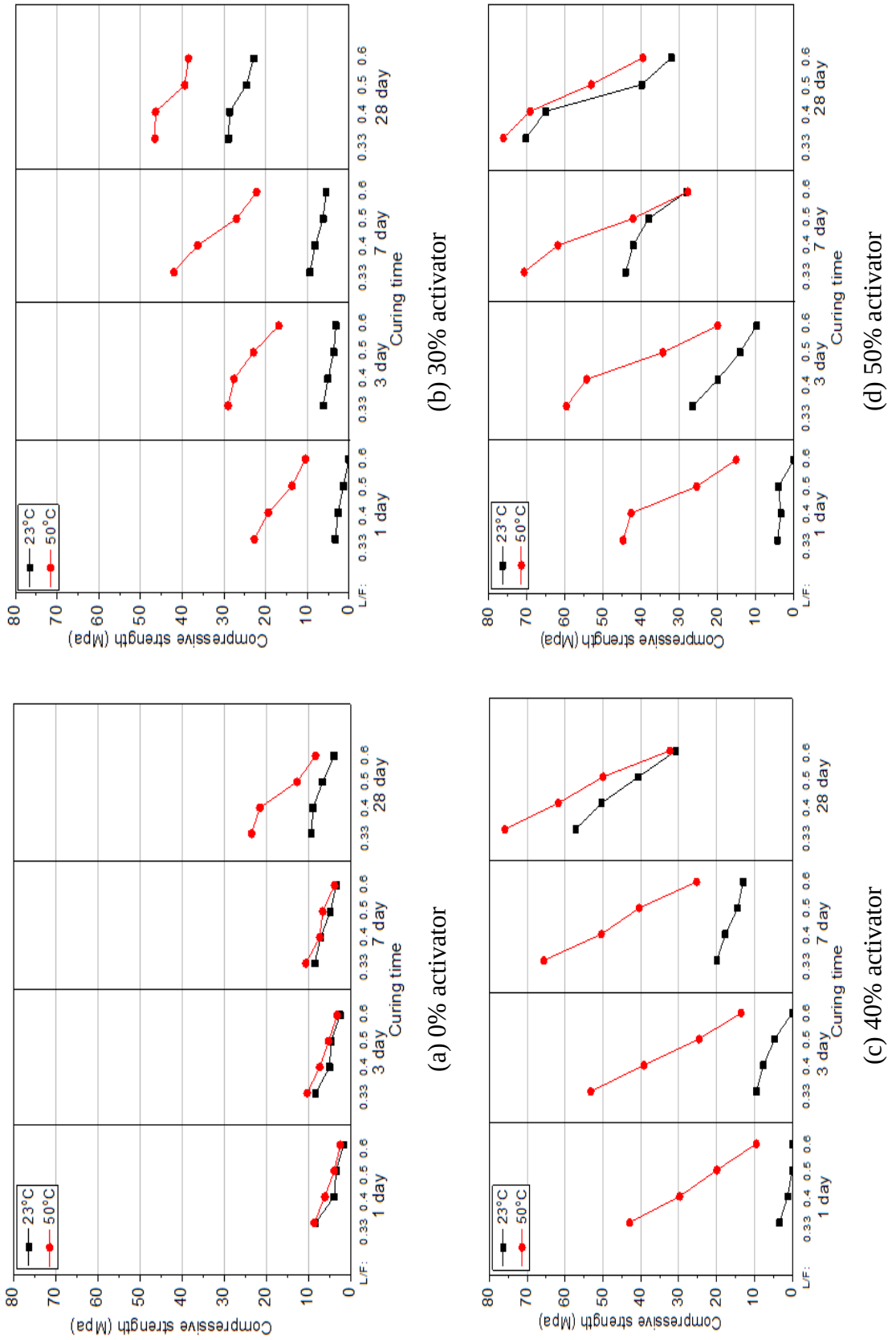

(a) 0% activator (b) 30% activator

(c) 40% activator (d) 50% activator

Figure 5. Compressive strength of mixes cured at different temperatures (Module = 1.0)

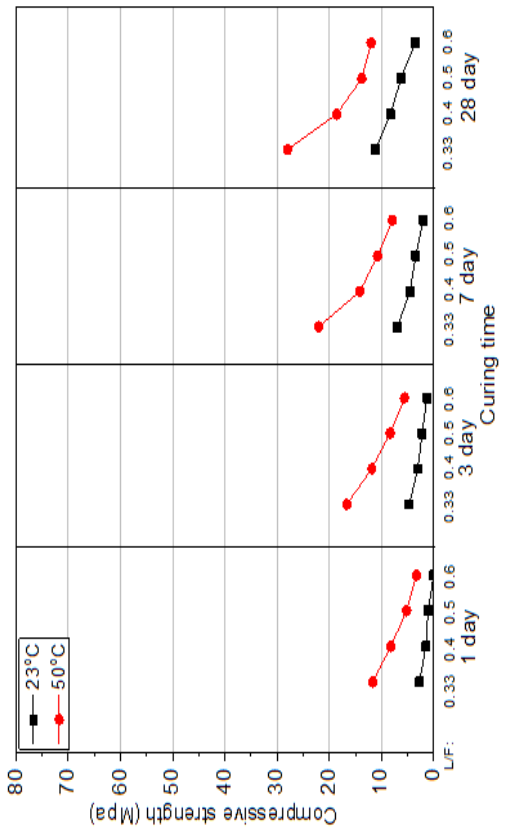

(a) 0% activator

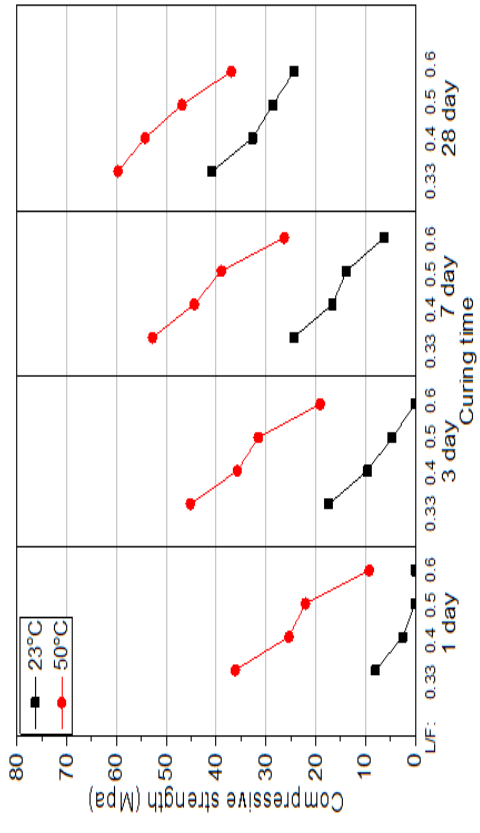

(b) 30% activator

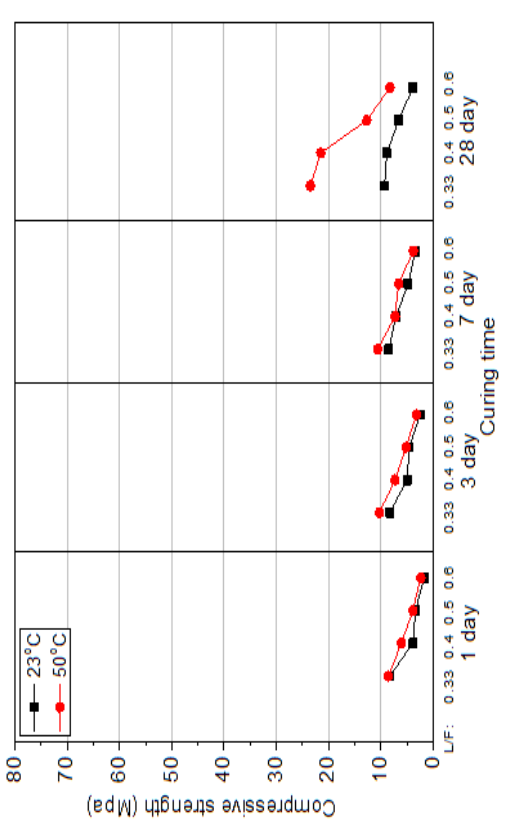

(c) 40% activator

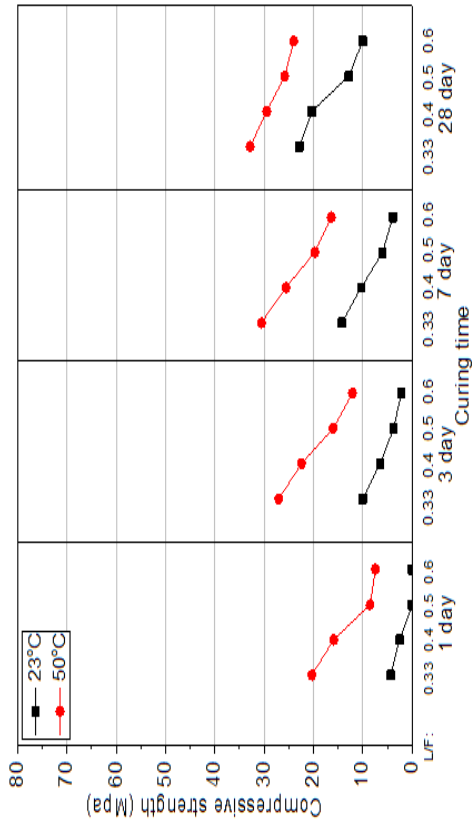

(d) 50% activator

Figure 6. Compressive strength of mixes cured at different temperatures (Module = 1.5)

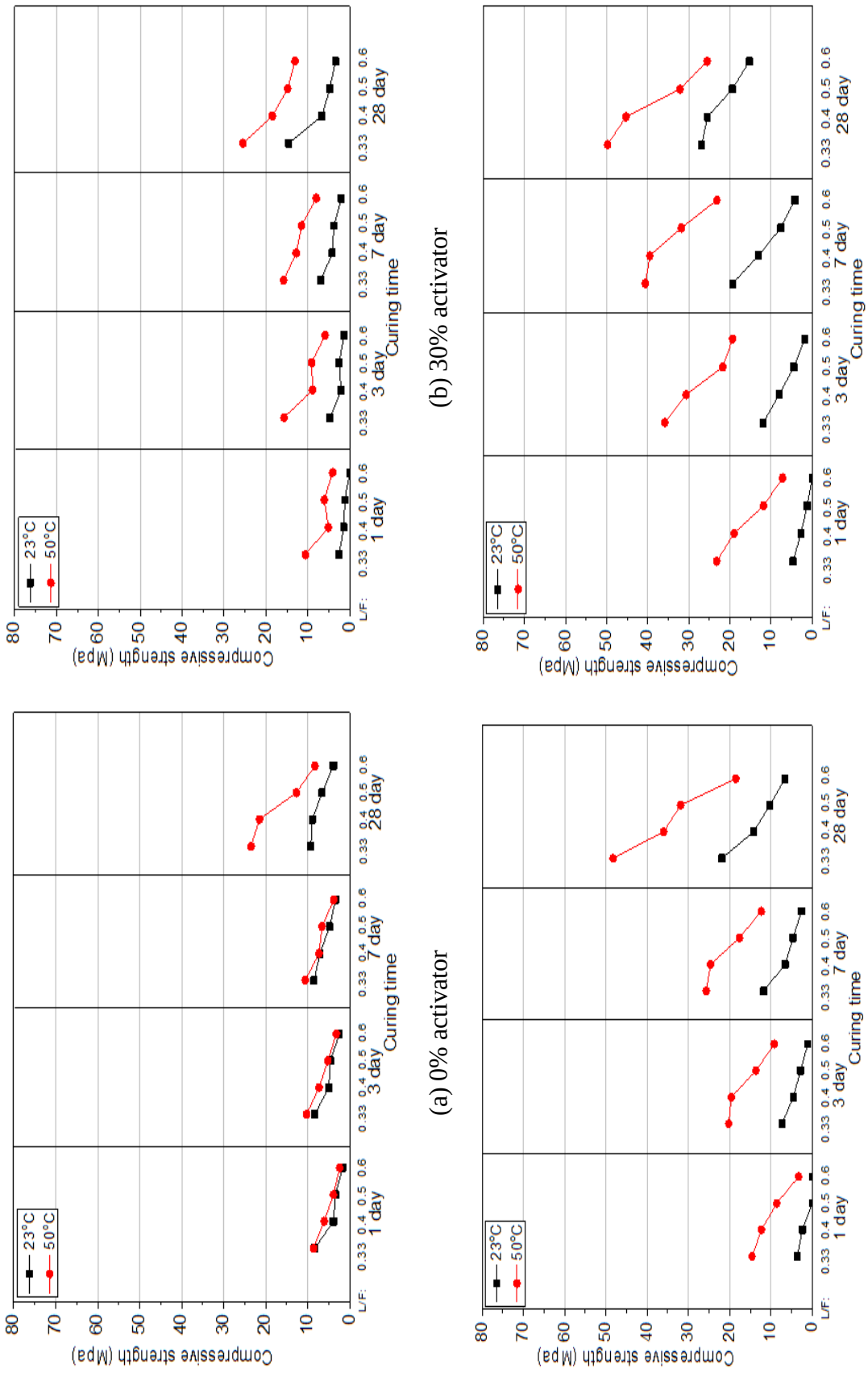

(a) 0% activator (b) 30% activator

(c) 40% activator (d) 50% activator

Figure 7. Compressive strength of mixes cured at different temperatures (Module = 2.0)

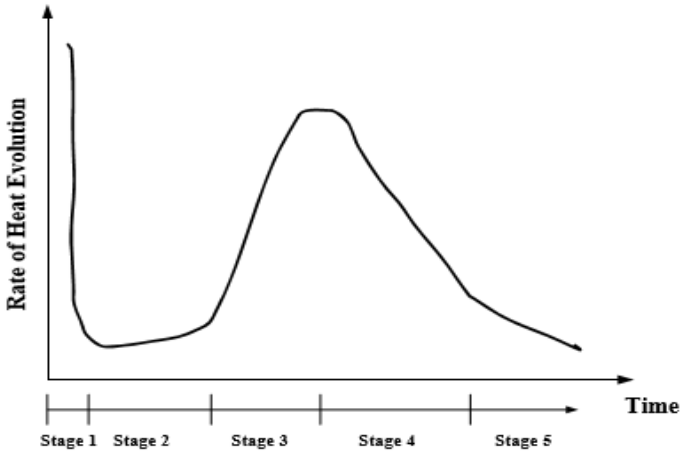

(a) Cement hydration process (Wang et al. 2006)

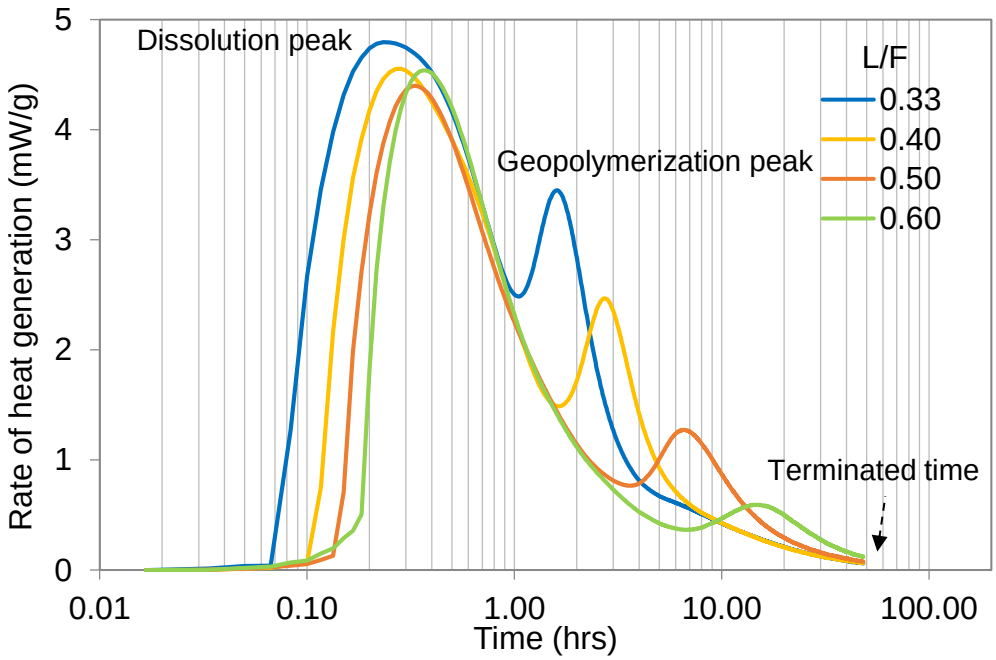

(b) Fly ash geopolymer hydration process

Figure 8. Heat generation curves for (a) typical cement paste and (b) the 2.0-40%-23C geopolymer mixture

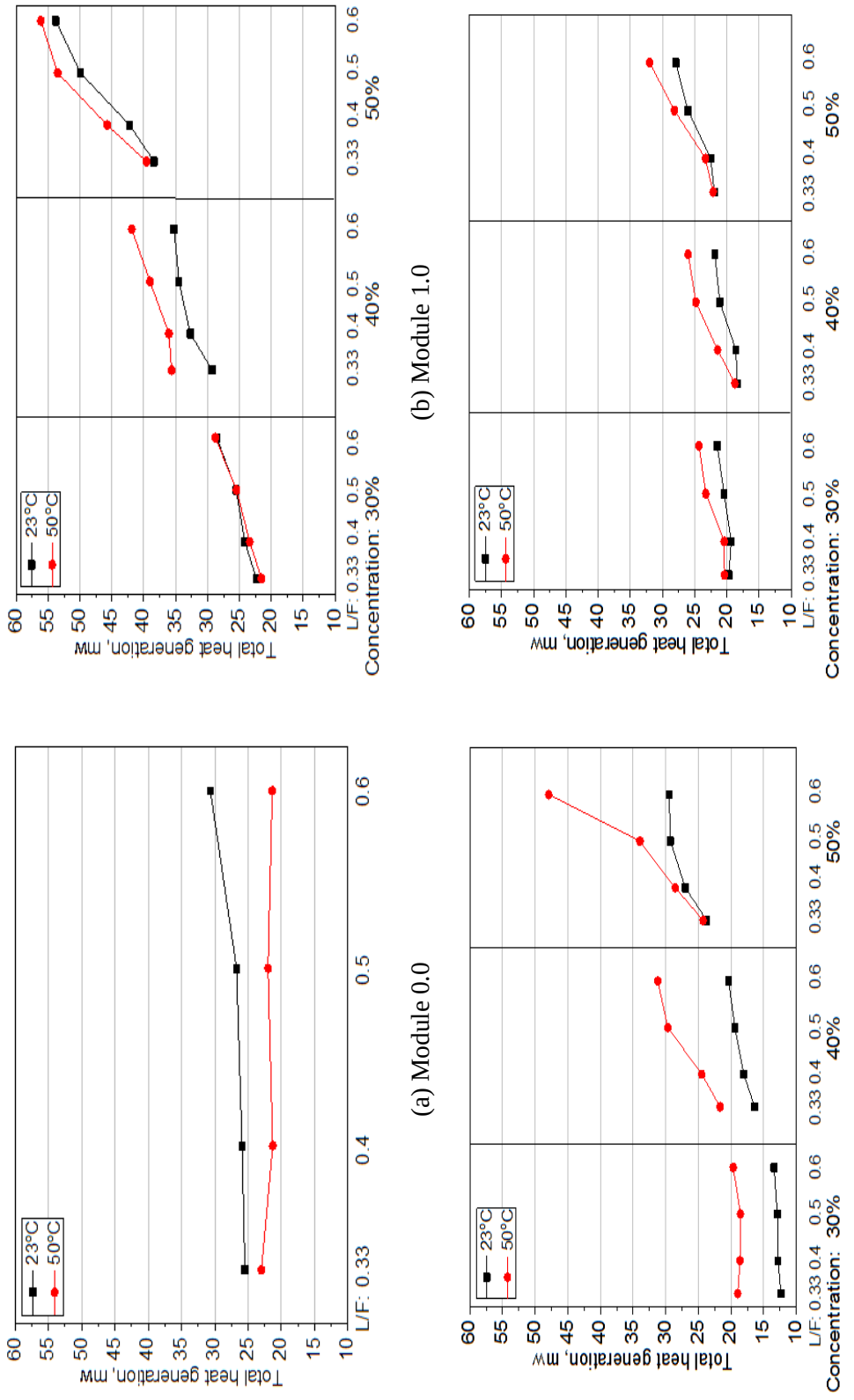

Figure 9. Total heat generation of geopolymer mixtures with various Modules

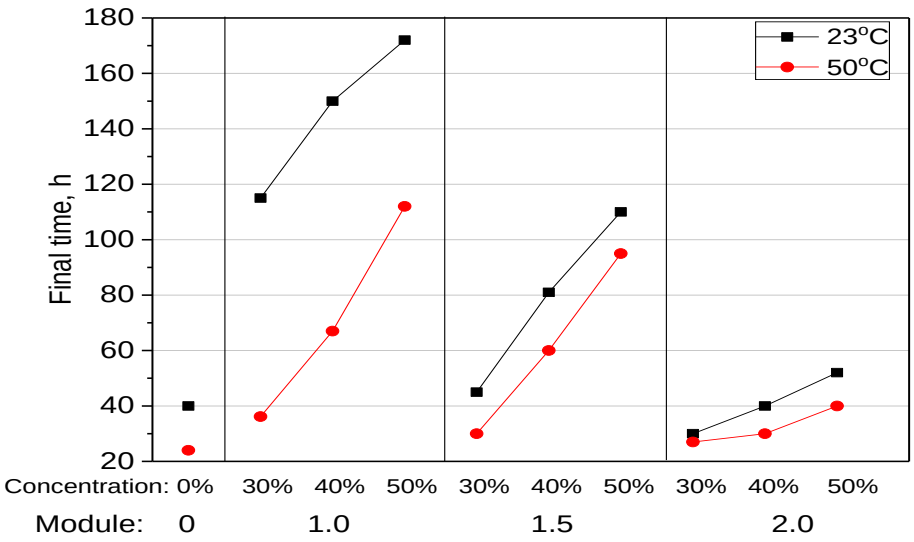

Figure 10. Terminated time of heat generation

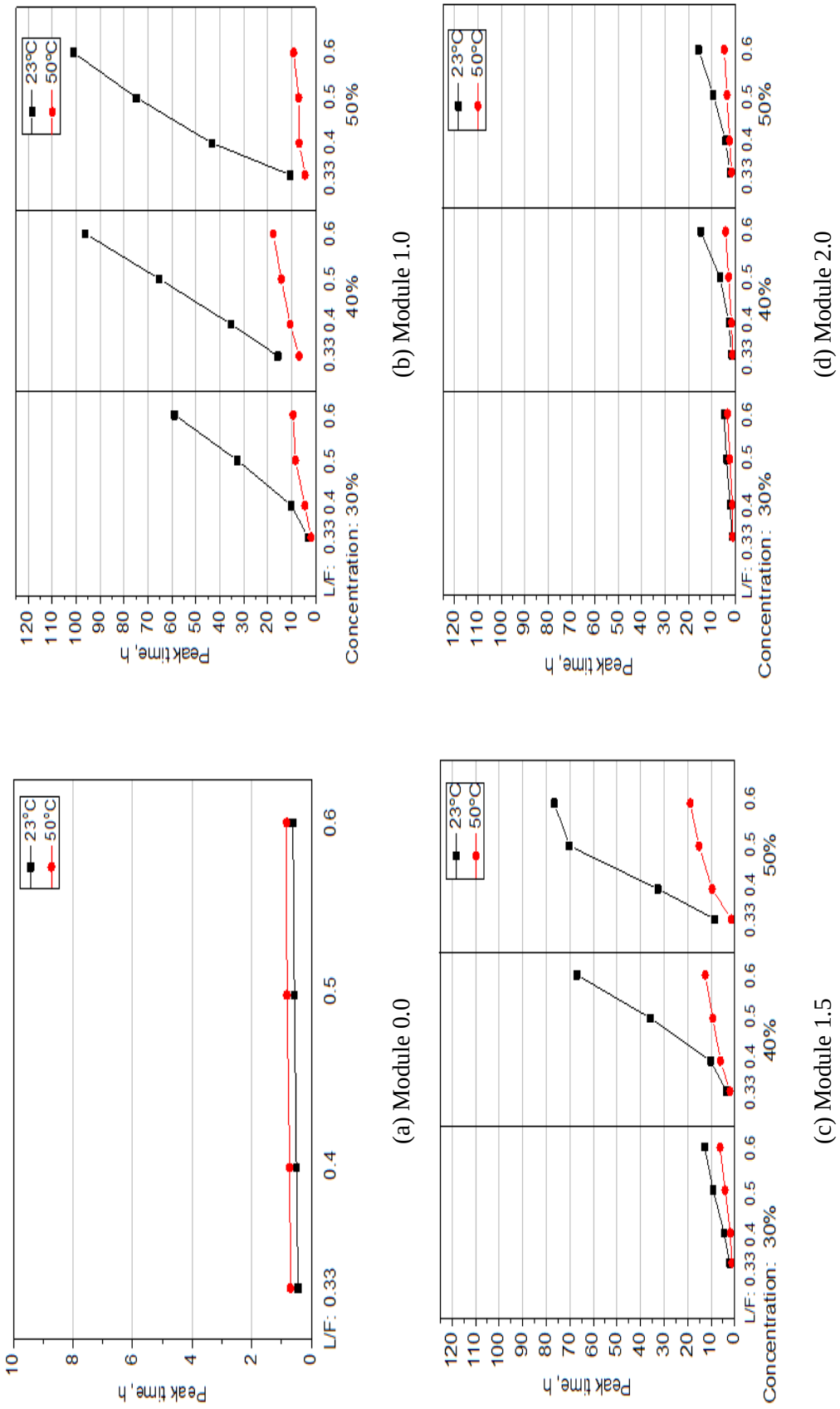

(a) Module 0.0 (b) Module 1.0 (c) Module 1.5 (d) Module 2.0

Figure 11. The peak time of geopolymerization

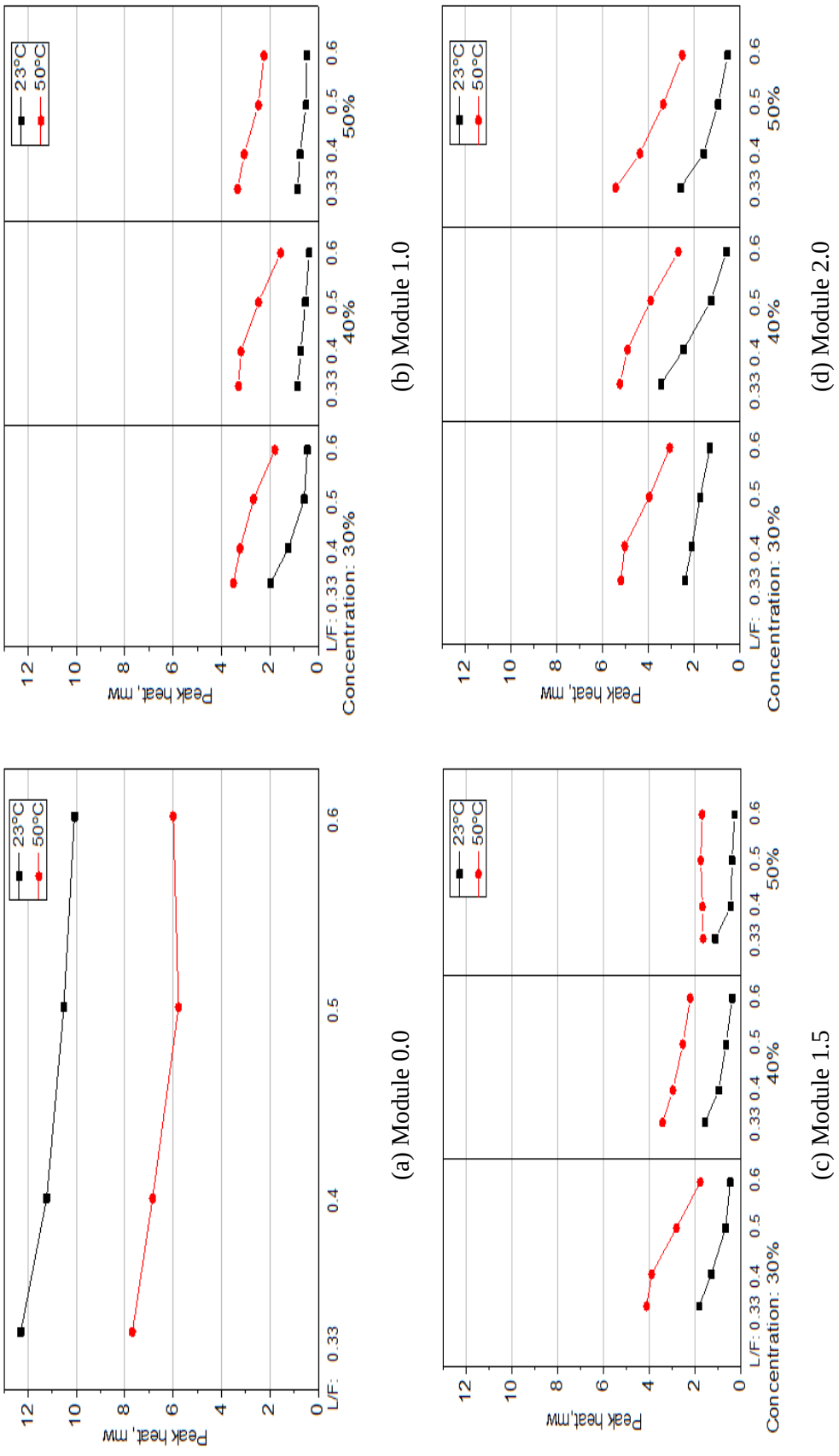

(a) Module 0.0 (b) Module 1.0

(c) Module 1.5 (d) Module 2.0

Figure 12. The peak heat of geopolymerization

CHAPTER 4. PREDICTION OF STRENGTH, SETTING TIME AND GEOPOLYMERIZATION HEAT OF FLY ASH GEOPOLYMER USING ARTIFICIAL NEURAL NETWORK

Yifeng Ling, Kejin Wang, Xuhao Wang

Department of Civil, Construction and Environmental Engineering, Iowa State University, Ames IA 50010

Abstract

Geopolymer has been studied as an innovative concrete binder due to its comparable properties to Portland cement and environmental benefits in recent years. However, the complexity of design parameters makes it difficult to systematically approach mix design. The SiO_2/Na_2O mole ratio in alkaline solution (Module), alkaline solution concentration in mass percent (Concentration), liquid-to-fly ash mass ratio (L/F), curing temperature and time have been shown to have significant influences on the setting time, compressive strength and heat of geopolymerization that are critical properties for a concrete binder. In the present study, an artificial neural network (ANN) has been applied to establish predictive models for identifying how mix design parameters result in favorable fly ash geopolymerproperties (i.e., compressive strength, setting time and heat generation). Results show good correlation between the experimental measurements and model predictions from ANN for setting time, compressive strength and heat generation properties. The effects of geopolymer mix design parameters on setting time, compressive strength and heat generation were also discussed in accordance with the prediction profiler generated from ANN models. This ANN-derived model can guide property prediction in high-calcium fly ash geopolymer mix design.

Key words: Geopolymer, Prediction, Strength, Setting time, Heat generation, ANN

Introduction

Geopolymer, as an artificial aluminosilicate material containing fly ash, slag and metakaolin activated by alkali solution, has become a popular alternative to ordinary Portland cement binder in recent years (Rangan 2008, Skvara et al. 2006). The advantages of using such a material are due to its excellent acid and fire resistance, low production cost, environmental friendliness and good heat resistance properties (Fernandez et al. 2006, Chareerat et al. 2006).

The biggest challenge of geopolymer mix design is that geopolymer properties (e.g., setting time, strength development and heat generation) are rather sensitive to mix design parameters, including SiO_2/Na_2O mole ratio in alkaline solution (Module), alkaline solution concentration in mass percent (Concentration), liquid to fly ash mass ratio (L/F), and curing conditions. A Module of 2.0 with an 8–16 M in Concentration were recommended as a geopolymer activator. It has also been recommended that L/F be maintained between 0.30 to 0.45 (Skvara et al. 2006), while a wider range of Module between 1.5 and 3.2 has also been reported (Fernandez et al. 2005). Song found that the Concentration for fly ash and slag mixes should range from 2-10 Module (Song 2007). Curing temperatures in the range of 50–80°C are widely accepted values used for successful geopolymer hydration (Rangan 2008, Skvara et al. 2006). With these recommended ranges in geopolymer mix design parameters, there is a need to assess the sensitivity of applying wide range design parameters to seek the best combination for a particular property, such as setting time of geopolymerization process, compressive strength development, and heat generation kinetics. In addition, a sensitivity study can reduce a large amount of trial and error in experimental work and labor intensity.

ANN models are inspired by biological nervous systems (Gerven and Bohte 2018). They can be trained to perform a particular function by adjusting the weights among elements so that inputs lead to specific outputs by continuously comparing with the target (Ozcan et al 2009, Yaprak et al 2011). Neural networks consist of many simple algorithm units called *nodes* with dense parallel interconnections. Each node receives weighted inputs from other nodes and transfers outputs to other nodes by using an activation function. Neural networks can be multilayered and with their remarkable ability to derive meaning from complicated or imprecise data, used to extract patterns and detect trends that are too complex to be noticed by other computer techniques due to adaptive learning (Kewalramani and Gupta 2012). A multi-layer perceptron consists of multiple layers of nodes with each layer fully connected to the next one and utilizes a back propagation for training the network. The main advantage of ANNs is that one does not have to explicitly assume a model form (all calculations are done in ANNs), which is a pre-requisite in the parametric approach. It does not need any specific equation form. ANN automatically manages the relationships between variables and adapt based on the data used for their training which makes it important to collect a large number of experimental data to carry out the modelling of the system.

Saridemir developed ANN models to predict compressive strength of Portland cement concrete with different water-to-cement ratios while Gupta applied sigmoidal activation function in ANNs for strength prediction (Saridemir 2009 and Gupta 2013). Diab et al. predicted the initial setting time of self-consolidating concrete using ANNs to demonstrate that their utility (Diab et al 2014). ANNs have been used to predict cement hydration heat with R^2 of 0.999 based upon a large dataset (Najafi and Ahangari 2013).

To date, however, little ANN modeling has been used to predict geopolymer mixture properties (Diab et al 2014, Yadollahi et al 2015), possibly due to its complexity of multiple design

parameters and lack of sensitivity studies on performance characteristics. In the present study, ANN technique has been applied to establish predictive models for the compressive strength, setting time and heat generation of fly ash geopolymer. Critical design parameters and the feasibility of ANN for predicting aforementioned properties of high-calcium fly ash geopolymer are discussed in order to provide an optimization and performance based geopolymer mixture design approach.

Database

The input data used for predictive model establishment and validation were all extracted from the results of laboratory experiment, including setting time determined by penetrometer test in accordance with ASTM WK27337, compressive strength measured up to 28 days in accordance with ASTM C109/C109M, and heat generation measured through isothermal calorimetry complied with ASTM C1702. The experimental test apparatus and method were reported in Paper 1. The detailed mix design matrix and critical design parameters are listed in Table 1. The setting time mentioned in this paper is the final setting time.

ANN Modeling

The architecture of the artificial neural network was constructed using a commercial statistical analysis tool, JMP Pro 13 (Ge et al. 2012). The Neural platform in JMP implements a fully connected multi-layer perceptron with one or two layers. The model launch of ANNs consists of five steps as validation method, hidden layer structure, boosting, fitting options and penalty method. Based on different ways to divide data sets, the validation methods can be sorted by excluded rows, holdback and KFold. Excluded rows uses row states to subset the data as the validation set. Holdback randomly divides the original data into training and validation sets. KFold

divides the original data into K subsets. In turn, each of the K sets is used to validate the model fit on the rest of the data, fitting a total of K models. The model giving the best validation statistic is chosen as the final model. This method is the better fit for small data sets, because it makes efficient use of limited amount of data. The hidden layer structure can fit in one or two-layer neural networks. Increasing the number of nodes in the first layer, or adding a second layer, makes the neural network more flexible.

- The functions applied at the nodes of the hidden layers are called activation functions. In JMP interface, there are three types of activation functions which are Linear, Gaussian and TanH: A linear activation function cannot be used in neural networks because neural networks with a linear activation function are effective only one layer deep, regardless of how complex their architecture are. It aims at finding the optimal weights that results in minimal vertical effect between the explanatory and target variables, when combine with the input. The identity activation function can be simply written as Eq. (1):

$$y(x) = x$$

- A Gaussian function is a bell-shaped curve that is continuous. It is used for radial basis function behavior or when the response surface is normal in shape. The node output (high/low) is interpreted in terms of class membership (1/0), depending on how close the net input is to a chosen value of average. The Gaussian function is notated as Eq. (2):

$$y(x) = e^{-x^2} \tag{2}$$

- TanH is the hyperbolic tangent function with expression as Eq. (3):

$$y(x) = \frac{e^{2x}-1}{e^{2x}+1} \tag{3}$$

Where x is a linear combination of the X variables.

It is mapped between 0 and 1, where zero means the feature is not there, while one means the feature is present. Therefore, nonlinear functions must be continuous and differentiable between this range. In this paper, the TanH sigmoid activation function was applied in two hidden three-node layers to model ANNs due to obtaining well-connected neutral networks.

Boosting is typically used for building a large additive neural network model by fitting a sequence of smaller models. The fitting options specify the model fitting. *Transform covariates* transforms all continuous variables to near normality using either the Johnson Su or Johnson Sb distribution. Transforming the continuous variables helps to mitigate the negative effects of outliers or heavily skewed distributions. *Robust fit* trains the model using least absolute deviations instead of least squares. This option is useful to minimize the impact of response outliers available only for continuous responses. *Penalty method* is to mitigate tendency of neural networks. *Squared penalty function* was used in modeling because the input variables are all contributing to the predictive ability.

Setting time

A total of 36 sets of input and output variables for setting time prediction was used. The variable input parameters are Module, Concentration and L/F. Their ranges of various input and output parameters used in training process are summarized in Table 2.

The three-fold cross-validation mode (i.e., repeatedly partitioning the original training dataset into a training dataset and a validation dataset with fitting option of transform covariates and squared penalty method) was implemented for setting time prediction as shown in Fig. 1. One of the main reasons for using cross-validation instead of using the conventional validation (e.g.,

partitioning the data set into two sets of 70% for training and 30% for test) is that there is not enough data available to partition it into separate training and test sets without losing significant modelling or testing capability (Seni and Elder. 2010). In these cases, a fair way to properly estimate model prediction performance is to use cross-validation as a powerful general technique. The properties of the neural network simulator used in this study have been shown in Table 3. The input layer consists of three parameters, Module, Concentration and L/F, which are the variables. The output is setting time for each path from input parameters. In addition, the final network contains two hidden layers with 3 nodes in each layer. A nonlinear sigmoid function was employed as an activation function for all nodes with full connection adopted between nodes in different layers within the network.

Compressive strength

273 sets of input data, including the variation of Module, Concentration, L/F, temperature and age were selected for compressive strength prediction. Table 4 lists the input and output parameters and their ranges for ANN training process.

The ten-fold cross-validation was chosen to establish the neural network of compressive strength using fitting options of transform covariates and robust fit to train with squared penalty method as seen in Table 5. The flow chart illustrating the training process of neural networks for compressive strength is shown in Fig.2.

Heat generation of geopolymerization peak

The ANNs model of heat generation of geopolymerization was created according to 72 sets of calorimetry results with a wide range of Module, Concentration, L/F and temperature. The ranges of calorimetry data were present in Table 6.

The heat generation model is launched using ten-fold cross-validation, transform covariates fitting and squared penalty as shown in Table 7. Fig. 3 exhibits the ANN architecture of heat generation at geopolymerization peak that was trained by activation functions in layers starting from the input parameters.

Results and Discussion

In this study, correlation coefficient (R^2), root mean square error (RMSE) and mean absolute deviation (MAD) are used to evaluate the performances of the multilayer neural networks models for setting time, compressive strength and heat generation prediction. They can be mathematically determined using Eqs. (4)-(6) and calculated for both training results and validation results.

$$R^2 = \frac{(n\sum_i to - \sum_i t \sum_i o)^2}{[n\sum_i t^2 - (\sum_i t)^2][n\sum_i o^2 - (\sum_i o)^2]} \quad (4)$$

$$\text{RMSE} = \sqrt{\frac{1}{n}\sum_{i=1}^{n}(t-o)^2} \quad (5)$$

$$\text{MAD} = \frac{1}{n}\sum_{i=1}^{n}|t-o| \quad (6)$$

where *t* is the target value, *o* is the output value and *n* is the number of data sets.

R^2, RMSE and MAD are used for investigating data fitting between prediction and experimental results. Those R^2 closer to 1 and comparatively small RMSE and MAD mean a good fitting behavior for prediction model.

Setting time

The setting time vs. Module, Concentration and L/F was predicted using ANNs model. The results from experimental and predicted values for training and validation sets with R^2, RMSE and MAD are shown in Fig. 4 and Table 8. The values obtained from the training and validation using

the ANNs model correlate well with experimental results. This can also be evidenced by high R^2 values of 0.991 and 0.999, low RMSE values of 112.8 and 34.4, and low MAD values of 66.0 and 28.1, for training and validation sets, respectively.

The prediction profiler of setting time as plotted in Fig. 5 demonstrates the effects of Module, Concentration and L/F on setting time tendency individually for the selected ranges. L/F seems to be the most significant influence parameter for geopolymer setting time according to the exponential curve indicating a dramatic increase. As Module varies from 1.0 to 2.0, two inflection points at around 1.4 and 1.8 can be observed. Generally, the dissolution and geopolymerization are two main processes in geopolymer formation. Although lower Module accelerated dissolution, it delayed geopolymerization (Petermann et al. 2010). These two contradictory effects of Module may be attributed to the two inflection points. In addition, Concentration has similar effect as L/F to setting time, but to a less extent.

From Fig. 6, the setting time results from experiments are almost overlapped with the predicted results from ANNs model. Furthermore, the linear fit of predicted and experimental setting time results has a high R^2 of 0.992.

Compressive strength

The results of geopolymer compressive strength prediction from training and validation process using ANNs model with the parameters of Module, Concentration, L/F, curing temperature and time are illustrated in Fig.7. Their statistical parameters R^2, RMSE and MAD are listed in Table 9. Based on these results, the ANNs model for compressive strength prediction in both training and validation processes is very accurate and evidenced by the large R^2 (0.952 and 0.961)

and relatively small RMSE and MAD which indicate the difference between the real value and the predicted value.

The effects of each selected parameter on geopolymer compressive strength is presented in Fig. 8 using prediction profiler. It can be observed that as the Module and L/F increase, the compressive strength generally decreases. While the increased Concentration, temperature and age can improve compressive strength of geopolymer. This observation is the same as the findings from the experimental results. It is noted that there is a large drop on compressive strength when Module increases from 1.0 to 1.5 while no further deduction can be observed when Module is higher than 1.5. This is likely due to saturation of silicon in the mixture (Petermann et al. 2010). Furthermore, the high-calcium fly ash geopolymer seems to rapidly gain strength at early age (i.e., less than 14 days), but gently increase afterwards.

The proposed ANNs model can accurately predict the compressive strength with a R^2 of 0.94 by considering the effects of Module, Concentration, L/F, temperature and age (Fig. 9).

Heat generation of geopolymerization peak

The heat generation of geopolymerization peak were predicted by ANNs based on the experimental data from isothermal calorimetry. The mix design parameters that related to heat generation are Module, Concentration, L/F and temperature. The goodness-of-fit model for training and validation processes with given R^2, RMSE and MAD is shown in Fig. 10 and Table. 10 which indicates that the ANNs system is able to predict the peak of heat generation during geopolymerization quite accurately.

The prediction profiler of model gives the information for the effects of Module, Concentration, L/F and temperature on heat generation as illustrated in Fig. 11. It can be found

that the heat generation increases with the increased Module, especially when Module is higher than 1.5. This phenomenon seems to comply with compressive strength development which is associated with the high soluble silica directly affects the reaction kinetics, the rate of crystallization, and promotes gel formation which is responsible for strength development (Zuda et al. 2006). The decreasing effects on heat generation from increased Concentration and L/F are similar in terms of magnitude while higher curing temperature yields a higher heat generation. According to the slope of heat generation and corresponding parameters, Module, L/F and temperature are very important parameters in the evaluation of heat generation.

The Fig. 12 plots the result of goodness-of-fit analysis which evaluates the ability of established ANNs model on prediction of heat generation. The correlation coefficient R^2 of 0.92 indicates that this ANN model is appropriate for heat generation prediction of high-calcium geopolymer mixtures with selected ranges of design parameters.

Conclusions

The present work utilizes ANN to predict setting time, compressive strength and heat generation of geopolymerization peak for fly ash geopolymer. The following conclusions can be drawn from the previously presented models:

1. By analyzing predictive models of setting time, compressive strength and heat generation, the effects of each geopolymer mix design parameter were clear in quantity using prediction profiler which was not apparent from experimental results. For example, the setting time has extremums at 1.4 and 1.8 when Module is changing within 1.0 to 2.0. L/F is a most effective parameter in setting time. Module over 1.5, affects compressive strength

a little while concentration influences compressive strength most. Module larger than 1.5 significantly impacts the heat generation.

2. Numerical modeling using ANNs shows an excellent performance to predict geopolymer properties. The well correlations between model predicted and laboratory results on setting time, compressive strength and heat generation with selected ranges of design parameters can be evidenced by high R^2 values of 0.99, 0.94 and 0.92 respectively.
3. The proposed model can be considered as a guidance for high-calcium fly ash geopolymer mix design in the future. ANN can be further used for geopolymer study to reduce trial and error and assist mix design sensitivity study.

References

ASTM C109/C109M, (2013). "Standard Test Method for Compressive Strength of Hydraulic Cement Mortars," Philadelphia: ASTM International.

ASTM C1702, (2017). "Standard Test Method for Measurement of Heat of Hydration of Hydraulic Cementitious Materials Using Isothermal Conduction Calorimetry," Philadelphia: ASTM International.

ASTM WK27337, (2010). "New Test Method for Pocket Penetrometer Test," ASTM International.

Chareerat, T., Lee-Anansaksiri, A., Chindaprasirt, P. (2006). "Synthesis of High Fly Ash and Calcined Kaolin Geopolymer Mortar," International Conference on Pozzolan, Concrete and Geopolymer, Khhon Kaen, Thailand, 24-25 May.

Diab, A., Elyamany, H., Abd Elmoaty, M., Shalan, A. (2014). "Prediction of Concrete Compressive Strength Due to Long Term Sulfate Attack Using Neural Network," Alexandria Engineering Journal 53(3), pp. 627–642.

Fernandez-Jimenez, A., Palomo, A., Criado, M. (2005). "Microstructure Development of Alkali-Activated Fly Ash Cement: A Descriptive Model," Cement and Concrete Research 35(6), pp.1204-1209.

Fernandez-Jimenez, A., Palomo, A., Lapez-Hombrados, C. (2006). "Engineering Properties of Alkali—Activated Fly Ash Concrete," ACI Materials Journal, 103(2), pp.106-112.

Ge, Z., Wang, K., and Gao, Z. (2012). "Prediction of Pavement Concrete Strength Development, Joint Sawing, and Opening Time Using FEMLAB," Journal of Performance of Constructed Facilities 26(2), pp. 162-169.

Gerven, M., and Bohte, S. (2018). "Artificial Neural Networks as Models of Neural Information Processing," DOI: 10.3389/978-2-88945-401-3.

Gupta, S. (2013). "Using Artificial Neural Network to Predict the Compressive Strength of Concrete Containing Nano-silica," Civil Engineering and Architecture 1(3), pp. 96-102.

Kewalramani, M.A., Gupta, R. (2006). "Concrete Compressive Strength Prediction Using Ultrasonic Pulse Velocity through Artificial Neural Networks," Automation in Construction 15(3), pp. 374-379.

Najafi, Z., and Ahangari, K. (2013). "The Prediction of Concrete Temperature during Curing Using Regression and Artificial Neural Network," Journal of Engineering, Volume 2013, Article ID 946829, 5 pages.

Ozcan, F., Atis, C.D., Karahan, O., Uncuoglu, E., Tanyildizi, H. (2009). "Comparison of Artificial Neural Network and Fuzzy Logic Models for Prediction of Long Term Compressive Strength of Silica Fume Concrete," Advances in Engineering Software 40 (9), pp. 856–863.

Petermann, J., Saeed, A., and Hammons, M. (2010). "Alkali- Activated Geopolymers: A Literature Review," Air Force Research Laboratory Materials and Manufacturing Directorate.

Rangan, B.V. (2008). "Fly Ash-Based Geopolymer Concrete," Research Report GC 4.

Saridemir, M. (2009). "Prediction of the Compressive Strength of Mortars Containing Metakaolin by Artificial Neural Networks and Fuzzy Logic," Advances in Engineering Software 40 (9), pp. 920–927.

Seni, G., and Elder, J.F. (2010). "Ensemble Methods in Data Mining: Improving Accuracy through Combining Predictions," Synthesis Lectures on Data Mining and Knowledge Discovery, 10.2200/S00240ED1V01Y200912DMK002.

Skvara, F., Dolezal, J., Svoboda, P., Kopecky, L., Pawlasova, S., Lucuk, M., Dvoracek, K., Beksa, M., Myskova, L., Sulc, R. (2006) "Concrete Based on Fly Ash Geopolymers," The Tenth East Asia-Pacific Conference on Structural Engineering and Construction August 3-5, Bangkok, Thailand.

Song, X. (2007) "Development and Performance of Class F Fly Ash Based Geopolymer Concretes against Sulphuric Acid Attack," Doctoral Thesis, School of Civil and Environmental Engineering, University of New South Wales, Sydney, Australia.

Yadollahi, M.M., Benli, A., and Demirboga, R. (2015). "Prediction of Compressive Strength of Geopolymer Composites Using an Artificial Neural Network," Materials Research Innovations 19(6), pp. 453-458.

Yaprak, H., Karaci, A., Demir, I. (2011). "Prediction of The Effect of Varying Cure Conditions and W/C Ratio on the Compressive Strength of Concrete Using Artificial Neural Networks," Neural Computing and Applications 22(1), pp. 133-141.

Zuda, L., Pavlik Z., Rovnanikova, P., Bayer, P., Cerny, R. (2006), "Properties of Alkali Activated Aluminosilicate Material after Thermal Load," International Journal of Thermophysics 27(4), pp. 1250-1263.

Table 1. Parameters in setting time, compressive strength and heat generation

Property	Module	Concentration (%)	L/F	Temperature (°C)	Curing time (day)
Setting time	1.0, 1.5, 2.0	30,40,50	0.33, 0.4, 0.5, 0.6	23	-
Compressive strength	1.0, 1.5, 2.0	30,40,50	0.33, 0.4, 0.5, 0.6	23, 50	1, 3, 7, 28
Heat generation	1.0, 1.5, 2.0	30,40,50	0.33, 0.4, 0.5, 0.6	23, 50	-

Table 2. Input and output variables for setting time

Variables	Parameter	Database Range
Input	Module	1.0, 1.5, 2.0
	Concentration, %	30, 40, 50
	L/F	0.33, 0.4, 0.5, 0.6
Output	Setting time, min	20~4415

Table 3. Properties of neural network simulator in setting time

Details	Selection
Network architecture	Back propagation network
Validation method	3-fold
Activation function	TanH Sigmoid
Boosting (number of models/learning rate)	0/0.1
Fitting options	Transform Covariates
Penalty method	Squared
Number of tours	1

Table 4. Input and output variables for compressive strength

Variables	Parameter	Database Range
Input	Module	1.0, 1.5, 2.0
	Concentration, %	30, 40, 50
	L/F	0.33, 0.4, 0.5, 0.6
	Temperature, ^{o}C	23, 50
	Age, day	1, 3, 7, 28
Output	Compressive strength, MPa	1.1~76

Table 5. Properties of neural network simulator in compressive strength

Details	Selection
Network architecture	Back propagation network
Validation method	10-fold
Activation function	TanH Sigmoid
Boosting (number of models/learning rate)	0/0.1
Fitting options	Transform Covariates and robust
Penalty method	Squared
Number of tours	1

Table 6. Input and output variables for heat generation

Variables	Parameter	Database Range
Input	Module	1.0, 1.5, 2.0
	Concentration, %	30, 40, 50
	L/F	0.33, 0.4, 0.5, 0.6
	Temperature, ℃	23, 50
Output	Heat generation at peak, mw/g	0.26~5.42

Table 7. Properties of neural network simulator in geopolymerization heat

Details	Selection
Network architecture	Back propagation network
Validation method	10-fold
Activation function	TanH Sigmoid
Boosting (number of models/learning rate)	0/0.1
Fitting options	Transform Covariates
Penalty method	Squared
Number of tours	1

Table 8. R^2, RMSE and MAD for training and validation results of setting time

Terms	Training	Validation
R^2	0.991	0.999
RMSE	112.8	34.4
MAD	66.0	28.1

Table 9. R^2, RMSE and MAD for training and validation results of compressive strength

Terms	Training	Validation
R^2	0.952	0.961
RMSE	631.0	543.0
MAD	419.8	355.3

Table 10. R^2, RMSE and MAD for training and validation results of compressive strength

Terms	Training	Validation
R^2	0.943	0.972
RMSE	0.34	0.23
MAD	0.20	0.18

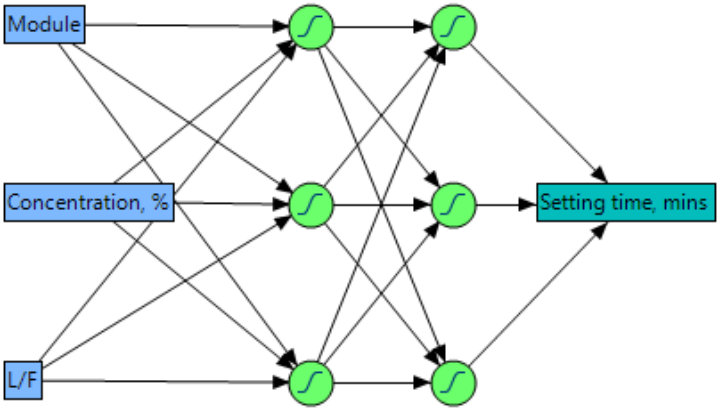

Figure 1. Neural network architecture of setting time

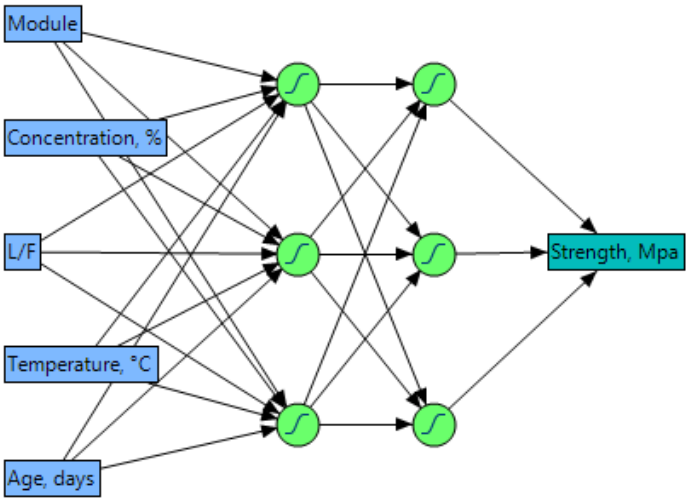

Figure 2. Neural network architecture of compressive strength

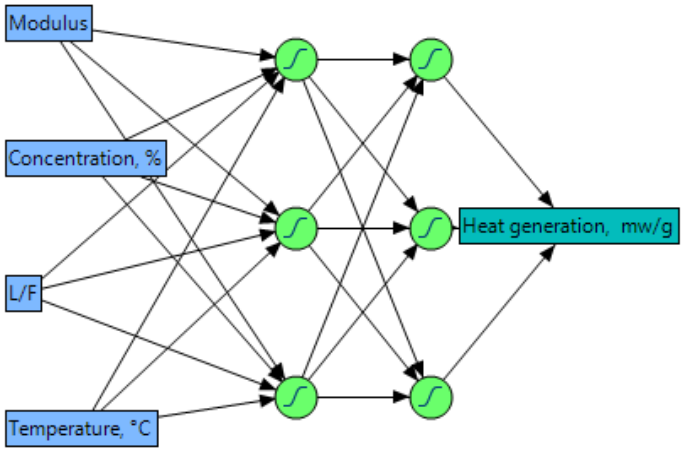

Figure 3. Neural network architecture of heat generation at geopolymerization peak

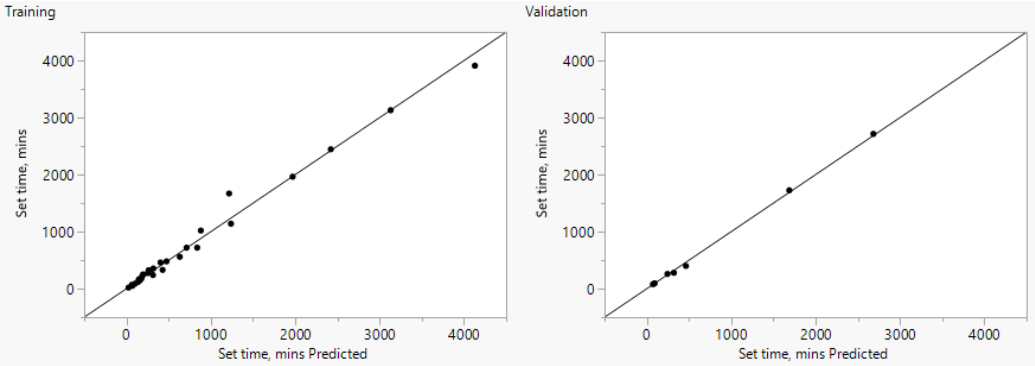

Figure 4. Experimental and predicted setting time for training and validation

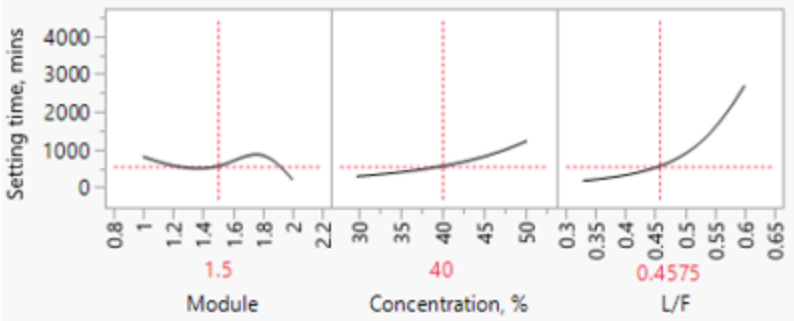

Figure 5. Prediction profiler of setting time model

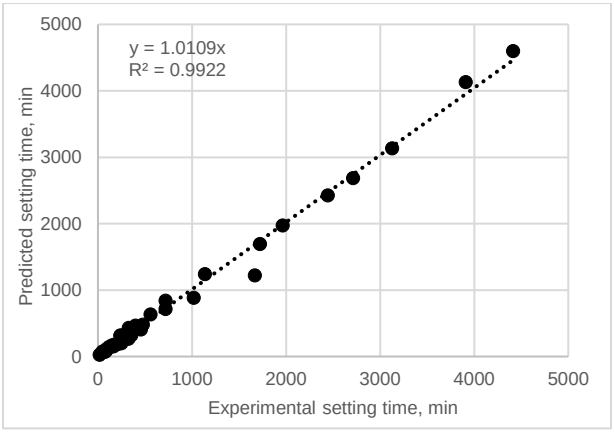

Figure 6. Predicted setting time vs. experimental setting time

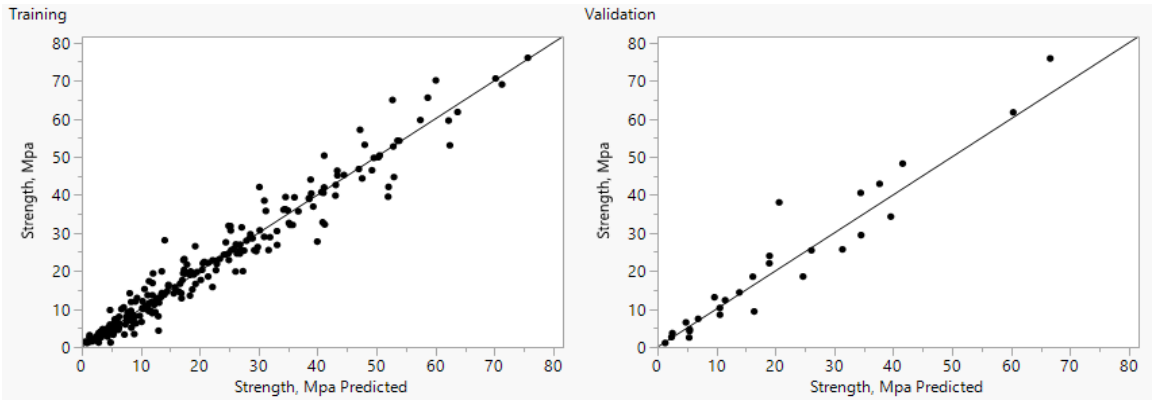

Figure 7. Experimental and predicted compressive strength for training and validation

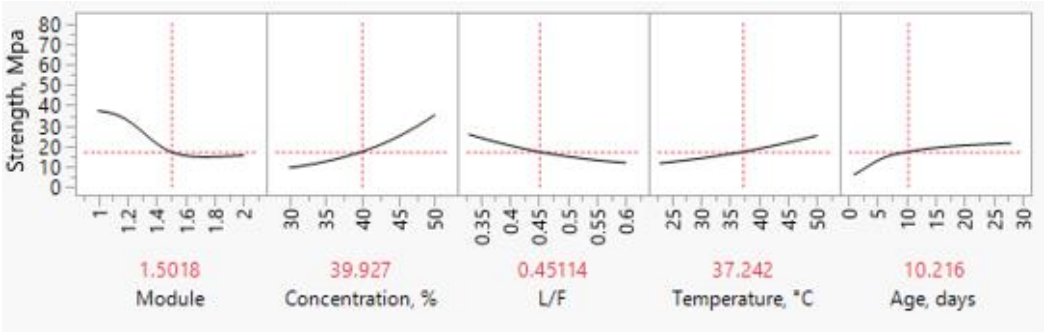

Figure 8. Prediction profiler of compressive strength model

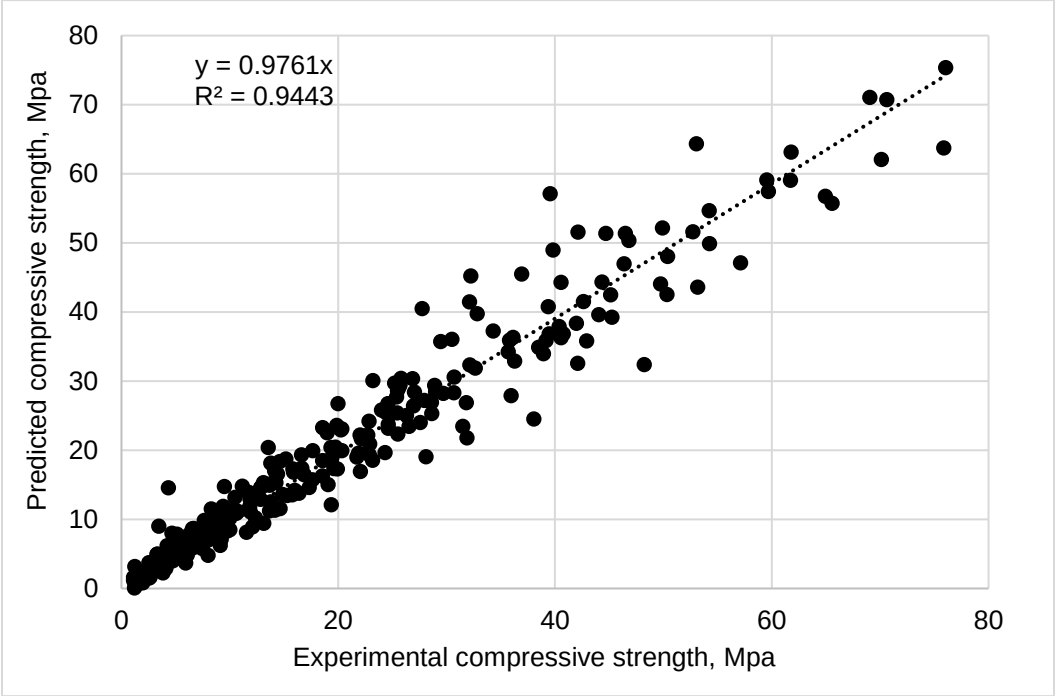

Figure 9. Predicted compressive strength vs. experimental compressive strength

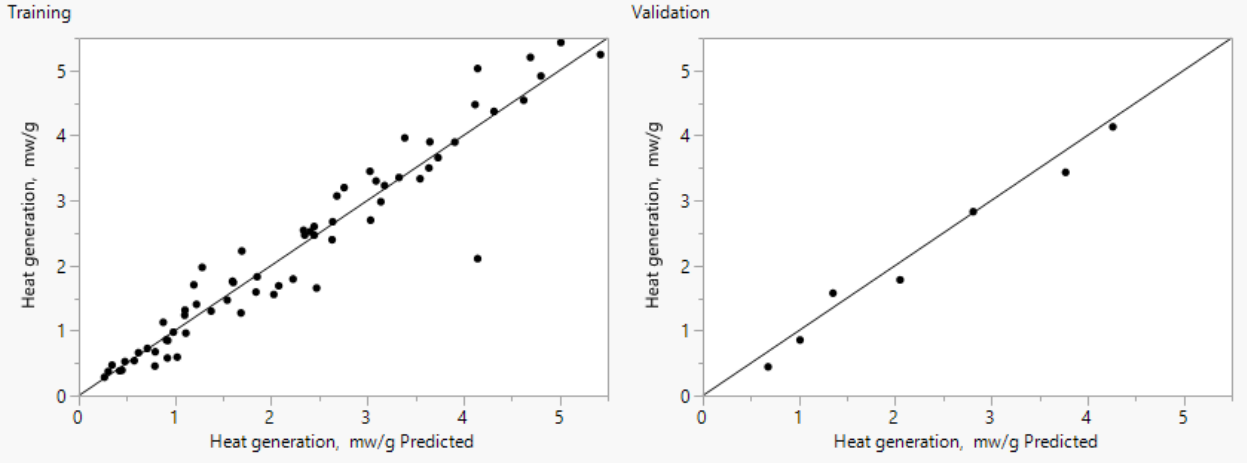

Figure 10. Experimental and predicted heat generation for training and validation

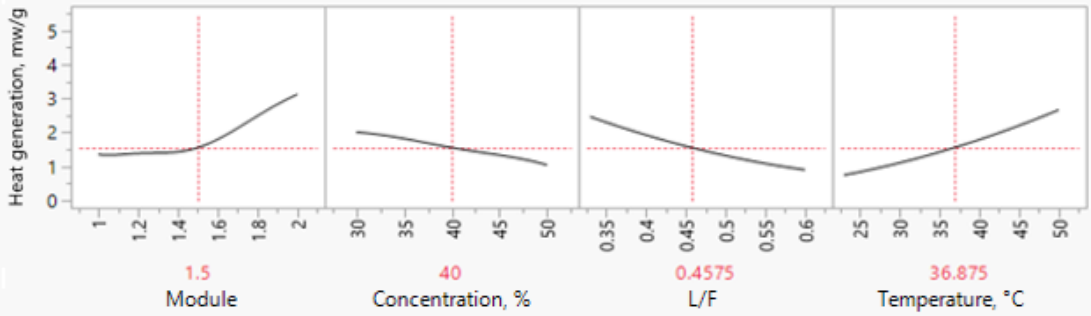

Figure 11. Prediction profiler of heat generation model

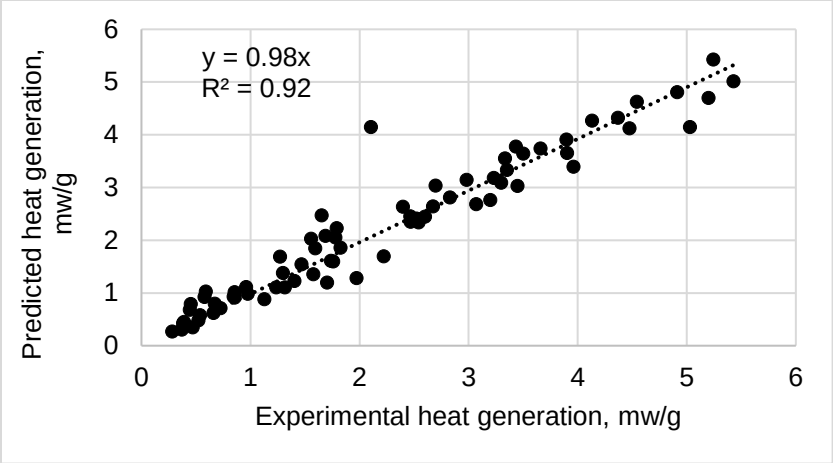

Figure 12. Predicted heat generation vs. experimental heat generation

CHAPTER 5. THE EFFECTS OF ACTIVATOR AND SHRINKAGE REDUCING ADMIXTURE ON SHRINKAGE BEHAVIOR OF FLY ASH GEOPOLYMER

Yifeng Ling[a], Kejin Wang[a], Chuanqing Fu[b]

[a]Department of Civil, Construction and Environmental Engineering, Iowa State University, Ames, IA 50010

[b]College of Civil Engineering and Architecture, Zhejiang University of Technology, Hangzhou, China 310023

Abstract

In this paper, a summary of several investigations was conducted to establish the influence of SiO_2/Na_2O mole ratio (Module), solute mass concentration (Concentration) and shrinkage reducing admixture (SR) on the flowability, compressive strength, drying and restrained shrinkage, restrained shrinkage cracking of fly ash geopolymer (FG) pastes. The flowability test was conducted by mini slump test. The drying and restrained shrinkage tests were carried out by subjecting the specimens to 25℃ temperature and 50% humidity. Drying shrinkage tests were performed by measuring length change of specimens with a micrometer and mass loss were determined as well. The time and width of cracks of the FG were recorded by using strain gauge and crack comparator respectively on restrained shrinkage test. The stress rate of FG during restrained shrinkage test was also derived from strain gauge. Finally, based on the obtained results, the FG has comparable flowability to PC. SR slightly decreased flowability of PC and FG. It's also found that the magnitude of drying shrinkage of FG was similar to that of PC, however not owing to mass loss for FG. The SR significantly reduced the drying shrinkage of FG up to 52% as well as PC. The SR decreased the restrained shrinkage up to 16%, delayed the cracking time,

reduced the crack width and lowered the cracking potential for both PC and FG. The FG mixtures had lower cracking potential than PC. The effect of Module and Concentration on drying shrinkage and restrained ring shrinkage was say what it was.

Keywords: Drying Shrinkage; Restrained ring shrinkage; Shrinkage reducing admixture; Fly ash geopolymer

Introduction

Fly ash geopolymer (FG), produced by combining fly ash and an alkaline activator, has been extensively studied due to its environmental benefits including lower energy requirements and lower emission of greenhouse gases with respect to the manufacturing of Portland cement (3-5 Refs). Freshly cast Portland cement concrete shrinks primarily due to negative capillary pressure that leads to a volume contraction of the cement paste during water evaporation (Cabrera et al. 1992, Soroushian and Ravanbakhsh 1998). When concrete is restrained against shrinkage, tensile stresses develop and can lead to cracking (Ref).

FG mixtures can be used as an alternative binder material to Portland cement (PC) in concrete. The shrinkage behavior of FG mixtures has begun to draw increased attention for its application in concrete (list 2-3 Refs). Several studies indicated that FG had lower drying shrinkage than ordinary Portland cement (Castel et al. 2016). The drying shrinkage of FG concrete has been shown to be comparable to that of ordinary Portland cement concrete of similar compressive strength (Deb et al. 2015). Lower shrinkage is believed to be favored in slag-based geopolymer with design parameters such as low activator solution/slag ratios, low water glass Modules and low activator Concentration (Collins and Sanjayan 2000, Shi 1996).

Very few authors, however, have studied the effect of SiO_2/Na_2O mole module (Module) and concentration of solute in alkaline solution (Concentration) on FG shrinkage and corresponding cracking behavior. The addition of polypropylene fibers has been reported to slightly decrease shrinkage in water glass-activated mortars cured at 50% relative humidity (RH) (Puertas et al. 2000). Bakharev et al. (2000) studied the effects of different admixtures on shrinkage in water glass-activated slag concrete, concluding that gypsum reduces both autogenous and drying shrinkage attributed to the formation of expansive phases, such as ettringite. The addition of shrinkage reducing admixture (SR) in Portland cement systems can decrease capillary stress in pore water, which in turn reduces cement paste shrinkage and shrinkage cracking of cement-based materials (Berke et al. 1997, Mora et al. 2003). However, the effects of SR on shrinkage of FG mixtures have not been widely reported. This constitutes the subject of the present study.

Some have studied the drying shrinkage of FG (Crentsil et al. 2013, Kheradmand et al. 2017), but very few results have been published with regards to restrained shrinkage of FG, let alone with addition of SR. The effectiveness of SR in reducing early-age shrinkage should be evaluated from drying shrinkage and restrained shrinkage tests because…?. Reduction in drying shrinkage does not necessarily give an indication of the overall reduction in crack tendency, which is a function of the plastic shrinkage and the effect of the SR in FG. To establish the cracking tendency, restrained shrinkage tests with different mix parameters and SR concentration need to be carried out. This study provides insight into the effect of activator (i.e., Module and Concentration) on flowability, drying shrinkage and crack behavior of FG paste and the effect of SR on reducing drying shrinkage, cracking potential and width comparing with PC as reference for the further application of FG.

Experimental Program

Materials

The chemical composition of ASTM C618 Class C fly ash used in this study is shown in Table 1 as well as ASTM C150 Type I/II Portland cement for reference. The Class C fly ash has a specific gravity of 2.52 and a fineness of 419.6 m^2/kg. The fly ash was alkali-activated with an activator (Na_2SiO_3+NaOH) having a SiO_2/Na_2O mole ratio (Module) of 1.0 and 1.5 and a solute (i.e. Na_2SiO_3 and NaOH) mass concentration (Concentration) of 40% and 50%. The products specifications of Na_2SiO_3 and NaOH are listed in Table 2. A hexylene-glycol -based SR was added at a dosage of 2% (by mass of binder) recommended by manufacture. The admixture was mixed with the activator solution.

Mix proportion and test method

FG and Portland cement (PC) pastes, with and without SR, were prepared with a liquid to binder ratio of 0.33 in a laboratory Hobart mixer following ASTM C305. The mix proportions are present in Table 3.

Flowability

The flowability of paste samples was measured using the mini slump cone in accordance with modified ASTM C1611 test method as shown in Fig. 1. In previous studies, it is shown that the workability of the paste is directly related to the spread it attains (Collins and Sanjayan 1998, Roussel 2006). The geometry of the plastic mini slump cone is 20 mm in top diameter, 40 mm in bottom diameter, and 54 mm in height. Fresh paste was immediately poured into the cone after mixing and the cone was lifted as slowly as possible (<0.005 m/s) (Gao and Fourie 2015) to minimize inertial effects. After 1 min, the spread of paste flow was measured using a ruler across

two perpendicular diameters as exhibited in Fig. 2. The slump flow was conducted three times for each mixture in order to obtain an average slump flow, D in mm, from the six measurements.

Compressive strength

FG and cement pastes (50.8 mm cube) with three replicates per mixture were prepared in accordance with ASTM C109. These specimens were cover with moist cloth and cured at 50±2℃ and 55% relative humidity (RH) for 24 h. They were subsequently removed from the molds and cured until the testing ages. The compressive strengths of the specimens were measured at the age of 3, 7 and 28 days.

Drying shrinkage

Six 10×10×60 mm prisms for each mixture were prepared for drying shrinkage measurement, stainless steel contact studs were positioned at each end of prisms similar to the test apparatus described in ASTM C157 as shown in Fig. 3. Fresh paste was poured into the mold in one layer and consolidated for five seconds using a vibration table. The prisms were then sealed and cured at 50±2℃ and 55% RH for seven days, then stored at 23±2℃ and 50±4 % RH in the laboratory condition. Length change of each prism was measured using a micrometer (Fig. 4) with a 0.01 mm accuracy up to 56 days. The initial reading was taken as the measurement after 7 days curing. The weight loss of each prism was recorded every time before shrinkage measurement.

Restrained ring shrinkage

Three restrained paste rings of each mixture were prepared in accordance with modified ASTM C1581. The geometry of the specimen is modified to 150 mm in external diameter, 100 mm in internal diameter and 30 mm in height as shown in Fig. 5. The restrained ring shrinkage of FG paste was studied using a ring type specimen. The mixtures were placed between the outer ring and the inner ring molds made of steel with the same thickness of 5 mm and height of 30 mm. The

outer ring and inner ring were fixed on a wooden board by a wooden bar on top with two screws tightened as shown in Fig 5.

In restrained ring tests, pastes were cast around a steel ring that resisted the free shrinkage of the paste. The compressive strain accumulation in the steel ring which induces tensile stresses in the paste was monitored using two strain gauges that were attached to the two symmetrical positions of the inside surface of the inner ring. If the shrinkage-induced tensile stresses are higher than the tensile strength of the paste, cracks develop in the paste. The occurrence of a crack in the paste was normally indicated by a sudden decrease of the measured compressive strain in the steel. The time to cracking is used as an index of the cracking tendency of the paste. The cast ring specimens were consolidated by a vibrating table for five seconds and then stored in drying condition at 23 ± 2°C temperature and a RH of 50 ± 4%. After removing the wooden bar and releasing outer ring, the lead-wires were connected to modules in data acquisition system (DAS) to collect data every minute. This DAS consisted of one battery, one CR1000 data logger and two AM16/32 multiplexers as shown in Fig. 6. The specimens were then covered with a polythene sheet and wet towel. After 24 hours, the outer steel ring was removed. The top surface was coated with paraffin wax as shown in Fig. 7. Strain gauge data were recorded automatically by the data logger. The test ended until a sudden decrease in compressive strain in one or both strain gauges occurred.

The time and width of cracking, and the stress rate were obtained from each restrained ring and average values were reported for each mixture. Three test specimens for each mixture were prepared and the averages of three replicates were exhibited for all results. The time to cracking of a ring specimen is used as a principal measure of the tendency of a paste mixture to crack. When cracks develop in the paste, the shrinkage induced tensile stress in the paste dissipates, and

correspondingly there is a sharp compressive strain drop in the steel ring. The time when the strain drops in the steel ring indicates that a crack has formed in the paste. The crack width was measured with a visual crack comparator right after crack appeared by taking the average from 3 uniformly distributed points along the crack. The stress rate determination is similar to ASTM C 1581. Eq. (1) introduces the strain rate factor for tested paste specimen:

$$\varepsilon_{net} = \alpha\sqrt{t} + k \quad (1)$$

Where:

ε_{net} is net strain, m/m, α is the strain rate factor for each strain gauge on the test specimen, i.e. slope of the line, (m/m)/day$^{1/2}$, t is elapsed time, days, and k is the regression constant.

The stress rate in each test specimen at cracking is expressed in Eq. (2):

$$q = \frac{G|\alpha_{avg}|}{2\sqrt{t_r}} \quad (2)$$

Where:

q is stress rate in each test specimen, MPa/day, G, a constant for the ring setup (See 2003), is given by Eq. (3) (42 GPa), $|\alpha_{avg}|$ is absolute value of the average strain rate factor for each test specimen, (m/m)/day$^{1/2}$, and t_r is elapsed time at cracking for each test specimen, days.

$$G = \frac{E_{st} r_{ic} h_{st}}{r_{is} h_c} \quad (3)$$

Where:

E_{st} is the modulus of elasticity of the steel (189 GPa), h_{st} and h_c are the thicknesses of the steel and specimen, respectively, and r_{is} and r_{ic} are the internal radii of the steel and specimen, respectively.

Finally, the average stress rate, MPa/day, is determined-based on the stress rates of three tested specimens which is an index for cracking potential.

Results and Discussion

Flowability

Fig. 8 reports the average slump flow values of each mixture. None of the pastes exhibited noticeable bleeding during the mini-slump test. The flowability of the geopolymer pastes depended on Concentration, Module and addition of SR. In general, mixtures with 2% SR addition howed decreased slump flow compared to those without SR. It is most likely due to the hexylene glycol-based SR used in this study is sticky, therefore increasing viscosity of mixtures and therefore yielding a lower slump flow as reported by Bilek (Bilek et al. 2017). Paste mixtures with 50% Concentration showed dramatically reduced slump flow while those with 40% Concentration showed increased slump flow compared to PC mixture. Chindaprasirt reported the similar results and stated that it was attributed to higher Concentration leading to an increased viscosity of the mixture (Chindaprasirt et al. 2007). Also, high Module results in a lower slump flow mixture due to more silica content promotes the precipitation of larger molecular species resulting in a stronger gel with an enhanced density (Zuda et al. 2006).

Compressive strength

Compressive strengths of all the mixtures are shown in Fig. 9. SR seems to have marginal effects on strength compared to their corresponding mixtures without SR. Mixtures with Module of 1.0 at 50% Concentration have the highest strength while higher Module of 1.5 seems to adversely affect strength at all ages. Higher Concentration yields a higher compressive strength regardless of Module. The effects of Modules and Concentration can be attributed to reaction rate and degree that lead to different porosity of products and the trends comply with previous (Fernandez and Palomo 2005, Rattanasak and Chindaprasirt 2009). A majority FG paste mixtures

have higher strength up to 28 days except the mixtures prepared with 1.5 Module at 40% Concentration.

Drying shrinkage

Mass loss of the specimens for free drying shrinkage test

The results of mass loss of paste specimens for all 10 mixtures are presented in Fig. 10. The specimens started free drying condition since day 0. It can be seen that the major portion of mass loss occurs during the first 14 days. PC-SR displays the least amount of mass loss and 1.5-50% shows the greatest amount of mass loss. For the pastes without SR, marked as solid lines, the FG pastes have more mass loss than PC paste and the pastes of 1.5 Module lose much more mass than those of 1.0 Module. Furthermore, with the same Module, pastes with 50% Concentration has more mass loss than 40% Concentration. The same trend of mass loss was found in the pastes with SR addition. Additionally, The SR addition reduced mass loss for all pastes. This effect is substantial on the pastes with 1.5 Module.

Free drying shrinkage

Fig. 11 illustrates the free drying shrinkage test results of PC and FG pastes, with and without SR in the course of 56 days. The primary shrinkage occurred in the first 14 days. The lowest drying shrinkage exhibited mixture of 1.5-40%-SR and the mixture of 1.0-50 had the highest drying shrinkage. Regardless of the addition of SR, the dependence that with decreasing Module or increasing Concentration the drying shrinkage increases is evident for FG mixtures. FG mixtures have comparable drying shrinkage with PC mixtures for either with or without SR. Comparing the specimens between with SR and without SR, the SR was able to significantly reduce the drying shrinkage up to 52% for 1.0-50% mixture. The effect of SR on FG mixtures was as strong as PC mixture.

Comparing the results of drying shrinkage and mass loss, it can be seen that the greater magnitude of mass loss did not lead to a higher drying shrinkage. For example, 1.0-50% mixture with maximum shrinkage has quite low mass loss among the other mixtures. This indicates that the mass loss is no longer the only dominant factor for drying shrinkage of FG mixture. It has been proposed that the drying shrinkage behavior of geopolymer is a function of pore size distribution and thermodynamic behavior of water in the pores (Shimomura and Maekawa 1997, Shimomura 1998). Collins put forward that capillary tensile forces set up during drying was a very significant factor for the drying shrinkage of geopolymer (Collins and Sanjayan 2000).

Restrained ring shrinkage

The restrained ring shrinkage results of PC and FG pastes, with and without SR, are present in Fig. 12. It is apparent that 1.0-50% mixture displayed the greatest amount of shrinkage and 1.5-40%-SR mixture occurred the least shrinkage. With or without SR, it can be found that the mixtures with 50% Concentration have more shrinkage than those with 40% Concentration and the shrinkage of 1.0 Module mixtures is larger than that of 1.5 Module because the drying shrinkage is a direct result of hydration heat and the increase in alkaline concentration and NaOH percentage could increase the degree of hydration reaction (Pacheco et al. 2007, Fernandez et al. 2007). The SR addition considerably decreases the shrinkage appeared in PC and FG pastes up to 16% for 1.0-50% mixture.

Based on the time of a sudden increase of strain, the time of cracking for all mixtures was given in Fig. 13. The PC mixture cracked earliest while the 1.5-40%-SR mixture cracked the latest. For mixtures with and without SR, PC mixtures cracked earlier than FG mixtures. Moreover, increasing Module leads to increased cracking time while increasing Concentration decreased cracking time. With the addition of SR, cracking time for all mixtures was postponed.

The crack width measured from cracked ring specimens for all pastes is shown in Fig. 14. The range of crack width is from 0.2 mm (1.5-40%-SR) to 6 mm (1.5-50%). The mixtures of 50% Concentration have wider crack width than PC mixture while those of 40% Concentration exhibit narrower crack than PC mixture for both with and without SR. Regarding to the same Concentration, the mixtures of 1.5 Module occurred less crack width than those of 1.0 Module. In the case of a certain Module, the 50% Concentration had an effect of larger crack width than 40% Concentration on FG mixtures. The existence of SR in mixtures apparently reduced the crack width, especially for 1.0-50% and 1.5- 50%.

The cracks from failure ring specimens were measured from photographs (Fig. 15). Since the crack width of replicates is similar, only one crack photo from each mix is presented. The width of crack is the average of three replicates for each mix.

The stress rate of all mixtures, with and without SR, were derived from Eq. (2). Their results are illustrated in Fig. 16. The magnitude of stress rate during restrained ring shrinkage indicates the cracking potential of pastes according to ASTM C1581. PC and 1.5-40% mixture show the highest cracking potential with SR and lowest cracking potential without SR. Without SR, FG mixtures exhibited lower cracking potential than PC. At equal Concentration, FG mixtures with 1.0 Module had higher cracking potential than those with 1.5 Module. However, for a given Module, the mixtures of 50% Concentration performed cracking earlier comparing with 40% Concentration mixtures. SR addition had a substantial effect towards reducing the cracking potential for both PC and FG pastes. This effect on PC was greater than on FG.

In general, if the tensile stresses caused by drying shrinkage of ring specimen are higher than the tensile strength of the pastes themselves, the cracks occur. However, the drying shrinkage is not only related to moisture loss but also the tensile force in pore structure for FG pastes (Collins

and Sanjayan 2000). Fig. 17 shows the relationship between stress rate and cracking time of all paste mixtures. Since the trend of stress rate is the same as that of cracking time, the time to cracking could be used to evaluate the cracking tendency of FG pastes.

Conclusions

1. FG has comparable flowability to PC. Increased Module and Concentration could reduce flowability of FG. SR slightly decreased flowability of PC and FG.

2. The FG exhibited considerably higher compressive strength than PC, especially for the mixtures with 1.0 Module and 50% Concentration.

3. Mass loss is not the only reason for drying shrinkage of FG. The drying shrinkage of FG was similar to that of PC. The drying shrinkage raised with decreasing Module or increasing Concentration for FG. The SR significantly reduced the drying shrinkage of FG up to 52% as well as PC.

4. Based on the results of ring shrinkage test, the FG with higher Concentration or lower Module have more shrinkage. The SR substantially decreased the restrained shrinkage appeared in both PC and FG pastes up to 16%. The PC cracked earlier than FG. An increment in Module or a decrease in Concentration brought the cracking forward on FG. With the SR addition, the cracking time was delayed for both PC and FG. The FG of 40% Concentration exhibited smaller crack than PC. The FG of increased Module or decreased Concentration occurred reduced crack width. The existence of SR apparently reduced the crack width, especially for 1.0-50% and 1.5-50%.

5. According to stress rate results of restrained ring shrinkage test, the FG mixtures performed lower cracking potential than PC and the decreased Module or increased Concentration made

them easier to crack. The SR addition lowered the cracking potential for both PC and FG pastes. It should be aware that the time to cracking could be used as an index for the cracking tendency of FG pastes.

Acknowledgments

Authors wish to thank the Robert F, Steffes and Gilson R, Lomboy for their support in materials and equipment used in this study.

References

ASTM C109/C109M, (2013). "Standard Test Method for Compressive Strength of Hydraulic Cement Mortars," Philadelphia: ASTM International.

ASTM C150, (2017). "Standard Specification for Portland cement," Philadelphia: ASTM International.

ASTM C1581/C1581M, (2016). "Standard Test Method for Determining Age at Cracking and Induced Tensile Stress Characteristics of Mortar and Concrete under Restrained Shrinkage," Philadelphia: ASTM International.

ASTM C1611/C1611M, (2014). "Standard Test Method for Slump Flow of Self-Consolidating Concrete," Philadelphia: ASTM International.

ASTM C305, (2014). "Standard Practice for Mechanical Mixing of Hydraulic Cement Pastes and Mortars of Plastic Consistency," Philadelphia: ASTM International.

ASTM C618, (2018). "Standard Specification for Coal Fly Ash and Raw or Calcined Natural Pozzolan for Use in Concrete," Philadelphia: ASTM International.

Bakharev, T., Sanjayan, J.G., Cheng, Y.-B. (2000). "Effect of Admixtures on Properties of Alkali-Activated Slag Concrete," Cement and Concrete Research 30 (9), pp. 1367–1374.

Berke, N.S., Dallaire, M.P., Hicks, M.C., Kerkar, A. (1997). "New Developments in Shrinkage-Reducing Admixtures," CANMET/ACI 5th International Conference on Superplasticizers and Other Chemical Admixtures in Concrete. Supplementary Papers. Ed. Malhotra, pp. 971–998.

Bilek, V., Kalina L., and Fojtik, O. (2017). "Shrinkage-Reducing Admixture Efficiency in Alkali-Activated Slag across the Different Doses of Activator," Key Engineering Materials 761, pp. 19-22.

Cabrera, J.G., Cusens. A.R., Brookes-Wang, Y. (1992). "Effect of Superplasticizers on the Plastic Shrinkage of Concrete," Magazine of Concrete Research 44(160), pp. 149–155.

Castel, A., Foster, S. J., Ng, T., Sanjayan, J. G., Gilbert, R. I. (2016), "Creep and Drying Shrinkage of A Blended Slag and Low Calcium Fly Ash Geopolymer Concrete," Materials and Structures 49(5), pp. 1619–1628.

Chindaprasirt, P., Chareerat, T., Sirivivatnanon, V. (2007). "Workability and Strength of Coarse High-calcium Fly Ash Geopolymer," Cement and Concrete Composites 29(3), pp. 224-229.

Collins, F., and Sanjayan, J.G. (1998). "Early Age Strength and Workability of Slag Pastes Activated by NaOH and Na_2CO_3," Cement and Concrete Research 28(5), pp. 655-664.

Collins, F., and Sanjayan, J.G. (2000). "Sanjayan, Effect of Pore Size Distribution on Drying Shrinking of Alkali-Activated Slag Concrete," Cement and Concrete Research 30 (9), pp. 1404–1406.

Crentsil, K.S., Brown, T., Taylor, A. (2013). "Drying Shrinkage and Creep Performance of Geopolymer Concrete," Journal of Sustainable Cement-Based Materials 2(1), pp. 35-42.

Deb, P.S., Nath, P., Sarker, P.K. (2015). "Drying Shrinkage of Slag Blended Fly Ash Geopolymer Concrete Cured at Room Temperature," Procedia Engineering 125, pp. 594-600.

Fernandez-Jimenez, A., Garcia-Lodeiro, I., Palomo, A. (2007). "Durability of Alkali-Activated Fly Ash Cementitious Materials," Journal of Materials Science 42(9), pp. 3055-3065.

Fernandez-Jimenez, A., Palomo, A. (2005). "Composition and Microstructure of Alkali Activated Fly Ash Binder: Effect of the Activator," Cement and Concrete Research 35(10), pp. 1984-1992.

Gao, J., Fourie, A. (2015) "Spread Is Better: An Investigation of the Mini-Slump Test," Minerals Engineering 71, pp. 120–132.

Kheradmand, M., Abdollahnejad, Z., Torgal, F.P. (2017). "Drying Shrinkage of Fly Ash Geopolymeric Mortars Reinforced with Polymer Hybrid Fibres," Construction Materials, 10.1680.

Mora, J., Aguado, A., Gettu, R. (2003). "The Influence of Shrinkage-Reducing Admixtures on Plastic Shrinkage," Materials Construction 53 (271–272), pp. 71–80.

Pacheco-Torgal, F., Castro-Gomes, J., Jalali, S. (2007). "Alkali-Activated Binders: A Review. Part 2. About Materials and Binders Manufacture," Construction and Building Materials 22(7), pp.1315-1322.

Puertas, P., Amat, T., Vazquez, T. (2000). "Behaviour of Alkaline Cement Mortars reinforced with Acrylic and Polypropylene Fibers," Materials Construction 50 (259), pp. 69–84.

Rattanasak, U., and Chindaprasirt, P. (2009). "Influence of NaOH Solution on the Synthesis of Fly Ash Geopolymer," Minerals Engineering 22(12), pp. 1073–1078.

Roussel, N., (2006). "Correlation between Yield Stress and Slump: Comparison between Numerical Simulations and Concrete Rheometers Results," Materials and Structures 39(4), pp. 501-509.

See, H. T., Attiogbe, E. K., and Miltenberger, M. A. (2003). "Potential for Restrained Shrinkage Cracking of Concrete and Mortar," Proceedings of the ASTM Symposium on Early-Age Cracking of Concrete, Dec. 2003.

Shi, C. (1996). "Strength, Pore Structure and Permeability of Alkali-Activated Slag Mortars," Cement and Concrete Research 26 (12), pp. 1789–1799.

Shimomura, T. (1998). "Modelling of Initial Defect of Concrete Due to Drying Shrinkage," Proc. CONSEC '98 Concrete Under Severe Conditions, Norway vol. 3, pp. 2071-2083.

Shimomura, T., Maekawa, K. (1997). "Analysis of the Drying Shrinkage Behavior of Concrete Using a Micromechanical Model Based on the Micropore Structure of Concrete Using A Micromechanical Model," Magazine of Concrete Research 49 (181), pp. 303-322.

Soroushian, P., Ravanbakhsh, S. (1998). "Control of Plastic Shrinkage Cracking with Specialty Cellulose Fibers," ACI Materials Journal 95(4), pp. 429–435.

Zuda, L., Pavlik Z., Rovnanikova, P., Bayer, P., Cerny, R. (2006). "Properties of Alkali Activated Aluminosilicate Material after Thermal Load," International Journal of Thermophysics 27(4), pp. 1250-1263.

Table 1. Chemical composition of fly ash and Portland cement

	SiO_2	Al_2O_3	Fe_2O_3	SO_3	CaO	MgO	Na_2O	K_2O	P_2O_5	LOI
Fly ash	30.7	16	6.8	3.5	28.8	6.74	2.97	0.27	0.64	0.49
PC	20.1	4.4	3.1	2.8	64	2.22	0.14	0.58	0.06	2.46

Note: All values in mass %, expressed on an oven-dry basis; LOI: loss on ignition at 1000°C

Table 2. Specification of sodium silicate solution and sodium hydroxide

Product	Sodium silicate solution (Na_2SiO_3)	Sodium hydroxide (NaOH)
Company	Sigma-Aldrich	Fisher Scientific
Grade	Reagent	Certified ACS
Composition	Na_2O: 10.6%, SiO_2: 26.5%	NaOH Solid
Density	1.39 g/ml	2.13g/ml
Formula	$(NaOH)_x(Na_2SiO_3)_yzH_2O$	NaOH

Table 3. Mix proportion of pastes

Mixture	Activator		Admixture
	Module	Concentration, %	
1.0-40% 1.0-40%-SR	1.0	40	– SR
1.0-50% 1.0-50%-SR	1.0	50	– SR
1.5-40% 1.5-40%-SR	1.5	40	– SR
1.5-50% 1.5-50%-SR	1.5	50	– SR
PC PC-SR	Water		– SR

Note: Mixtures in this paper are all identified as Module-Concentration-Admixture

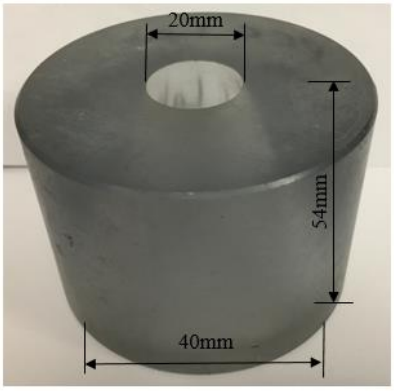

Figure 1. Mini slump cone

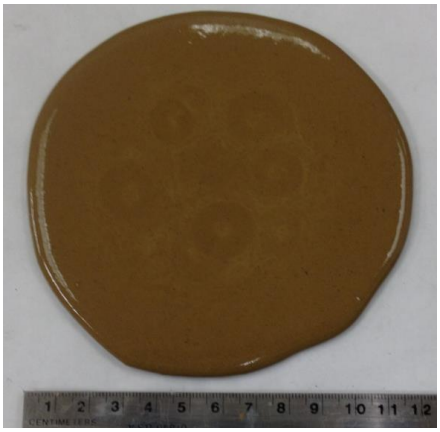

Figure 2. Paste spread flow in mini slump test

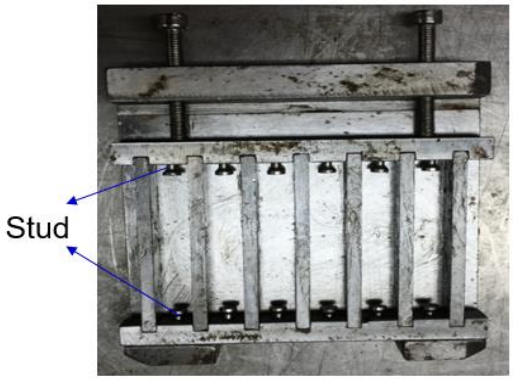

Figure 3. Mold for drying shrinkage

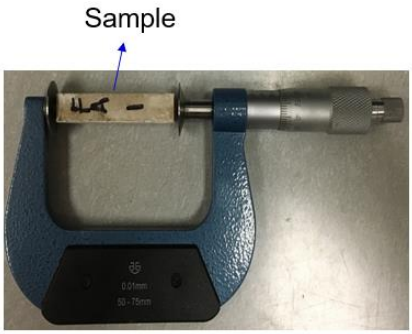

Figure 4. Micrometer for drying shrinkage measurement

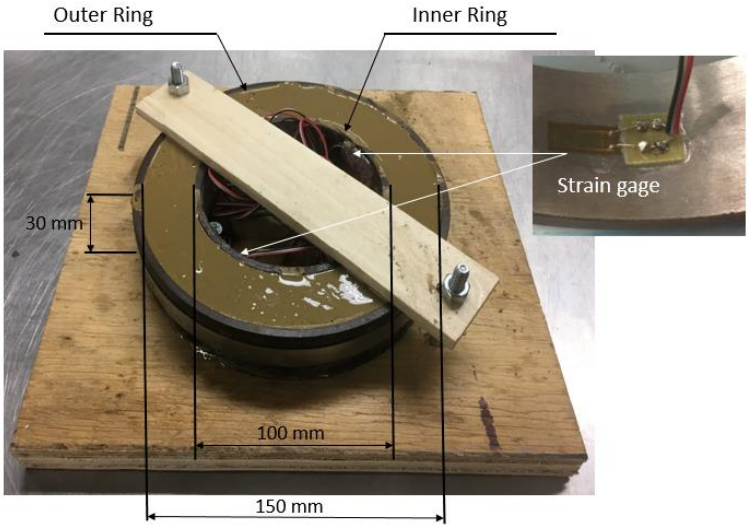

Figure 5. Restrained ring shrinkage test set-up

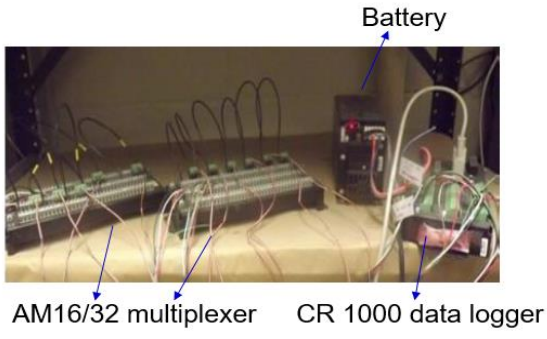

Figure 6. DAS for restrained ring shrinkage test

Figure 7. Paste ring specimen under drying

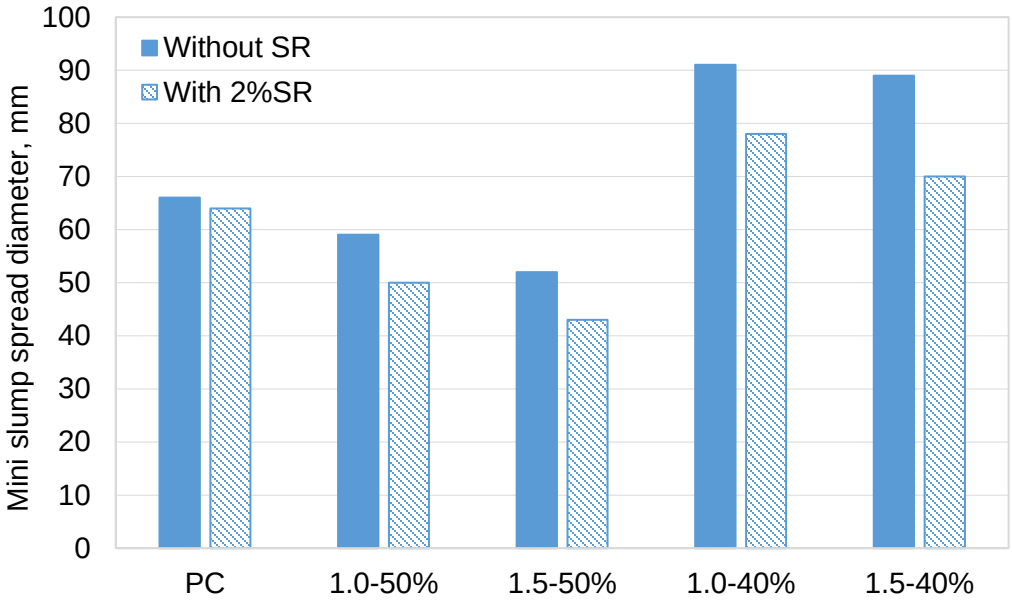

Figure 8. Mini slump spread diameter of FG and cement paste

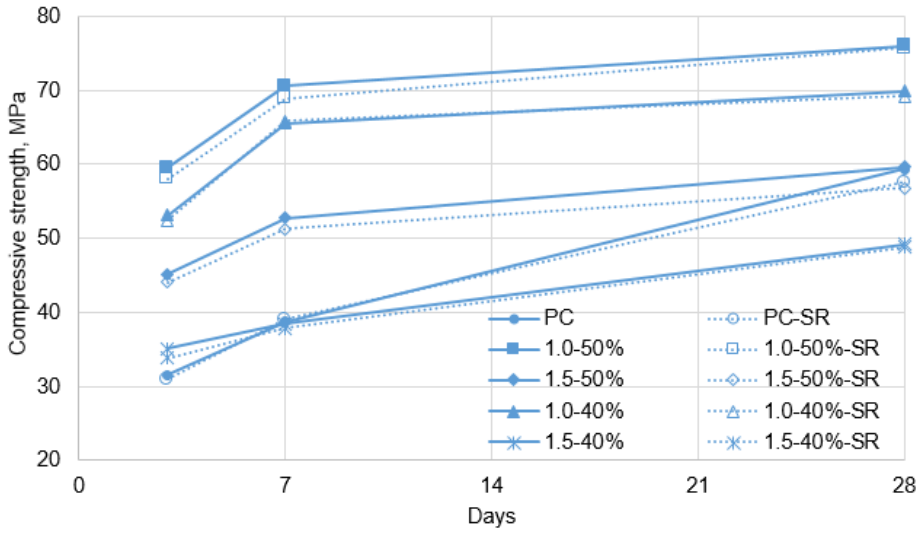

Figure 9. Compressive strength of FG and PC paste with and without SR

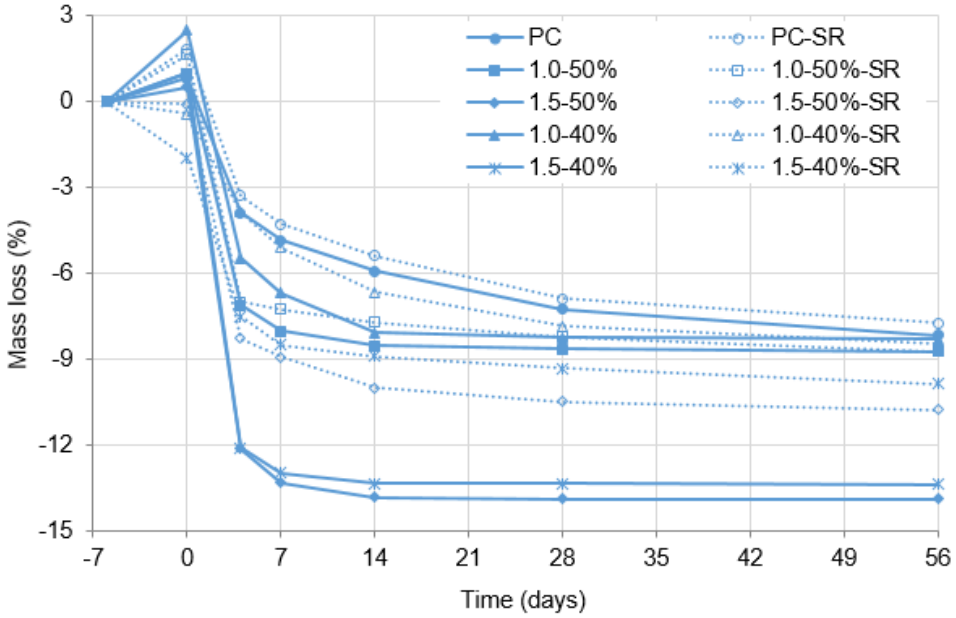

Figure 10. Mass loss of PC and FG pastes

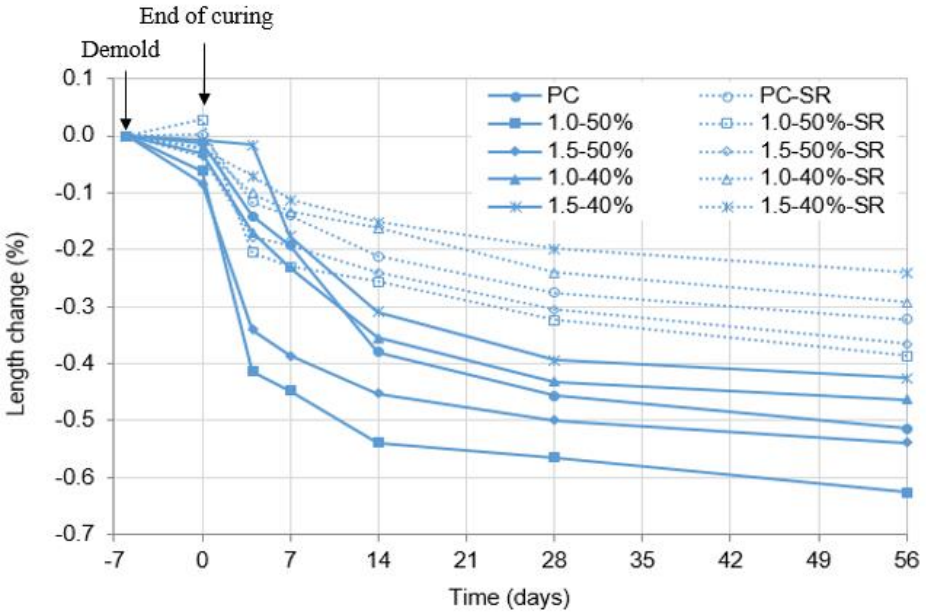

Figure 11. Free drying shrinkage of PC and FG pastes

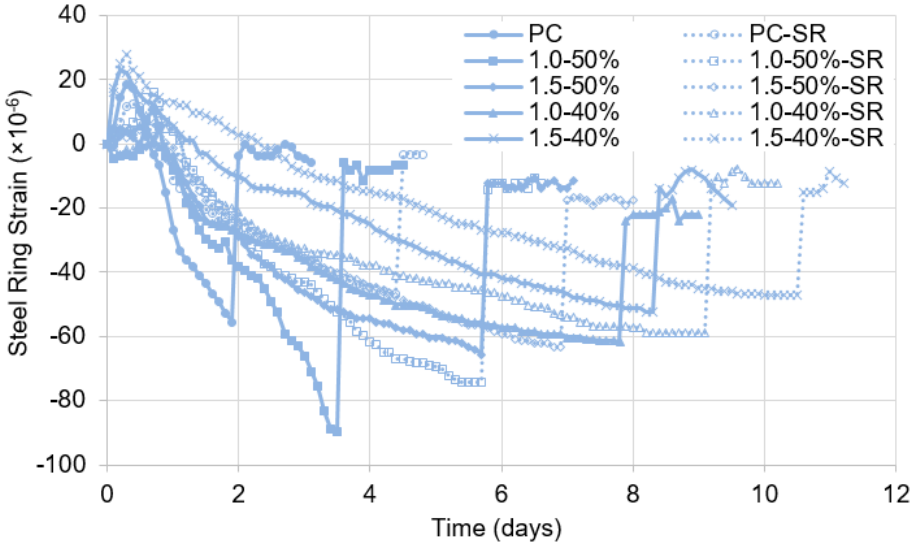

Figure 12. Restrained ring shrinkage for PC and FG pastes

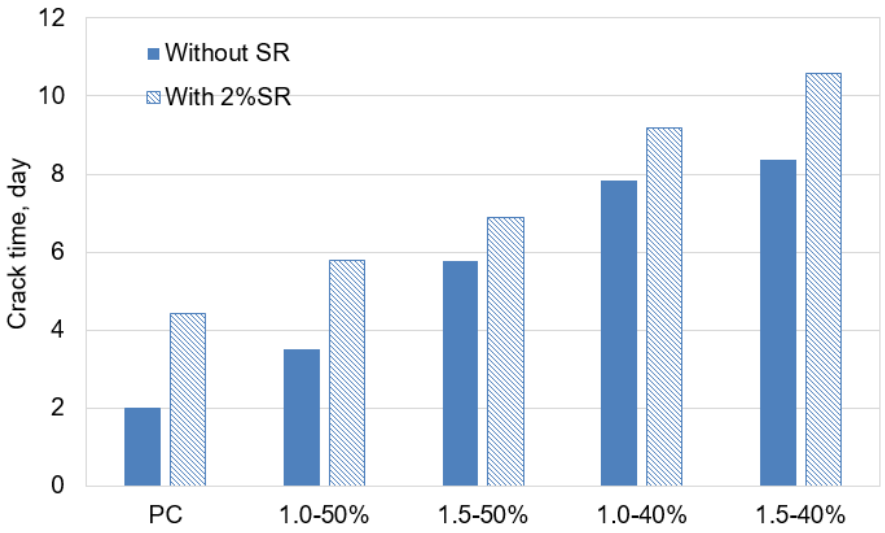

Figure 13. Cracking time of PC and FG pastes in restrained rig test

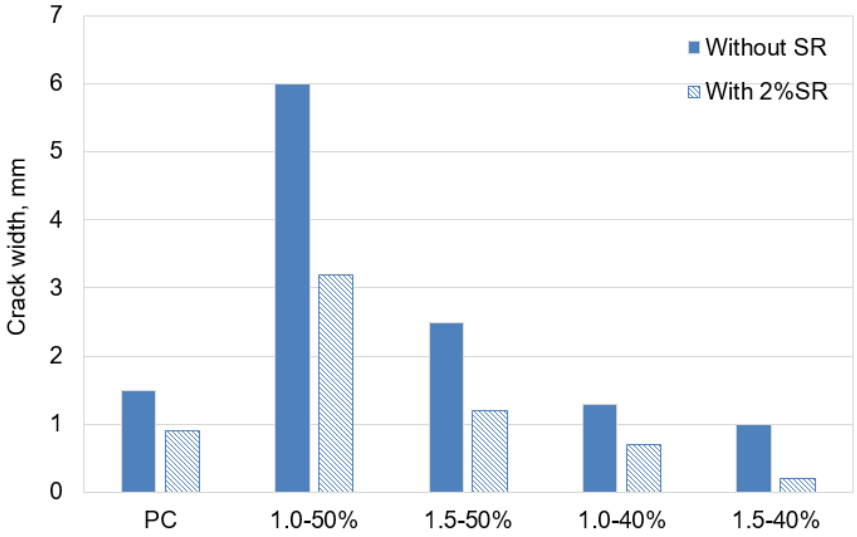

Figure 14. Crack width of PC and FG pastes in restrained ring test

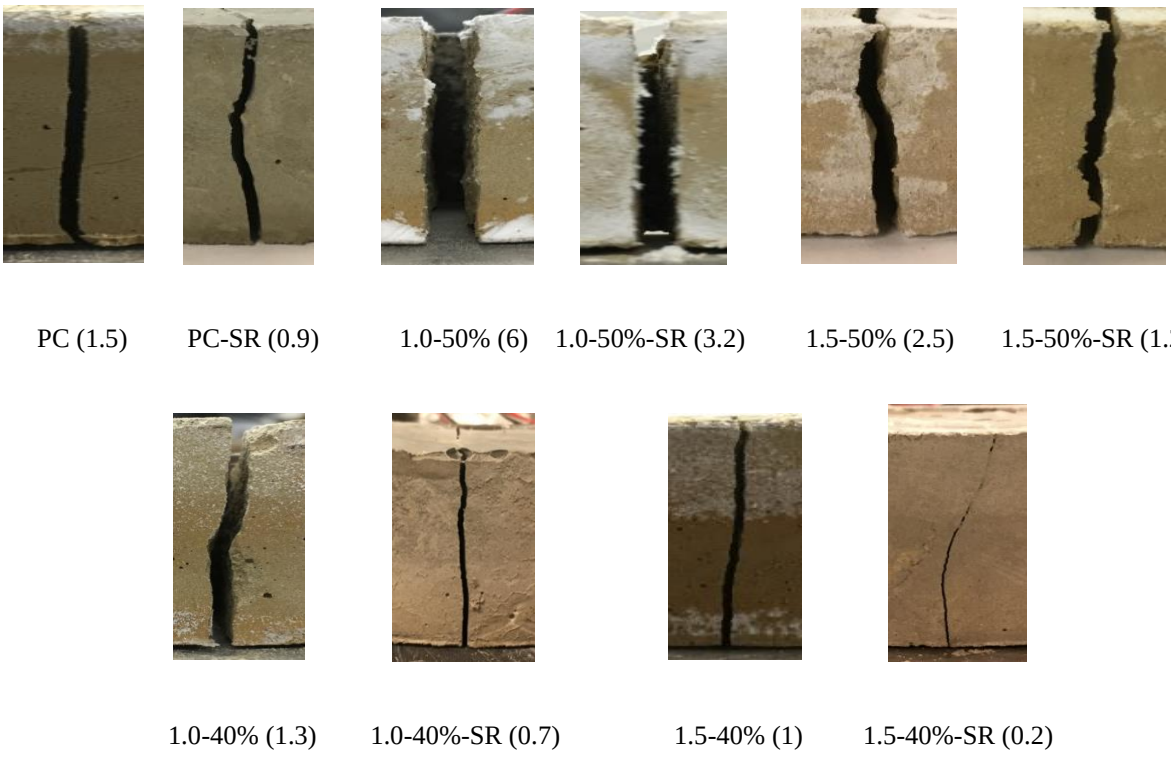

Figure 15. Cracks on ring specimens (widths were presented in mm)

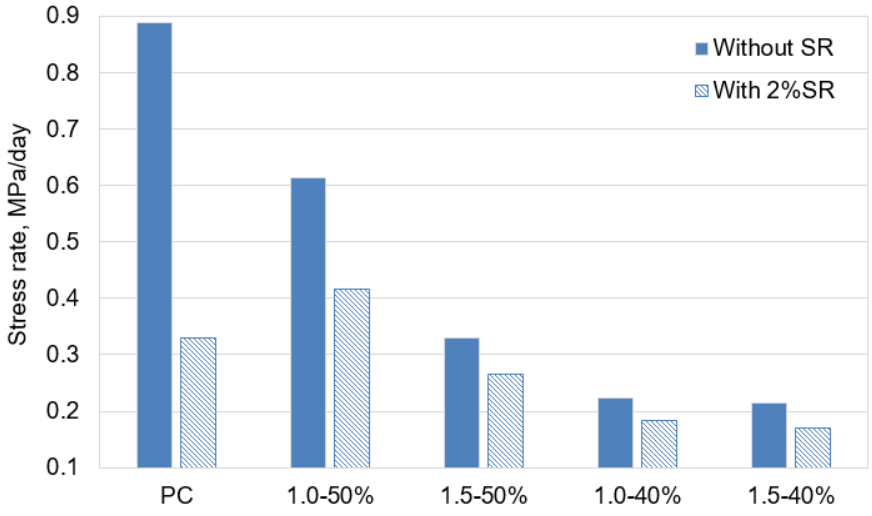

Figure 16. Stress rate of PC and FG pastes during restrained ring shrinkage

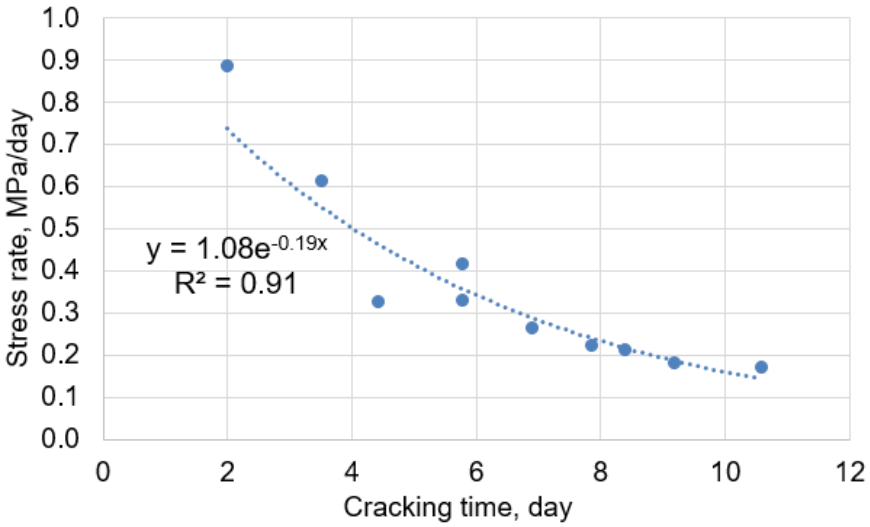

Figure 17. Stress rate vs. cracking time of PC and FG pastes

CHAPTER 6.THE EFFECT OF SLAG ON MECHANICAL PROPERTIES OF ENGINEERED GEOPOLYMER COMPOSITE

Yifeng Ling, Kejin Wang, Guyu Shi

Department of Civil, Construction and Environmental Engineering, Iowa State University, Ames IA 50010

Abstract

This paper aimed to investigate the effect of slag replacement on mechanical properties of low-calcium (Class F) fly ash-based engineered geopolymer composite (EGC). In this regard, four different percentages of slag replacement (i.e., 0%, 10%, 20%, 30%) were used with NaOH and Na_2SiO_3 combined activator to develop the fly ash-based EGCs exhibiting strain hardening behavior under uniaxial tension. Randomly oriented short polyvinyl alcohol (PVA) fibers (2% by volume of matrix) were employed to reinforce the relatively brittle fly ash-based geopolymer matrix. The mechanical properties of the EGCs, including compressive strength, elasticity, uniaxial tensile behavior, flexural bending strength and pullout bond strength, were evaluated. Experimental results revealed that all EGCs exhibited strain hardening behavior. 20% slag replacement improved the mechanical strength most. However, as slag replacement was increased, the tensile strain capacity, ultimate deflections, toughness and ductility decreased. In addition, bond strength can be estimated from compressive strength of EGCs.

Key words: Engineered geopolymer composite (EGC), Fly ash, Slag, Pullout test, Mechanical property

Introduction

Engineered cementitious composite (ECC) incorporating a small amount of discontinuous fibers (typically 2% or less by volume) is about 600 times as ductile as normal Portland cement concrete in tension (Li and Kanda 1998) and exhibits a tensile strain capacity of up to 6% (Kong et al. 2003). However, a typical ECC mix design has a two to three times higher cement content compared to conventional Portland cement (PC) concrete (Wang and Li 2007). The high cement content in ECC mix design apparently compromises sustainability performance of this material (Wang and Li 2007). Hence, it is necessary to develop economical ECCs with lower CO_2 emissions during cement production, while maintain the tensile ductility properties. The best solution to achieve this goal is to completely replace the PC binder in the ECC mix design by an alternative cementless binder, such as geopolymer.

Recent studies (e.g., Fernandez et al. 2006, Sofi et al. 2007) have reported similar mechanical properties of geopolymer concrete that are favorable for its use as a construction material. The bonding behavior between the concrete and the reinforcing steel is an important mechanism for the performance of reinforced concrete as a composite material. It is important to understand the bonding behavior of geopolymer composite in order to use it as an alternative to PC concrete in reinforced concrete structures. Limited research (i.e., pull-out tests) have been conducted to assess bonding strength of fly ash geopolymer mixtures (Fernandez et al. 2006, Sofi et al. 2007). Comparable results were derived for both fly ash geopolymer and PC mixtures.

Recently, a feasibility study was conducted to develop a geopolymer-based ECC, known as engineered geopolymer composite (EGC), where the PC binder was completely replaced by a fly-ash-based geopolymer binder. Mechanical test results indicated that the EGC exhibited strain hardening and deflection hardening behaviors (in uniaxial tension and bending, respectively) were

accompanied by multiple cracking (Ohno and Li 2014). However, their proposed fly-ash-based EGC mixtures possessed low compressive and uniaxial tensile strengths, ranging from 17.4 to 27.6 MPa and 2.9 to 3.4 MPa, respectively, comparing with typical ECC (50 - 60 MPa in compressive strength and 4 – 5 MPa in tensile strength. These low strengths may limit widespread application of these composites in the construction industry. Another study added slag to fly ash-based geopolymer mixtures, yielding significantly improved strength (Li and Liu 2007). This study in Chapter 6 aimed to investigate the mechanical properties, including compressive, flexural bending, tensile and bonding strengths, of the newly developed fly ash-based EGC with partial slag cement replacement. In order to furthest improve strength of fly ash-based EGC, the activator to binder mass ratio was reduced, and the concentration of activator was increased in this paper. These modifications would greatly reduce the workability of fly ash-based EGC. Therefore Class F fly ash was used in this paper to maintain the good workability of EGC because geopolymer made by Class F fly ash has higher workability than Class C fly ash due to lower CaO content in Class F fly ash.

Experimental Program

Materials

The fly ash (FA) used was low-calcium (Class F) with a specific gravity of 2.61 g/cm^3 based on ASTM C618. A ground granulated blast furnace slag with a specific gravity of 2.50 g/cm^3 was also employed in this study. The major chemical components of fly ash and slag are provided in Table 1 as determined by x-ray fluorescence (XRF). The activator was a combination of NaOH and Na_2SiO_3 (water glass). Their products specifications are listed in Table 2. The polyvinyl alcohol (PVA) fibers used in the research were supplied by Kuraray of Japan. The characteristics of used PVA fiber are presented in Table 3.

Mix proportion

Solid NaOH, Na_2SiO_3 solution and tap water were mixed together with a SiO_2/Na_2O mole ratio (Module) of 1.0 and solute (i.e., NaOH and Na_2SiO_3) mass concentration (Concentration) of 60% to prepare the activator. Four fly-ash-based EGC mixtures with 0%, 10%, 20%, and 30% slag replacement by weight of fly ash content were prepared (denoted as (1) FA-0%S, (2) FA-10%S (3) FA-20%S, and (4) FA-30%S respectively). The activator solution to binder (i.e., FA and slag cement) ratio of 0.27 was selected to prepare the EGC mixtures. According to the recommendation from the manufacturer, 2% PVA fibers by volume of matrix was added to EGC mixtures. Table 4 presents mix proportions of fly ash-based EGC mixtures reported in this paper.

Mixing

The mixing procedure was initiated by combining and mixing the binder (i.e., FA and slag) for 2 min in a laboratory Hobart mixer. The alkaline activator solution was prepared 24 h prior to incorporation into the dry mix. This allowed for dissipation of heat attributed to the exothermic chemical reaction of Na_2SiO_3 and NaOH. The solution was then added gradually to the mixer and mixed for another 3 min to ensure a homogeneous and uniform mixture. In each batch, once a consistent matrix was reached, PVA fibers were gradually added, taking care to ensure uniform fiber dispersion. The whole mixing procedure for each composite generally took 8–10 min.

Compressive strength test

As per ASTM C109, the fresh EGC was placed and tamped in two layers in 50.8 mm cubic molds. Cast specimens were compacted for 10 s on a vibrating table. All EGC specimens were subjected to heat curing. In this regard, all molds were sealed to minimize moisture loss and placed in an oven at 50°C for 24 h. At the end of heat curing period, the specimens were removed from

the molds and cured in the oven at 50°C until the day of testing. All EGC specimens were tested 3 days, 7 days and 28 days after casting. For each testing, three replicates were tested in order to check the variability of performance under compression.

Tensile strength test

Uniaxial tension tests were conducted to evaluate the tensile behavior of the developed fly ash-based EGCs. For each mixture, two composite panels in the shape of a dog bone were cast and cured for 28 days in the same environmental conditions as specimens prepared for compressive strength. The schematic of the test specimen and apparatus is illustrated in Fig. 1.

All specimens were tested in uniaxial tension under displacement control using a mechanical testing system (MTS) testing machine with hydraulic wedge grips. In accordance with the Japan Society of Civil Engineers (JSCE), the displacement rate was 0.5 mm/min. Panel specimens were polished on the two ends to facilitate gripping. Specimens were in proper alignment with the machine hydraulic grips. The MTS machine had a fully digital control panel and software to automatically run the tests and collect the load. In addition, two linear variable differential transformers (LVDTs) were also employed to measure displacements between two points on the specimen with a gauge length of 110 mm, as shown in Fig. 1. Resulting load versus displacement data were recorded and tensile stress versus strain curves were plotted.

According to previous studies on micromechanical design of conventional ECCs (Kanda and Li 1999), criteria (i.e., stress-based condition) must be satisfied in order to achieve pseudo-strain hardening (PSH) behavior accompanied with multiple fine cracks. The stress-based condition can be expressed as

$$\sigma_{fc} \leq \sigma_0 \quad (1)$$

where σ_0 = maximum fiber bridging stress (i.e., ultimate tensile strength of the composite); and σ_{fc} = tensile first-crack strength of the composite. Fig. 2 illustrated typical stress (σ) versus strain (ε) curves for strain hardening behavior. According to the stress-based condition, if σ_0 exceeds σ_{fc}, multiple cracking occurs with increasing load. Otherwise, the composite immediately fails after initiation of first crack from a defect site.

In accordance with the stress condition for PSH behavior, Kanda and Li proposed a performance index σ_0/σ_{fc} (Kanda and Li 2006). Theoretically, this index must exceed unity to achieve PSH behavior in a fiber-reinforced composite. The higher the performance index value, the greater the possibility of saturated multiple cracking or saturated PSH behavior, resulting in a higher tensile strain capacity of the composite. The area under the stress-strain curve up to failure can be derived as the tensile toughness of the EGC, which is an indication of the total energy absorption capacity of the material. The tensile toughness and the tensile elasticity (the slope of elastic portion i.e., $\sigma_{fc}/\varepsilon_{fc}$) of EGC were derived from stress-strain curve as shown in Fig. 2.

Flexural bending test

A four-point flexural bending test was carried out on EGC overlay slab to evaluate flexural bending behavior of EGC mixes. For each mix, two slabs with the dimensions of 711 × 108 × 13 mm were cast and cured similar to the cube specimens for 28 days before testing. Each slab was loaded under four-point bending with span of 457 mm between supports and loading was applied symmetrically at 152 mm from the supports using an MTS testing machine. The loading configuration is shown in Fig. 3. Two LVDTs were employed to monitor the midspan deflection of the slab at both sides of middle. In accordance with Martin et al. (2007) and Sarker et al. (2013), the displacement control rate was 0.2 cm/min until its failure. Fig 4. illustrates the EGC slab under bending test.

According to four-point flexural bend model and the loading span is one-third of the support span, the flexural stress could be calculated following Eq. (2):

$$\sigma = \frac{FL}{bd^2} \quad (2)$$

where σ is flexural stress; F is the load at the fracture point; L is the length of the support span; b is the width of slab and d is thickness of slab.

Pullout bond strength test

Direct tension pullout bond test was conducted to investigate the bond strength of steel bar embedded in EGCs. For each mix, two cylinders of Φ152 × 152 mm (Φ=diameter) with a Φ12.6 × 609.6 mm smooth steel bar embedded in the center of specimen as shown in Fig. 5, were cast and cured similar to the cube specimens for 28 days before testing. The properties of the used steel bar are shown in Table 5. The steel bar was covered by a 76 mm long polyvinyl chloride (PVC) tube along the top half of cylinder where the steel bar is free to move and embedded all the way through the cylinder with 19 mm out of specimen bottom as shown in Fig. 5. Therefore, the effective bond length between EGC and steel bar is 76 mm. The reason for PVC tube covering is to avoid stress concentration on EGC during pullout. During the test, the top of steel bar was gripped by the wedge on MTS machine. An alloy plate was placed on the top surface of EGC cylinder by four bolts tightened on four threaded rods to fix the EGC cylinder as seen in Fig. 5. The steel bar was subjected to a tensile force that is transferred to the EGC as tensile stresses throughout the bond stresses between the EGC and the steel.

An average result of two specimens was derived for each EGC mixture. The bar slip was recorded by the two LVDTs installed on the two sides of cylinder for until failure. In order to compensate the displacement on the steel bar itself caused by tension, a micro-strain gauge was

pre-installed on the steel bar surface. The strain of the steel during the pullout test was recorded by a data logger until failure. The bond stress was computed using Eq. (3):

$$\tau = P/(\pi L_e d_b) \quad (3)$$

where τ is the bond stress; P is the load; L_e is the contacted length of bar in EGC; and d_b is the bar diameter. The slip of bar (s) was calculated according to Eq. (4)

$$s = d_L - \varepsilon \times L_e \quad (4)$$

where d_L is the displacement of bar from LVDT; and ε is the microstrain of bar from the strain gauge.

All specimens were tested under displacement control rate of 0.3 mm/min in accordance with Qian and Li. (2011). A schematic of the pullout test setup is shown in Fig. 5.

Results and Discussion

Compressive strength

The compressive strength of each EGC mixture with standard error bars is presented in Fig. 6. The 20% slag EGC mixture exhibited the highest compressive strength at all testing ages that is likely due to the production of aluminosilicate hydrate and calcium silicate hydrate gels (Palomo 1999, Chi 2012). However, further replacement of slag to 30% led to a decreased compressive strength. This is consistent with a previous report that attributed to excessive Ca undergoes a hydration reaction forming $Ca(OH)_2$ which might lead to expansion therefore decreased the strength (Wardhono et al. 2017). The compressive strength of 10% slag replacement EGC mixture only slightly increased at 28 days compared to 0% slag cement replacement mixture. The same

trend on compressive strength with different percentage of slag replacement has been reported previously (Hassan and Ismail 2018).

Tensile strength

Tensile stress-strain behaviors of the EGC mixtures are presented in Fig. 7. all the mixtures exhibited strain hardening behavior accompanied by multiple cracking because of the bridging mechanism of the PVA fibers. The uniaxial tensile strength of the EGC mixtures with slag addition developed in this paper are higher than those of the slag-based EGCs developed by Lee et al. (2012) and the fly ash-based EGCs developed by Ohno and Li (2014).

The first-crack strength (σ_{fc}), tensile elasticity, ultimate tensile strength (σ_0), tensile strain capacity, toughness and stress index (σ_0/σ_{fc}) of each mix are list in Table 6. The ultimate tensile strengths of all the EGC mixtures were significantly higher than the first crack strength. FA-20%S exhibited the highest first-crack strength which corresponds to its highest ultimate tensile strength. The first-crack strength of FA-30%S, FA-10%S, and FA-0%S were 16.1, 32.3, and 45.2% lower, respectively. The ultimate tensile strength of FA-30%S, FA-10%S, and FA-0%S were 10.3, 25.0, and 30.9% lower, respectively than that of FA-20%S. The decrease in the ultimate tensile strength could be due to the interfacial properties. In other words, the chemical bonding energy and the frictional bond strength of FA-20%S increased more than the cracking strength compared to the other EGC composites, resulting in higher fiber-bridging strength (Lee et al. 2012). However, the tensile elasticity was increased with the increment of slag addition up to 2.98 GPa for FA-30%S which is attributed to C-A-S-H gel formed through the activation of slag leading to reduce porosity (Criado et al. 2016). Among all EGCs, FA-0%S exhibited the highest tensile strain capacity. With slag content increasing, the tensile strain capacity decreased. One of the underlying reasons for this considerable reduction in the tensile strain capacities with slag addition lies in their different

stress indices. The stress index of FA-0%S was the highest among the EGCs. In addition, the stress indices of FA-10%S, FA-20%S, and FA-30%S were 12.3%, 13.8%, and 15.2% lower, respectively, than that of FA-0%S. As mentioned previously, the higher the stress index value, the greater the possibility of saturated PSH behavior, which results in a higher tensile strain capacity of the composite. Therefore, the stress-based condition for PSH behavior (i.e., Eq. 1) is satisfied. The toughness results also reveal that with slag increase from 0% to 30%, toughness reduced from 12.6 to 3.7 J/cm^3 which means that the energy absorption of the EGC decreased as slag content increasing. This trend corresponds to tensile strain capacity. Generally, the incorporation of slag implied that the EGCs exhibited a low ductility and toughness but a high ultimate tensile strength.

The multiple cracking pattern of each mix is presented in Fig. 8. After unloading, a clear trace of all visible cracks was obtained by water spray. Mixture without slag cement addition, FA-0%S, exhibited the uniform and enormous micro-cracks distribution with tightly controlled crack width (i.e., saturated cracking behavior) were observed, which corresponds to its significantly high tensile strain capacity. However, with the increase of slag addition from 10% to 30%, the crack spacing was bigger and the crack distribution was not uniform (i.e., unsaturated cracking behavior). As slag content increasing, the EGC tended to be more brittle.

Flexural bending strength

The stress-deflection curves of flexural bending test are shown in Fig. 9. The stress deflection of all EGCs was reinforced with PVA. It was found that for the 20% and 30% slag addition of EGC, the material demonstrated relative brittle behavior, the stress decreases rapidly at around 10 mm midspan deflection. However, for the FA-0%S and FA-10%S, the curves were flatter and the midspan deflection increased up to 39.81 and 35.32 mm respectively. Moreover, the pseudo hardening responses appeared generally, which were much dependent on the slag addition.

In the four-point bending test, the ductility index can be obtained as the ratio of mid-span deflection at failure to that at the first crack (Jaejer et al. 1997). The greater ductility index indicates better ductility. A summary of modulus of rupture (MOR), deflection at first crack (D_{fc}), deflection at failure (D_{fl}) and ductility index (D_{fl}/ D_{fc}) is reported in Table 7. Slag addition increased MOR. Among the three percentage of slag addition, the mix with 20% slag gave the highest MOR, while the mix with 0% slag gave the lowest MOR. This founding corresponds to compressive strength results. The midspan deflection at first crack increased with MOR rising. The maximum mid-span deflection at failure reached 39.81 mm without slag and it was declined as slag addition increasing. Especially from 10% to 20% slag addition, 68.8% reduction in mid-span deflection at failure was observed. The data showed that the ductility was decreased with increment of slag content. FA-0%S gave the highest ductility index value. However, the ductility characteristics were dramatically reduced from 10% to 20% slag addition. It should be noted that FA-20%S gave the lowest flexural ductility.

In order to show multiple cracks clear, water was used to dampen the surface of failure specimens. Multiple cracks were uniformly distributed along the bending moment for all EGCs (Fig. 10). The number of cracks reduced and their spacing increased as slag content increased. The cracking pattern also indicated that the EGCs had very good deflection hardening.

Pullout bond strength

The general profile of pullout curve is illustrated in Fig. 11. It can be decomposed into three regimes. After debonding, the fiber can undergo sliding with either slip hardening, constant friction or slip softening behavior based on the different fiber properties (Redon et al. 2001).

Fig. 12 shows the bond stress-slip relationship for EGC specimens. All EGC mixtures exhibited pullout mode of failure with post-peak slip development. After the peak load, the pullout load dropped a little quickly and still maintain a constant bond stress until complete failure. They showed low bond stress reduction with slip evidenced by a high ductility measurement after peak load which indicated certain improvement in bond strength with some enhanced post-peak behavior (more ductility) due to high fiber confinement. The ultimate bond strength (τ_u), ultimate slip (s_u) and compressive strength (f_{cu}) of the EGCs are listed in Table 8.

It is obvious that bond strength of FA-20%S is the highest, and FA-0%S is the lowest which is coherent with compressive strength. This is associated with the decreased porosity in the interfacial zone, which can lead to an increase of the fiber-matrix contact surface, resulting in a higher frictional bond (Kim et al. 2007). Moreover, the ultimate slip reduced significantly as the slag content increased. This also reveals that the slag addition could decrease ductility of the EGC.

Based on BS 8110, the relationship between bond strength (τ_u) and compressive strength (f_{cu}) of concrete can be expressed as:

$$\tau_u = \beta\sqrt{f_{cu}} \tag{5}$$

Where τ_u is bond strength; β is a coefficient dependent on specimen; and f_{cu} is compressive strength.

The following equation was proposed to predict bond strength according to compressive strength for the fly ash/slag blended EGCs,

$$\tau_u = \begin{cases} 0.4\sqrt{f_{cu}} & for\ f_{cu} < 80MPa \\ 0.6\sqrt{f_{cu}} & for\ f_{cu} \geq 80MPa \end{cases} \tag{6}$$

The experimental bond strength and predicted bond strength are present in Table 9. Their linear regression is plotted in Fig.13. Comparing with the predicted bond strength determined using Eq. (6) and experimental bond strength from pullout test, it can be concluded that the predicted bond strength obtained using proposed equation agree well with the values obtained from the test. Regarding the fly ash/slag blended EGCs, BS equation is still valid with $\beta = 0.4$ for compressive strength less than 80 MPa and with $\beta = 0.6$ for compressive strength greater than or equal to 80 MPa.

Conclusions

Based on the test results, the following conclusions can be drawn:

1. Compressive strength of EGC can be enhanced by adding slag. However, peak strength is at 20% slag addition. The proposed EGC mixes have ultrahigh compressive strength by using low l/b of 0.27 and adding slag. The highest strength is 102 MPa with 20% slag addition for 28-day strength.
2. All EGCs exhibited strain hardening behavior in tension. Slag addition improved tensile strength of EGCs as well and the maximum was from the EGC with 20% slag addition. The strength turns to decrease when slag addition is over 20%. The highest tensile strain capacity of 3.14% was obtained without slag addition. With slag addition increasing up to 30%, the tensile strain capacities of composites decreased significantly, which was 0.74% as minimum. The higher stress index (σ_0/σ_{fc}) of the EGCs is one of the underlying reasons for its significantly high tensile strain capacity. The toughness of EGCs was reducing as slag content increasing.
3. For the EGC slabs, replacement of fly ash by slag can considerably improve the Modulus of Rupture, but on the other hand, significantly reduced deflection at failure and ductility.

MOR reached 18.5 MPa with 20% slag addition which is twice of the EGC without slag. The most reduction of 76.2% in deflection at failure comes from the EGC with 30% slag addition. 83.2% reduction in ductility were captured after 20% slag addition. Additionally, the deflection at first crack is dependent upon MOR instead of slag addition.

4. As the slag content increases, the bond strength increases up to maximum 6.2 MPa for 20% slag and the corresponding ultimate slip decreases. The 20% slag addition gained a 77.1% increase in bond strength of pure fly ash EGC.
5. There is excellent relationship between compressive strength and bond strength of EGCs. Equation to calculate the EGC's bond strength based on compressive strength are proposed. There is a good agreement between experimental results of bond strength and those of predicted equation. The BS equation is still working for the bond strength calculation of the EGC.
6. Addition of slag is a good approach to improve strength meanwhile maintain the strain hardening behavior for fly-ash-based EGC.

Acknowledgements

The authors acknowledge help provided by Chuanqing Fu during his visiting in Iowa State University and Douglas Wood for the mechanical tests in the structures lab of Iowa State University.

References

ASTM C109/C109M. (2016). "Standard Test Method for Compressive Strength of Hydraulic Cement Mortars (Using 2-in. Or [50-mm] Cube Specimens)," West Conshohocken (PA): ASTM International.

ASTM C618, (2017). "Standard Specification for Coal Fly Ash and Raw or Calcined Natural Pozzolan for Use in Concrete," Philadelphia: ASTM International.

BS 8110-1. (1997). "Structural Use of Concrete - Part 1: Code of Practice for Design and Construction," pp. 89–90.

Chi, M. (2012). "Effects of Dosage of Alkali-Activated Solution and Curing Conditions on the Properties and Durability of Alkali-Activated Slag Concrete," Construction and Building Materials 35, pp.240-245.

Criado, M., Aperador, W., and Sobrados, I. (2016). "Microstructural and Mechanical Properties of Alkali Activated Colombian Raw Materials," Materials 9(3), pp. 158.

Fernandez-Jimenez, A.M., Palomo, A., Lopez-Hombrados, C. (2006). "Engineering Properties of Alkali-Activated Fly Ash Concrete," ACI Materials Journal 103(2), pp. 106–112.

Hassan, H., Ismail, N. (2018). "Effect of Process Parameters on the Performance of Fly Ash/GGBS Blended Geopolymer Composites," Journal of Sustainable Cement-Based Materials 7(2), pp. 122-140.

Jaejer, L.G., Mufti, A.A., and Tadros, G. (1997). "The Concept of the Overall Performance Factor in Rectangular- Section Reinforced Concrete Beams," Proceedings of the 3rd International Symposium on Non-metallic (FRP) Reinforcement for Concrete Structure(FRPRCS-3), Japan Concrete Institute, Sapporo, Japan, pp. 551–558.

Japan Society of Civil Engineers. (2008). "Recommendations for Design and Construction of High Performance Fiber Reinforced Cement Composites with Multiple Fine Cracks (HPFRCC)," Testing Method 82, pp. 6-10.

Kanda, T., and Li, V.C. (1999). "New Micromechanics Design Theory for Pseudo-Strain Hardening Cementitious Composite," Journal of Engineering Mechanics 125(4), pp. 373–381.

Kanda, T., and Li, V.C. (2006). "Practical Design Criteria for Saturated Pseudo Strain Hardening Behavior in ECC," Journal of Advanced Concrete Technology 4(1), pp. 59–72.

Kim, J., Kim, J., Ha, G., Kim, Y. (2007). "Tensile and Fiber Dispersion Performance of ECC (Engineered Cementitious Composites) Produced with Ground Granulated Blast Furnace Slag," Cement and Concrete Research 37(7), pp. 1096–1105.

Kong, H-J., Bike, S.G., and Li, V.C. (2003). "Development of a Self-consolidating Engineered Cementitious Composite Employing Electrosteric Dispersion/Stabilization," Cement Concrete Composites 25(3), pp. 301–309.

Lee, B. Y., Cho, C-G., Lim, H-J., Song, J.K., Yang, K.H., and Li, V.C. (2012). "Strain Hardening Fiber Reinforced Alkali-Activated Mortar — A Feasibility Study," Construction and Building Materials 37, pp.15–20.

Li, V.C., and Kanda, T. (1998). "Engineered Cementitious Composites for Structural Applications," Journal of Materials in Civil Engineering 2(66), pp. 66–69.

Li, Z., and Liu, S. (2007). "Influence of Slag as Additive on Compressive Strength of Fly-ash-based Geopolymer," Journal of Materials in Civil Engineering 19(6), pp. 470-474.

Martin, J., Stanton, J., Mitra, N., and Lowes, L. N. (2007). "Experimental Testing to Determine Concrete Fracture Energy Using Simple Laboratory Test Setup," ACI Materials Journal 104(6), pp. 575–584.

Ohno, M., and Li, V.C. (2014). "A Feasibility Study of Strain Hardening Fiber Reinforced Fly ash-based Geopolymer Composites," Construction and Building Materials 57, pp. 163–168.

Palomo, A., Grutzeck, M.W., Blanco, M.T. (1999). "Alkali-Activated Fly Ashes: A Cement for the Future," Cement and Concrete Research 29(8), pp. 1323–1329.

Qian, S., and Li, V. (2011). "Headed Anchor/Engineered Cementitious Composites (ECC) Pullout Behavior," Journal of Advanced Concrete Technology 9(3), pp. 339-351.

Redon, C., Li, V., Wu, C., Hoshiro, H., Saito, T., Ogawa, A. (2001). "Measuring and Modifying Interface Properties of PVA Fibers in ECC Matrix," Journal of Materials in Civil Engineering 13(6), pp. 399-406.

Sarker, P. K., Haque, R., and Ramgolam, K. V. (2013). "Fracture Behavior of Heat Cured Fly-ash-based Geopolymer Concrete," Materials & Design 44, pp. 580–586.

Sofi, M., van Deventer, J.S.J., Mendis, P.A., Lukey, G.C. (2007). "Engineering Properties of Inorganic Polymer Concretes (IPCs)," Cement and Concrete Research 37(2), pp. 251–257.

Sofi, M., van Deventer, J.S.J., Mendis, P.A., Lukey, G.C. (2007). "Bond Performance of Reinforcing Bars in Inorganic Polymer Concretes (IPCs)," Journal of Materials Science 42(9), pp. 3107–3116.

Wang, S., and Li, V.C. (2007). "Engineered Cementitious Composites with High-Volume Fly Ash," ACI Materials Journal 104(3), pp. 233–241.

Wardhono, A., Law, D.W., Sutikno, and Dani, H. (2017). "The Effect of Slag Addition on Strength Development of Class C Fly Ash Geopolymer Concrete at Normal Temperature," AIP Conference Proceedings 1887, 020030.

Table 1. Chemical composition of fly ash and slag

	SiO_2	Al_2O_3	Fe_2O_3	SO_3	CaO	MgO	Na_2O	K_2O	Others	LOI
Fly ash	57.06	18.82	5.43	0.45	11.8	2.89	0.64	1.12	1.74	0.03
Slag	36.5	8.54	0.83	0.6	41.1	9.63	0.29	0.44	2.07	2.46

Note: All values in mass %, expressed on an oven-dry basis; LOI: loss on ignition at 1000 °C

Table 2: Specification of Sodium silicate solution and sodium hydroxide

Product	Sodium silicate solution (Na_2SiO_3)	Sodium hydroxide (NaOH)
Company	Sigma-Aldrich	Fisher Scientific
Grade	Reagent	Certified ACS
Composition	Na_2O: 10.6%, SiO_2: 26.5%	NaOH Solid
Density	1.39 g/ml	2.13g/ml
Formula	$(NaOH)_x(Na_2SiO_3)_y \bullet zH_2O$	NaOH

Table 3. Properties of PVA Fiber

Parameter	Value
Fiber label	RECS 15
Diameter (μm)	40
Length (mm)	12
Young's modulus (GPa)	41
Elongation (%)	6.7
Density (g/cm3)	1.3
Tensile strength (MPa)	1,586

Table 4. Mix Proportions of EGCs

Mix designation	Fly ash	Slag	Activator	PVA fiber
FA-0%S	1.0	-	0.27	0.02
FA-10%S	0.9	0.1	0.27	0.02
FA-20%S	0.8	0.2	0.27	0.02
FA-30%S	0.7	0.3	0.27	0.02

Note: All numbers are mass ratios of fly ash weight except fiber content (volume fraction).

Table 5. Properties of used steel bar

Diameter (mm)	Length (mm)	Yield strength (MPa)	Ultimate strength (MPa)	Elongation (%)
12.6	609.6	531	680	16

Table 6. Tensile strength test results

Mix	σ_{fc} (MPa)	Tensile elasticity, (GPa)	σ_0 (MPa)	Tensile strain capacity, (%)	Toughness, (J/cm^3)	Stress index, (σ_0/σ_{fc})
FA-0%S	3.4	1.18	4.7	3.14	12.6	1.38
FA-10%S	4.2	1.41	5.1	1.62	6.9	1.21
FA-20%S	5.7	1.58	6.8	1.04	5.5	1.19
FA-30%S	5.2	2.98	6.1	0.74	3.7	1.17

Table 7. Flexural strength test results

Mix	MOR (MPa)	D_{fc}, (mm)	D_{fl}, (mm)	Ductility index
FA-0%S	9.3	1.26	39.81	31.6
FA-10%S	10.4	1.41	35.32	25.0
FA-20%S	18.5	2.07	11.03	5.3
FA-30%S	15.3	1.60	9.46	5.9

Table 8. Pullout bond strength test results

Mix	τ_u, (MPa)	s_u, (mm)	f_{cu}, (MPa)
FA-0%S	3.5	16.3	72.6
FA-10%S	3.7	11.9	73.9
FA-20%S	6.2	9.4	102.3
FA-30%S	5.9	7.4	82.3

Table 9. Experimental (τ_u) and predicted (τ_p) bond strength

Mix	τ_u, (MPa)	τ_p, (MPa)
FA-0%S	3.5	3.41
FA-10%S	3.7	3.44
FA-20%S	6.2	6.07
FA-30%S	5.9	5.44

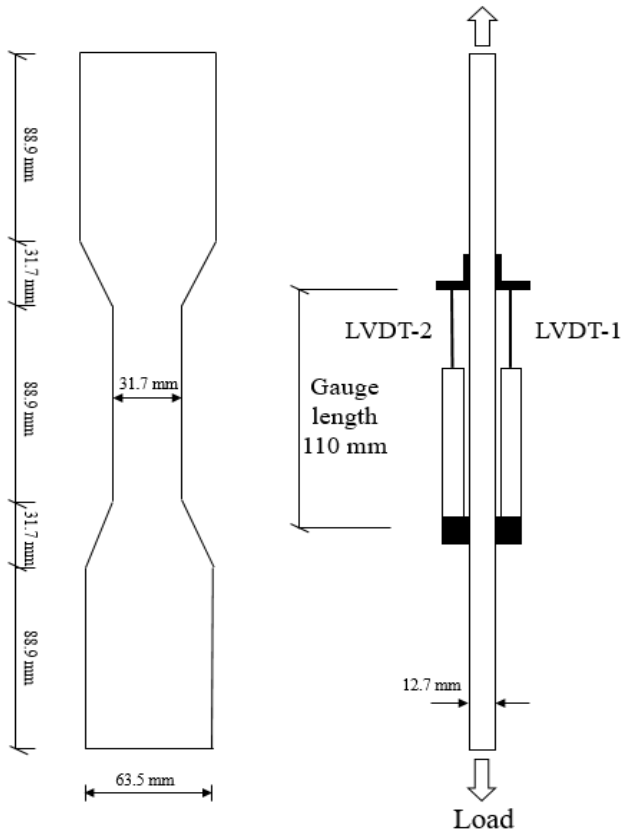

Figure 1. Uniaxial tension test setup

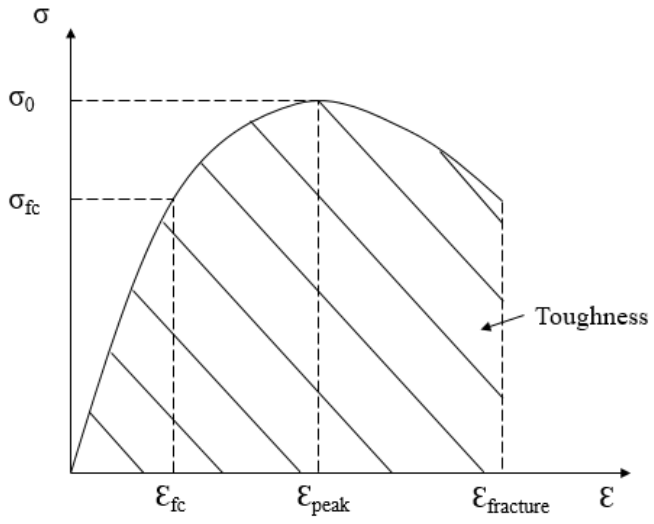

Figure 2. Typical stress/strain curve of strain hardening composites

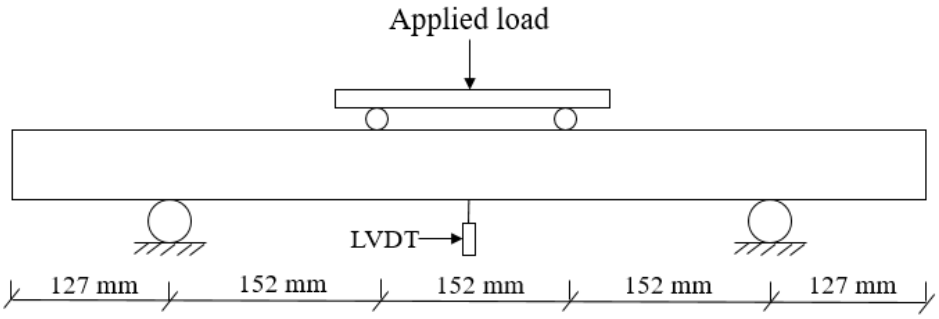

Figure 3. Schematic illustration of bending test setup

Figure 4. EGC slab under bending test

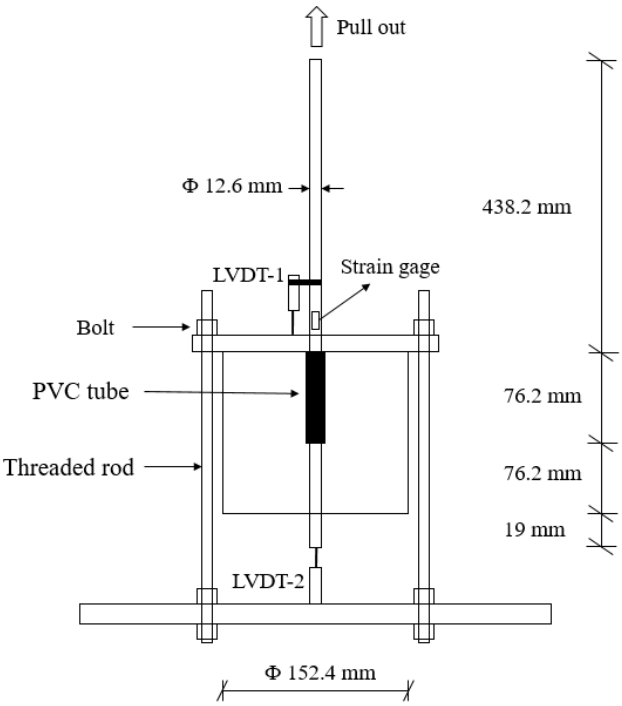

Figure 5. Pullout test setup

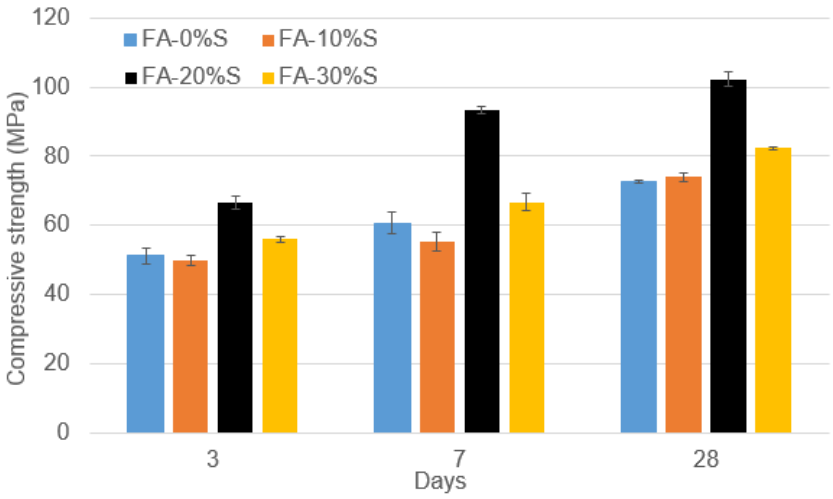

Figure 6. Compressive strength of EGCs

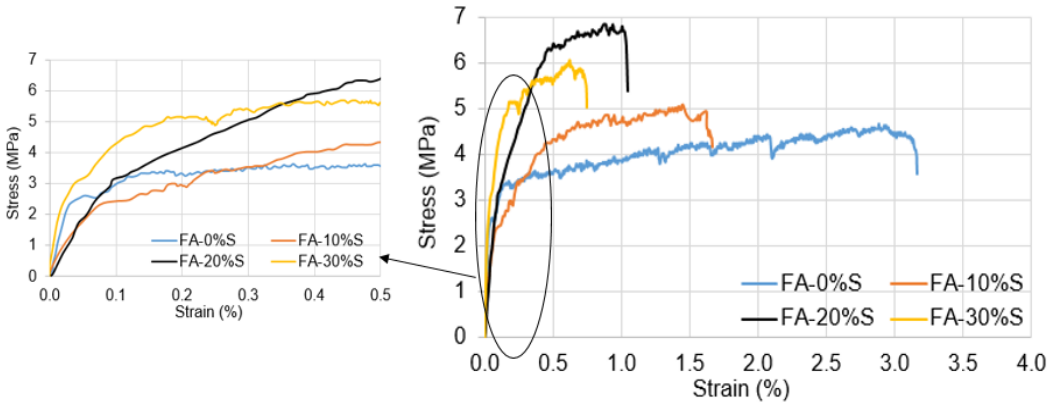

Figure 7. Tensile stress-strain responses of EGCs

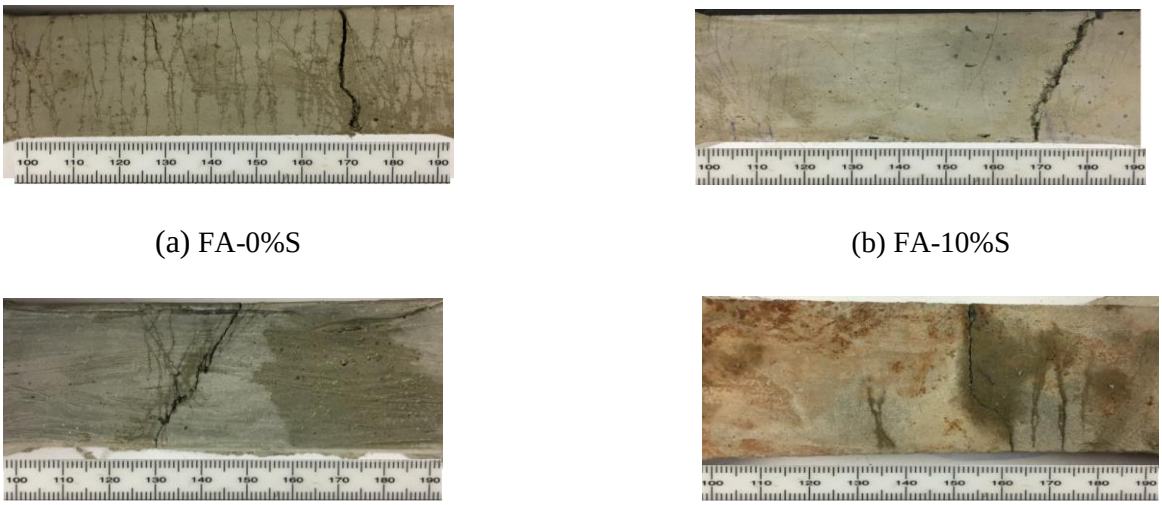

(a) FA-0%S

(b) FA-10%S

(c) FA-20%S

(d) FA-30%S

Figure 8. Multiple cracking behavior of EGCs on tension test

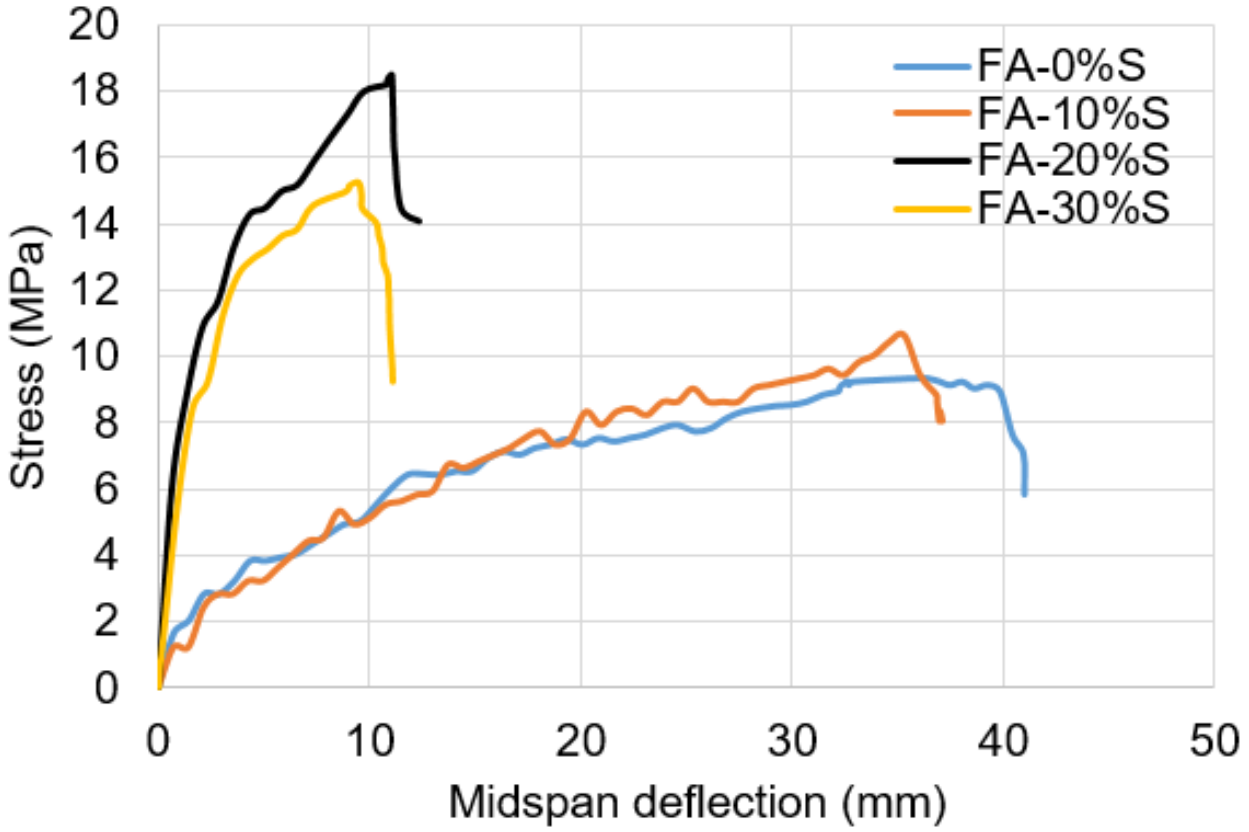

Figure 9. Flexural stress-deflection responses of EGCs

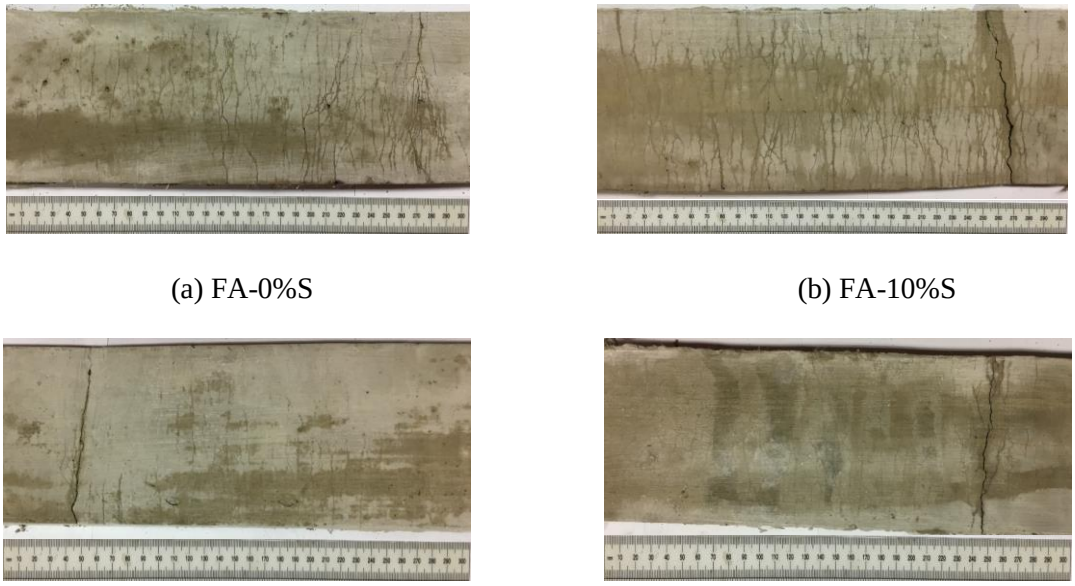

(a) FA-0%S (b) FA-10%S

(c) FA-20%S (d) FA-30%S

Figure 10. Multiple cracking pattern of EGCs under flexural loading.

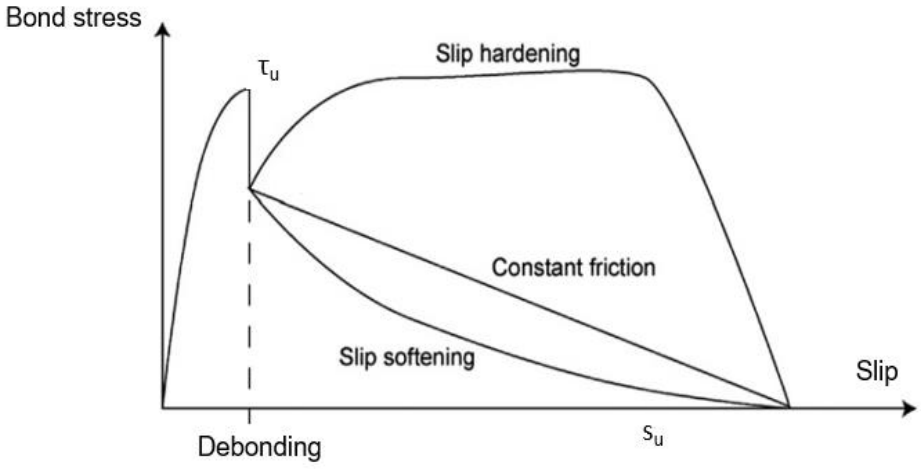

Figure 11.Typical curves for pullout test

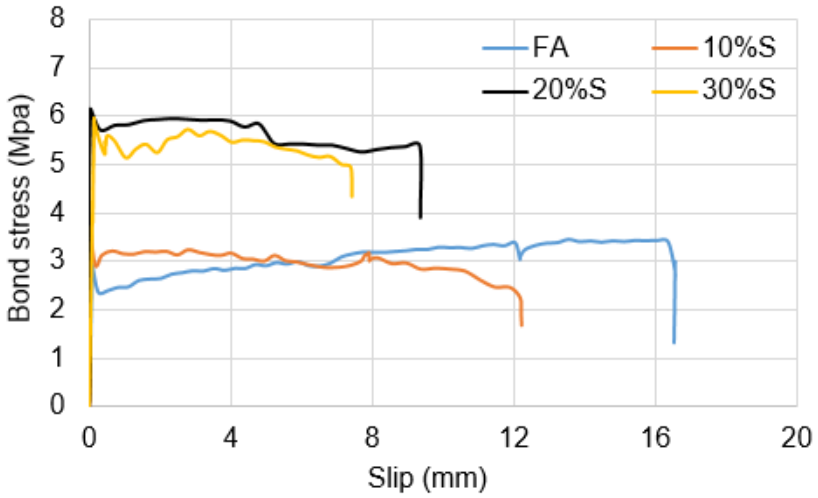

Figure 12. Bond stress-slip relationships for EGCs

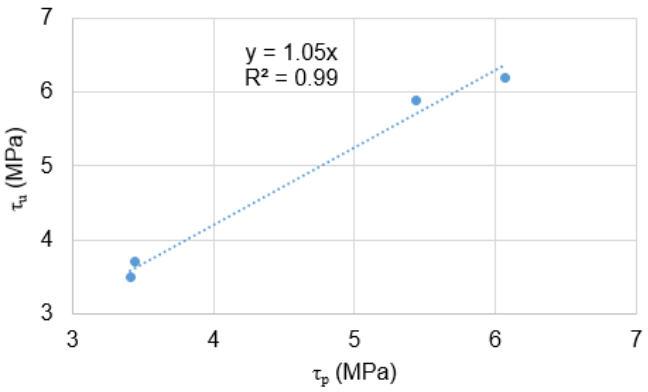

Figure 13. Experimental bond strength versus predicted bond strength

CHAPTER 7. CONCLUSIONS

This study investigates the effect of design parameters namely Module, Concentration, L/F, and temperature and time on setting time, compressive strength and hydration of FG. The statistical analysis and modeling on the prediction of setting time, compressive strength, and heat generation were conducted to understand the effect of each design parameter FG performance. The flowability, compressive strength and shrinkage behavior of FG paste were studied in terms of Module and Concentration. Comparing with PC, the effect of SR on reducing FG shrinkage was also evaluated by using free drying shrinkage and restrained ring shrinkage. In addition, a study of fly ash/slag blended EGC was provided in this dissertation. The effectiveness was determined of slag addition up to 30% in mechanical properties of EGC (i.e. compressive strength, tensile strength, flexural bending strength and pullout bond strength). Tensile strain capacity, toughness and ductility of fly ash/slag blended EGCs were assessed. Furthermore, a predictive model of bond strength based on compressive strength was established for EGC.

The main conclusions of this study are drawn as follows:

1. The increase in Module of an activator solution accelerated setting time, but reduced strength, total heat generation, reaction time and geopolymerization peak time. As solute Concentration increased, setting time for mixtures of 1.0 and 1.5 Modules became longer, but shorter for mixtures with 2.0 Module, while compressive strength, total heat, terminated time and peak time increased. The Modules less than 1.5, the Concentrations between 40% and 50%, the lower L/F ratios less than 0.40, and higher curing temperature, such as 50℃, were preferred to synthesize a geopolymer system using high-calcium fly ash.

2. From the predictive ANN models of setting time, compressive strength and heat generation, it revealed that the setting time had extremums at Module of 1.4 and 1.8 respectively, when Module changed from 1.0 to 2.0. It means the trend of setting time with various Module changed at Module of 1.4 and 1.8. L/F is the most influential parameter on setting. When Module is over 1.5, it has limited effect on strength while the solute Concentration influences compressive strength most. The heat generation is significantly dependent on the Module.
3. At a given liquid-to-fly ash ratio (L/F), FG paste exhibited similar flowability and drying shrinkage behavior, considerably higher compressive strength, and less shrinkage potential than PC.
4. Increased Module of activator could reduce flowability, compressive strength, drying shrinkage and cracking potential of FG. An increased solute Concentration could reduce flowability of FG and increase compressive strength, drying shrinkage and shrinkage potential of FG.
5. SR slightly decreased flowability and compressive strength of FG, but significantly reduced the drying shrinkage up to 52% and shrinkage potential for both FG and PC.
6. Mass loss is not the only reason for drying shrinkage of FG. The time to cracking could be used as an index for the cracking tendency of FG pastes.
7. Mechanical properties of EGC including compressive, tensile, flexural and bond strength could be enhanced by adding slag. However, there is a maximum strength at 20% addition. The proposed EGC mixes have ultrahigh 28-day compressive strength up to 102 MPa with 20% slag addition by using low l/b of 0.27. All EGCs exhibited strain hardening behavior in tension. The highest tensile strain capacity of 3.14% was obtained without slag addition.

With slag addition increasing up to 30%, the tensile strain capacities of composites decreased significantly, which was 0.74% as minimum. The stress index could be used to assess tensile strain capacity of the EGCs. The toughness of EGCs was reducing as slag content increasing.

8. The replacement of fly ash by slag can considerably improve the modulus of rupture, but on the other hand, significantly reduced deflection at failure and ductility. MOR reached 18.5 MPa with 20% slag addition which is twice of the EGC without slag. The deflection at failure decreases with the slag addition increasing. 83.2% reduction in ductility were captured for the EGC with 20% slag addition.
9. As the slag addition increases, the bond strength increases up to maximum 6.2 MPa for 20% slag and the corresponding ultimate slip decreases. The 20% slag addition gained a 77.1% increase in bond strength of pure fly ash EGC.
10. Equations to calculate the EGC's bond strength based on compressive strength are proposed. These models work for the bond strength calculation of the EGC.
11. The slag addition is a good approach to improve strength while maintaining the strain hardening behavior for fly-ash-based EGC.

CHAPTER 8. RECOMMENDATIONS FOR FUTURE RESEARCH

The work in this dissertation has provided optimized mix proportions regarding the basic design parameters based on the given fly ash from a stable source (certain power plant). However, the parameters from fly ash composites (e.g., Si to Al ratio in fly ash) need to be considered if the source of fly ash changes. Following the hydration process of FG investigated in this study, the phases on the hydration curve should be specified related to initial setting, final setting or even strength development using more accurately calorimetry test in future so that the theory of geopolymer reaction could be established.

Efforts have been made to develop predictive models of FG performance using ANNs. However, one of the biggest disadvantages of ANNs is the expression of ANN model. Further research is required, particularly to derive straightforward equations to predict FG performance or even for performance-based mix design.

The endeavor presented here attempts to evaluate the shrinkage cracking potential of geopolymer pastes according to the stress rate from restrained ring test. Since the magnitude of stress rate is dependent on the dimension of device. A specification of shrinkage cracking potential based on stress rate for geopolymer paste with a specified dimension of test device=should be demonstrated or even published in future. Therefore, the evaluations on shrinkage cracking potential of geopolymer paste could be qualitative from low to high.

The mechanisms of drying shrinkage for FG are not clear in this study. Since the moisture loss is not the only reason governing drying shrinkage, it is necessary to characterize pore structure of FG to figure out the reasons causing drying shrinkage. More shrinkage related properties such as

autogenous shrinkage, creep and shrinkage control methods should be explored for geopolymer paste.

Only geopolymer paste was studied in this dissertation. Geopolymer grout and concrete should be studied in future for practical use which are the major applications in sealing joints and construction respectively.

Only physical and mechanical properties of the designed geopolymer mixes were studied. The chemical interactions among the activators, admixtures, fly ash and slag that dominate the performance of geopolymer need to be studied in future.

Geopolymer paste samples produced in this study were cured at an elevated temperature (50 ºC). For field use, ambient temperature curing for the strength development of fly ash geopolymer should be studied in order to reduce the cost.

Durability of a construction material significantly influence its service life. Although SR and shrinkage of the geopolymer paste were studied, other durability properties such as freezing and thawing durability have not been studied.

REFERENCES

ACI Committee 232. (2004). "Use of Fly Ash in Concrete," Report, American Concrete Institute 232.2R-18.

Alomayri, T., Vickers, L., Shaikh, F.U.A., Low, I.M. (2014). "Mechanical Properties of Cotton Fabric Reinforced Geopolymer Composites at 200–1000 ℃," Journal of Advanced Ceramics 3(3), pp. 184–193.

ASTM C109. (2016). "Standard Test Method for Compressive Strength of Hydraulic Cement Mortars," American Society for Testing and Materials, Pennsylvania.

ASTM C1581/C1581M, (2016). "Standard Test Method for Determining Age at Cracking and Induced Tensile Stress Characteristics of Mortar and Concrete under Restrained Shrinkage," Philadelphia: ASTM International.

ASTM C1611. (2014). "Standard Test Method for Slump Flow of Self-Consolidating Concrete," American Society for Testing and Materials, Pennsylvania.

ASTM C1679. (2018). "Standard Practice for Measuring Hydration Kinetics of Hydraulic Cementitious Mixtures Using Isothermal Calorimetry," American Society for Testing and Materials, Pennsylvania.

ASTM C618. (2017). "Standard Specification for Coal Fly Ash and Raw or Calcined Natural Pozzolan for Use in Concrete," Philadelphia: ASTM International.

ASTM WK27337. (2010). "New Test Method for Pocket Penetrometer Test," ASTM International.

Banfill, P. F. G. (2006). "Rheology of Fresh Cement and Concrete," Rheology Reviews, pp.61-131.

Chareerat, T., Lee-Anansaksiri, A., Chindaprasirt, P. (2006). "Synthesis of High Fly Ash and Calcined Kaolin Geopolymer Mortar," International Conference on Pozzolan, Concrete and Geopolymer, Khhon Kaen, Thailand, 24-25 May.

Chindaprasirt, P., Chareerata, T., and Sirivivatnanon, V. (2007). "Workability and Strength of Coarse High Calcium Fly Ash Geopolymer," Cement and Concrete Composites 29, pp. 224-229.

Collins, F., and Sanjayan, J.G. (1998). "Early Age Strength and Workability of Slag Pastes Activated by NaOH and Na_2CO_3," Cement and Concrete Research 28(5), pp. 655-664.

Collins, F., and Sanjayan, J.G. (2000). "Effect of Pore Size Distribution on Drying Shrinkage of Alkali-Activated Slag Concrete," Cement and Concrete Research 30(9), pp. 1401-1406.

Criado, M., Fernandez-Jimenez, A., de la Torre, A.G., Aranda, M.A.G., Palomo, A. (2007). "An XRD Study of the Effect of the SiO_2/Na_2O Ratio on the Alkali Activation of Fly Ash," Cement and Concrete Research 37, pp. 671-679.

Dan E., Janotka I. (2003). "Chemical Resistance of Portland cement, Blast-Furnace Slag Portland cement and Sulphoaluminate-Belite Cement in Acid, Chloride and Sulphate Solution: Some Preliminary Results," Ceramics 47(4), pp. 141-148.

Davidovits, J. (1994). "Properties of Geopolymer Cements," Alkaline cements and concretes, KIEV Ukraine.

Deb, P., Natha, P., Sarker, P. (2015). "Drying Shrinkage of Slag Blended Fly Ash Geopolymer Concrete Cured at Room Temperature," Procedia Engineering 125, pp. 594 - 600.

Diab, A.M., Elyamany, H. E., Elmoaty A.E.M.A., Shalan, A.H. (2014). "Prediction of Concrete Compressive Strength Due to Long Term Sulfate Attack Using Neural Network," Alexandria Engineering Journal 53(3), pp. 627-642.

Dias, W.P.S., Pooliyadda, S.P. (2001). "Neural Networks for Predicting Properties of Concretes with Admixtures," Construction and Building Materials 15(7), pp. 371-379.

Fernandez-Jimenez, A., Garcia-Lodeiro, I., Palomo, A. (2007). "Durability of Alkali-Activated Fly Ash Cementitious Materials," Journal of Materials Science 42, pp.3055-3065.

Fernandez-Jimenez, A., Palomo, A., Criado, M. (2005). "Microstructure Development of Alkali-Activated Fly Ash Cement: A Descriptive Model," Cement and Concrete Research 35, pp.1204-1209.

Fernandez-Jimenez, A., Palomo, A., Sobrados, I., Sanz, J. (2006). "The Role Played by the Reactive Alumina Content in the Alkaline Activation of Fly Ashes," Microporous and Mesoporous Materials 91, pp. 111-119.

Filho, R.D.T, Ghavami, K., Sanjuan, M.A., England, G.L. (2005). "Free, Restrained and Drying Shrinkage of Cement Mortar Composites Reinforced with Vegetable Fibres," Cement & Concrete Composites 27 (5), pp. 537–546.

Gourley, J. T. (2003). "Geopolymers; Opportunities for Environmentally Friendly Construction Materials," Presented as a keynote paper at Materials conference, Adaptive Materials for a Modern Society, Institute of Materials Engineering Australasia, Sydney.

Hardjito, D., Cheak, C.C., Ing, C.H.L. (2008). "Strength and Setting Times of Low Calcium Fly Ash-based Geopolymer Mortar," Modern Applied Science 2(4), pp. 3-11.

Hossain, A.B., Weiss, J. (2006). "The Role of Specimen Geometry and Boundary Conditions on Stress Development and Cracking in the Restrained Ring Test," Cement and Concrete Research 36(1), pp. 189-199.

Intergovernmental Panel on Climate Change (IPCC) (1997). Revised 1996 IPCC Guidelines for National Greenhouse Gas Inventories. Reference Manual (Revised).Vol 3. J.T. Houghton et al., IPCC/OECD/IEA, Paris, France.

Jaarsveld, J. G. S. V., Deventer, J. S. J.V., and Lukey, G. C. (2003). "The Characterization of Source Materials in Fly Ash-based Geopolymers," Materials Letters 57(7), pp. 1272-1280.

Jo, M., Soto, L., Arocho, M., St John, J., Hwang, S. (2015). "Optimum Mix Design of Fly Ash Geopolymer Paste and Its Use in Pervious Concrete for Removal of Fecal Coliforms and Phosphorus in Water," Construction and Building Materials 93, pp. 1097−1104.

Karakoca, M.B., Turkmen, I., Maras M.M., Kantarcia, F., Demirboga, R., Toprak, M. U. (2014). "Mechanical Properties and Setting Time of Ferrochrome Slag Based Geopolymer Paste and Mortar," Construction and Building Materials 72, pp.283−292.

Khale, D., Chaudhary, R. (2007). "Mechanism of Geopolymerization and Factors Influencing Its Development: A Review," Journal of Materials Science 42, pp. 729-746.

Kong, D.L.Y., and Sanjayan, J.G. (2008). "Damage Behavior of Geopolymer Composites Exposed to Elevated Temperatures," Cement and Concrete Composites 30(10), pp. 986-991.

Krizan, D., Zivanovic, B. (2002). "Effects of Dosage and Modulus of Water Glass on Early Hydration of Alkali-Slag Cements," Cement and Concrete Research 32, pp. 1181-1188.

Lee, B., Cho, C-G., Lim, H-J., Song, J-K., Yang, K-H., Li, VC. (2012). "Strain Hardening Fiber Reinforced Alkali-activated Mortar - A Feasibility Study," Construction and Building Materials 37, pp. 15-20.

Li, V.C., Kanda, T. (1998). "Engineered Cementitious Composites for Structural Applications," ASCE Journal of Materials in Civil Engineering 10(2), pp. 66-69.

Li, V.C., Wu, H-C. (1992). "Conditions for Pseudo Strain-hardening in Fiber Reinforced Brittle Matrix Composites," Applied Mechanics Reviews 45(8), pp. 390-398.

McDonald, M., and Thompson, J. (2005). "Sodium Silicate: A Binder for the 21st Century," The PQ Corporation, Industrial Chemicals Division.

Nematollahi, B., Sanjayan, J., Shaikh, F. (2015). "Tensile Strain Hardening Behavior of PVA Fiber-Reinforced Engineered Geopolymer Composite," Journal of Materials in Civil Engineering 27(10): 04015001.

Nicholson, C., Fletcher, R., Miller, N., Stirling, C., Morris, J., Hodges, S., MacKenzie, K., and Schmücker, M. (2005). "Building Innovation through Geopolymer Technology," Chemistry in New Zealand, pp.10-12.

Ohno, M., Li, VC. (2014). "A Feasibility Study of Strain Hardening Fiber Reinforced Fly Ash-based Geopolymer Composites," Construction and Building Materials 57, pp. 163-168.

Pacheco-Torgal, F., Castro-Gomes, J., Jalali, S. (2007). "Alkali-Activated Binders: A Review. Part 2. About Materials and Binders Manufacture," Construction and Build Materials 22, pp. 1315-1322.

Palacios, M., Banfill, Ph., and Puertas, F.F.G. (2008). "Rheology and Setting of Alkali-Activated Slag Pastes and Mortars: Effect of Organic Admixture," ACI Materials Journal 105, pp. 140-148.

Palacios, M., Puertas, F. (2005). "Effect of Superplasticizer and Shrinkage-Reducing Admixtures on Alkali-Activated Slag Pastes and Mortars," Cement and Concrete Research 35, pp. 1358 - 1367.

Patankar, S., Ghugal, Y., Jamkar, S. (2014). "Mix Design of Fly-ash-based Geopolymer Concrete," Advances in Structural Engineering, pp. 1619-1634.

Petermann, J., Athar, S., and Hammond, M. (2010). "Alkali-activated Geopolymers: A Literature Review," Air Force Research Laboratory Materials and Manufacturing Directorate.

Ridtirud, C., Chindaprasirt, P., Pimraksa, K. (2011). "Factors Affecting the Shrinkage of Fly Ash Geopolymers," International Journal of Minerals, Metallurgy and Materials 18(1), pp. 100-104.

Roussel, N. (2006). "Correlation Between Yield Stress and Slump: Comparison Between Numerical Simulations and Concrete Rheometers Results," Materials and Structures 39(4), pp. 501-509.

Roussel, N., and Coussot, P. (2005). "Fifty-cent Rheometer for Yield Stress Measurements: From Slump to Spreading Flow," Journal of Rheology 49(3), pp. 705-718.

Rupnow T.D. (2013). "Quality Control Tools to Identify Source Variability of Class C Fly Ash and Its Impact on Freshly Mixed Cement-Fly Ash Paste," World of Coal Ash (WOCA) conference, Lexington, KY, 22-25 April.

Sarker, P.k. (2011). "Bond Strength of Reinforcing Steel Embedded in Fly Ash-based Geopolymer Concrete," Materials and Structures 44(5), pp.1021-1030.

Skvara, F., Dolezal, J., Svoboda, P., Kopecky, L., Pawlasova, S., Lucuk, M., Dvoracek, K., Beksa, M., Myskova, L., Sulc, R. (2006). "Concrete Based on Fly Ash Geopolymers," The Tenth East Asia-Pacific Conference on Structural Engineering and Construction, Bangkok, Thailand, 3-5 August.

Song, S., Sohn, D., Jennings, H.M., Mason, T.O. (2000). "Hydration of Alkali-Activated Ground Granulated Blast Furnace Slag," Journal of Materials Science 35, pp. 249-257.

Sumajouw, D.M.J., Hardjito , D., Wallah , S.E., and Rangan , B.V. (2004). "Geopolymer Concrete for a Sustainable Future," Green Processing Conference, Fremantle, WA, 10-12 May.

Suryadi, A., Triwulan, Aji, P. (2011). "Predicting the Initial Setting Time of Self Compacting Concrete Using Artificial Neural Networks (ANNs) with the Various of Learning Rate Coefficient," Journal of Applied Sciences Research 7(3), pp. 314-320.

Tang, T., Ouyang, C., Shah, S.P. (1996). "A Simple Method for Determining Material Fracture Parameters from Peak Loads," ACI Materials Journal 93(2), pp. 147-157.

Vijaya Rangan, B. (2008). "Fly Ash-Based Geopolymer Concrete," Research Report GC 4.

Wang, X. (2011). "Drying Shrinkage of Ternary Blends in Mortar and Concrete," Graduate Theses and Dissertations. Iowa State University, 10105.

Williams, P.J., Biernacki, J.J., Walker, L.R., Meyer, H.M., Rawn, C.J., Bai, J. (2002). "Microanalysis of Alkali-Activated Fly Ash-CH Pastes," Cement and Concrete Research 32, pp. 963-972.

Xie, Z., Xi, Y. (2001). "Hardening Mechanisms of an Alkaline-Activated Class F Fly Ash," Cement and Concrete Research 31, pp. 1245-1249.

Yadollahi, M., Benli, A., Demirboga, R. (2015). "Prediction of Compressive Strength of Geopolymer Composites Using an Artificial Neural Network," Materials Research Innovations 19(6), pp. 453-458.

Yao X., Zhang Z., Zhu H., Chen Y. (2009). "Geopolymerization Process of Alkali–Metakaolinite Characterized by Isothermal Calorimetry," Thermochimica Acta 493, pp.49–54.

Yuan, J., Darwin, D., Browning, J. (2011). "Development and Construction of Low-cracking High-performance Concrete Bridge Decks: Free Shrinkage Tests, Restrained Ring Tests, Construction Experience, and Crack Survey Results," Structural Engineering and Engineering Materials SM Report No. 103.

Zheng, Y. C. (2009). "Shrinkage of Geopolymer," Thesis, University of Melbourne.

Zivica, V., Palou M.T., Krizma, M. (2014). "Geopolymer Cements and Their Properties: A Review," Building Research Journal 61(2), pp. 85 -100.

Zivica, V., Palou, M. T., and Bagel, L. (2014). "High Strength Metahalloysite Based Geopolymer," Composites, Part B: Engineering 57, pp.155-165.

Zuda, L., Pavlik Z., Rovnanikova, P., Bayer, P., Cerny, R. (2006), "Properties of Alkali Activated Aluminosilicate Material after Thermal Load," International Journal of Thermophysics 27(4), 1250-1263.

APPENDIX. REPORT ABSTRACT FROM ADDITIONAL RESEARCH

PERVIOUS CONCRETE PHYSICAL CHARACTERISTICS AND EFFECTIVENESS IN STORMWATER POLLUTION REDUCTION

Final Report
April 2016

Principal Investigator
Say Kee Ong, Professor
Institute for Transportation, Iowa State University

Co-Principal Investigator
Kejin Wang, Professor
Institute for Transportation, Iowa State University

Research Assistants
Guyu Shi and Yifeng Ling

Authors
Say Kee Ong, Kejin Wang, Yifeng Ling, and Guyu Shi

Sponsored by
the Midwest Transportation Center and
the U.S. Department of Transportation
Office of the Assistant Secretary for Research and Technology

A report from
Institute for Transportation
Iowa State University
2711 South Loop Drive, Suite 4700
Ames, IA 50010-8664
Phone: 515-294-8103
Fax: 515-294-0467
www.intrans.iastate.edu

Executive Summary

The objective of the research was to investigate the physical/chemical and water flow characteristics of various pervious concrete mixes made of different concrete materials and their effectiveness in attenuating water pollution. Four pervious concrete mixes were prepared with Portland cement and with 15% cementitious materials (slag, limestone powder, and fly ash) as a Portland cement replacement.

All four pervious concrete mixtures had acceptable workability, with mixtures made with Portland cement and 15% fly ash replacement having better workability than those made with 15% slag and 15% limestone powder replacement. The unit weight of these fresh pervious concrete mixtures ranged from 115.9 lb/yd$_3$ to 119.6 lb/yd$_3$, with the mixture made with 15% slag having the lowest unit weight (115.9 lb/yd$_3$) and the mixture made with 15% fly ash having the highest unit weight (119.6 lb/yd$_3$). The 28 day compressive strength of the pervious concrete mixes ranged from 1858 psi (mix with 15% slag) to 2285 psi (pure cement mix). The compressive strength generally increased with unit weight and decreased with total porosity (air void ratio). The permeability of the four mixes generally decreased with unit weight and increased with total porosity. The permeability coefficients ranged from 340 in./hr for the pure cement mix to 642 in./hr for the mix with 15% slag. The total porosities (or air void ratios) of these pervious concrete mixes ranged from 24.00% (mix with 15% slag) to 31.41% (pure cement mix) as measured by the flatbed scanner test method, while the porosities ranged from 18.93% (mix with 15% slag) to 24.15% (pure cement mix) as measured by the RapidAir method. It was not clear why the concrete porosities were not correlated to unit weight. The total porosity of the four pervious concrete mixes measured by the flatbed scanner method were all higher than those measured by the Rapid Air

method, but the specific surface areas measured by the flatbed scanner method were all lower than those measured by the Rapid Air method.

For the pollution abatement experiments, mixes with fly ash and limestone powder removed about 30% of the input naphthalene concentration, while the mix with pure cement removed 10% and the mix with slag only removed 0.5% of the influent naphthalene concentration. The water volume balance showed that less than 1% of the water added was retained in the experimental column setup.